UNIVERSITY OF CALIFORNIA SAN DIEGO

Circuit Mechanisms of Noradrenergic Function in Descending Pain Modulation

A dissertation submitted in partial satisfaction of the requirements
for the degree Doctor of Philosophy

in

Neurosciences

by

Susan Therese Lubejko

Committee in charge:

Professor Matthew Banghart, Chair
Professor Wendy Campana
Professor Sung Han
Professor Byungkook Lim

2024

The Dissertation of Susan Therese Lubejko is approved, and it is acceptable in quality and form for publication on microfilm and electronically.

University of California San Diego

2024

DEDICATION

For Mom, Dad, Emily, and Chris.

TABLE OF CONTENTS

LIST OF FIGURES

LIST OF ABBREVIATIONS

4-AP	4-aminopyridine
AAV	adeno-associated virus
ACSF	artificial cerebrospinal fluid
AMPA	α-amino-3-hydroxy-5-methyl-4-isoxazoleproprionic acid
ANOVA	analysis of variance
AP	action potential
AP	anterior-posterior axis
Casp3	Caspase 3
CFA	complete Fruend's adjuvant
ChR2	channelrhodopsin 2
CNO	clozapine-n-oxide
CPP	3-(I-2-Carboxypiperazin-4-yl)-propyl-1-phosphonic acid
cVLM	caudal ventrolateral medulla
DAMGO	[d-Ala^2,Nme-Phe^4, Gly-ol^5]enkephalin
DAPI	4',6-diamidino-2-phenylindole
DBH	dopamine beta-hydroxylase
DPMS	descending pain modulatory system
DREADD	designer receptors exclusively activated by designer drugs
DV	dorsal-ventral axis
EPM	elevated plus maze
EPSC	excitatory postsynaptic current

f-I	firing rate vs. current input
FISH	fluorescence *in situ* hybridization
GABA	γ- aminobutyric acid
GIRK	G protein-coupled inward rectifier potassium channel
i.p.	intraperitoneal injection
IPSC	inhibitory postsynaptic current
LC	locus coeruleus
LH	lateral hypothalamus
mEPSC	miniature excitatory postsynaptic current
mIPSC	miniature inhibitory postsynaptic current
ML	medial-lateral axis
MOR	mu-opioid receptor
MRG	Mas-related G protein-coupled receptor
NA	noradrenaline
NBQX	2,3-dioxo-6-nitro-7-sulfamoyl-benzo[f]quinoxaline
NMDA	N-methyl-D-aspartate
NTX	naltrexone
oEPSC	optically-evoked excitatory postsynaptic current
oIPSC	optically-evoked inhibitory postsynaptic current
PAG	periaqueductal gray
PBS	phosphate buffered saline
peri-LC	pericoerulear area of the locus coeruleus
PFC	prefrontal cortex

PrH	nucleus prepositus hypoglossi
RMP	resting membrane potential
RVM	rostroventromedial medulla
RVLM	rostroventrolateral medulla
s.c.	subcutaneous injection
SEM	standard error of the mean
tdTom	tdTomato
TH	tyrosine hydroxylase
TTX	tetrodotoxin
vlPAG	ventrolateral periaqueductal gray
YFP	yellow fluorescent protein

ACKNOWLEDGEMENTS

I would like to thank my advisor Dr. Matt Banghart for handing me the reigns to this project and allowing me to run with it, and for cultivating my skills in becoming an independent thinker, leader, and communicator.

I would like to thank my committee members Dr. Sung Han, Dr. Wendy Campana, and Dr. Byungkook Lim for asking the tough questions every year while still encouraging me on my progress as a scientist and thinker.

Thank you to the Banghart Lab, especially Giulia Livrizzi, Shannan McClain, Desiree Johnson, Caroline Johnson, Jenny He, and Aryanna Layden, for picking me up and dusting me off after failed experiments and creating an environment in which I could thrive as a scientist and a person.

Thank you to my 2017 cohort mates, San Diego friends, and friends near and far that continue to check up on me, especially when I'm spending too much time in lab. Your encouragement, fun, and friendship have made these seven years not only possible, but some of my most enjoyable.

Finally, thank you to my husband Chris, who probably deserves a degree for listening to all of my joys and disasters every night on our walks. Your patience has finally paid off!

Chapter 2, in full, has been submitted for publication of the material as it may appear in Science Advances, 2024, Lubejko, Susan T.; Livrizzi, Giulia; Patel, Janki; Yung, Jean C.; Yaksh, Tony L., Banghart, Matthew R. "Inputs to the locus coeruleus

from the periaqueductal gray and rostroventral medulla shape opioid-mediated descending pain modulation." The dissertation author was the primary researcher and author of this paper.

Chapter 3, in part, is being prepared for submission for publication of the material. Lubejko, Susan T; Banghart, Matthew R. The dissertation author was the primary investigator and author of this material.

Chapters 4 & 5 contain unpublished material coauthored with Banghart, Matthew R. The dissertation author was the primary researcher and author of these chapters.

VITA

2015	Bachelor of Science in Physiology and Neurobiology, University of Maryland, College Park
2015-2017	Postbaccalaureate Fellow, National Institute on Aging, National Institutes of Health
2024	Doctor of Philosophy in Neurosciences, University of California San Diego

PUBLICATIONS

Lubejko ST, Livrizzi G, Patel J, Yung JC, Yaksh TL, Banghart MR. "Inputs to the locus coeruleus from the periaqueductal gray and rostroventral medulla shape opioid-mediated descending pain modulation." *BioRxiv* (2023). *Manuscript in revision.*

McClain SP, Ma X, Johnson DA, Johnson CA, Layden AE, Yung JC, **Lubejko ST**, Livrizzi G, He XJ, Zhou J, Chang-Weinberg J, Ventriglia E, Rizzo A, Levinstein M, Gomez JL, Bonaventura J, Michaelides M, Banghart MR. "*In vivo* photopharmacology with light-activated opioid drugs." *Neuron* **111**, 1-15 (2023).

Lubejko ST, Graham RD, Livrizzi G, Schaefer R, Banghart MR, Creed MC. "The role of endogenous opioid neuropeptides in neurostimulation-driven analgesia." *Frontiers in Systems Neuroscience* **16,** 1044686 (2022).

Lubejko ST, Fontaine B, Soueidan SE, MacLeod KM. "Spike threshold adaptation diversifies neuronal operating modes in the auditory brain stem." *Journal of Neurophysiology* **122,** 2576-2590 (2019).

Sah N, Peterson BD, **Lubejko ST**, Vivar C, van Praag H. "Running reorganizes the circuitry of one-week-old adult-born hippocampal neurons." *Scientific Reports* **7,** 10903 (2017).

Moon HY, Becke A, Berron D, Becker B, Sah N, Benoni G, Janke E, **Lubejko ST**, Greig NH, Mattison JA, Duzel E, van Praag H. "Running-induced systemic cathepsin B secretion is associated with memory function." *Cell Metabolism* **24,** 332-340 (2016).

Fontaine B, MacLeod KM, **Lubejko ST**, Steinberg LJ, Koppl C, Pena JL. "Emergence of band-pass filtering through adaptive spiking in the owl's cochlear nucleus." *Journal of Neurophysiology* **112**, 430-445 (2014).

Ahn JA, Kreeger LJ, **Lubejko ST**, Butts DA, MacLeod KM. "Heterogeneity of intrinsic biophysical properties among cochlear nucleus neurons improves the population coding of temporal information." *Journal of Neurophysiology* **111**, 2320-2331 (2014).

FIELDS OF STUDY

Major Field: Neurosciences

Studies in Neurobiology of Pain
Professor Matthew Banghart, University of California San Diego

ABSTRACT OF THE DISSERTATION

Circuit Mechanisms of Noradrenergic Function in Descending Pain Modulation

by

Susan Therese Lubejko

Doctor of Philosophy in Neurosciences

University of California San Diego, 2024

Professor Matthew Banghart, Chair

Our perception of pain is an important survival mechanism to avoid potentially damaging noxious stimuli. However, chronic pain is debilitating. While opioids remain the best treatment for pain, chronic use can lead to dangerous side effects including addiction, tolerance, and respiratory depression that have contributed to the U.S. Opioid Crisis. A better understanding of the underlying circuitry that modulates pain perception and contributes to opioid analgesia will

lead to alternative strategies to suppress pain in the absence of dangerous side effects. The supraspinal descending pain modulatory system (DPMS) shapes pain perception through terminals in spinal cord and is thought to be crucial for opioid analgesia. DPMS release of noradrenaline in the spinal dorsal horn inhibits pain. However, the circuit mechanisms by which the DPMS evokes this release remain unclear. Using anatomy, behavior, slice electrophysiology, and calcium activity measurements in transgenic mice, we establish a major role for the locus coeruleus (LC) in opioid-mediated antinociception. We also define the synaptic inputs by which canonical DPMS nodes, the ventrolateral periaqueductal gray (vlPAG) and rostroventral medulla (RVM), interface with LC. To this end, we discover that a significant portion of opioid antinociception is driven by excitatory output from vlPAG to LC and uncover a previously unstudied opioid-sensitive inhibitory output from RVM to LC, inhibition of which is antinociceptive. We also find that these circuit elements are responsive to noxious stimulation. Finally, we begin to define plasticity within the LC and excitatory inputs to LC in the context of persistent pain. These findings serve to revise circuit models of descending monoaminergic pain modulation and establish promising new targets for pain relief.

CHAPTER 1: Introduction

Pain and human health

The International Association for the Study of Pain defines pain as "an unpleasant sensory and emotional experience associated with, or resembling that associated with, actual or potential tissue damage" (Raja et al., 2020). Given this definition, acute pain is an important mechanism for survival and for preserving our physical well-being by avoiding potentially damaging stimuli. However, persistent or chronic pain is debilitating and produces a substantial burden on public health. The Centers for Disease Control and Prevention recently reported that in 2021, an estimated 51 million, or 20.9%, of U.S. adults experienced chronic pain, with 17 million, or 6.9% of the U.S. adult population, experiencing high-impact chronic pain. Chronic pain has been shown to disrupt work and life activities, and is linked with other comorbidities such as depression, suicide risk, and substance abuse (Rikard et al., 2023). While opioids remain the most effective treatment for pain due to their strong modulation of pain processing pathways within the brain and spinal cord, their propensity to cause addiction, tolerance, and respiratory depression, among many other side effects, has led to the current U.S. Opioid Crisis, which sees more than 90 overdose deaths per day (Volkow et al., 2017). Given these impacts on human health, it is imperative to understand the underlying circuitry that contributes to our perception of acute and chronic pain in an attempt to locate circuit elements that may be modulated without the use of opioid drugs for long-lasting pain relief.

Pain vs. nociception

As defined above, pain encompasses both a sensory and emotional experience. Pain is processed in the brain by a distinct group of structures known as the "pain matrix" (Wager et al., 2013). Different structures involved in the pain matrix differentially encode the sensory discriminative components of pain (where on the body, what the stimulus is, how intense it is, etc.) vs. the affective and emotional components (pain unpleasantness, expression of negative emotions as a result). Generally, in healthy humans, the sensory and affective components are inseparable in the pain experience.

However, in rodent studies, such as those performed in this dissertation, measurement of experience with a noxious stimulus often relies on reflexive behaviors, such as paw withdrawal or tail flick. In this case, we use the term "nociception" to refer to the sensory, discriminative aspect of encoding a noxious stimulus alone without implying an affective component that was not measured (IASP Terminology). Similarly, when analgesic drugs are used to modulate these reflexive behaviors, we use the term "antinociception" instead of "analgesia". The terms nociception and antinociception are used throughout this dissertation for these reasons. However, as more recent pain research does find strategies to measure affective behaviors in rodents, such as attending, escape, and avoidance, it is becoming possible to measure "pain" in rodent models as well (Kimmey et al., 2022).

Neurobiology of pain processing

Pain information is processed through two major pathways: the ascending and descending pathways (**Figure 1.1A)**.

Ascending pain pathways

The ascending pain pathway begins in the periphery at the site of tissue injury. Primary afferents, in this case Aδ- and C-fiber nociceptors, transmit peripheral noxious information via cell bodies located in the dorsal root ganglion to the dorsal horn of the spinal cord. Within the dorsal horn, noxious information flows to projection neurons and interneurons mainly in the superficial laminae, with a smaller portion of afferents contacting deeper wide dynamic range neurons in lamina V (Dubin and Patapoutian, 2010). After receiving peripheral pain information, the ascending spinal projection neurons generally decussate before projecting supraspinally through three major pathways.

The spinothalamic tract represents the classical pain processing pathway. Secondary spinal projection neurons in this pathway synapse in the thalamus on the way to cortical sites that are involved in the pain matrix, including the somatosensory cortex, insula, and cingulate cortex to encode the sensory discriminative and affective components of pain. The spinomesencephalic and spinoreticular tracts transmit pain information to the midbrain (including the periaqueductal gray and parabrachial region) and medullary reticular formation, respectively (Sengul and Watson, 2015).

Descending pain pathways

The second major pain processing pathway, which is the focus of this dissertation, is the descending pain modulatory system (DPMS). The DPMS begins supraspinally and passes through key midbrain and brainstem structures to gate spinal outflow of ascending nociceptive signals at the level of the dorsal horn *before* these signals ascend to the brain. The major midbrain DPMS node is the ventrolateral periaqueductal gray (vlPAG), which organizes pain

modulatory signals from cortical and subcortical regions, such as the amygdala, prefrontal cortex, insula, and cingulate cortex.

The most canonically studied descending pathway involves synapses from the vlPAG onto the medial portion of the rostroventral medulla (RVM), the neurons of which synapse in the dorsal horn to enhance or suppress incoming pain information through opioidergic and serotonergic mechanisms (Millan, 2002; François et al., 2017). The RVM, and to some extent vlPAG, contain electrophysiologically defined neuronal classes known as On- and Off- cells, which are thought to facilitate and inhibit neurons in the dorsal horn, respectively, in response to noxious stimuli (Heinricher et al., 1994). Exogenous and endogenous opioids exert many of their antinociceptive effects through this pathway: vlPAG-RVM glutamatergic projection neurons are under tonic inhibitory control from local GABAergic interneurons in vlPAG. It is posited that opioids cause antinociception by releasing this inhibition. Opioids suppress the local GABAergic interneurons by binding to inhibitory ($G_{i/o}$) G protein-coupled mu-opioid receptors (MORs), thereby disinhibiting the activity of vlPAG-RVM projections (Basbaum and Fields, 1984; Heinricher et al., 2009). The serotonergic output from RVM in the dorsal horn can be either pain inhibitory or pain facilitatory depending on the RVM neurons conveying the signal and the receptor identity of targets in the dorsal horn (Millan, 2002).

Descending noradrenergic pain modulation

In addition to the complicated role of serotonergic output in descending pain modulation and despite the apparent focus on this more canonical pathway, rodent intrathecal pharmacological studies have long indicated an almost purely pain inhibitory role of spinal release of noradrenaline (NA). These studies have implicated spinal noradrenergic signaling in a

variety of models of DPMS suppression of pain, including that which is caused by application of opioid drugs systemically or directly to the vlPAG via microinfusion (Yaksh, 1979; Proudfit and Hammond, 1981; Hammond and Yaksh, 1984).

Previous work points to three midbrain and brainstem noradrenergic structures as the likely sources of spinal NA that mediate antinociception: A5, A6 (also known as the locus coeruleus), and A7. All three of these structures exhibit anatomical projections to the spinal dorsal horn (Clark and Proudfit, 1991c, 1991b; Proudfit and Clark, 1991; Clark and Proudfit, 1993; Bruinstroop et al., 2012). A body of prior literature focused on the A7 nucleus alone as the primary driver of spinal NA in rats. Electrical stimulation of A7 produces spinal noradrenaline release and antinociception (Miller and Proudfit, 1990; Yeomans and Proudfit, 1992; Holden et al., 1999; Nuseir and Proudfit, 2000). Most recently, the A5 nucleus has been demonstrated as a crucial relay point for a specific type of descending pain modulation known as diffuse noxious inhibitory control, otherwise known as the "pain inhibits pain" phenomenon (Kucharczyk et al., 2023).

A large body of evidence encompassing early lesion studies to more modern neuroscience methods strongly implicates the locus coeruleus (LC) in descending pain modulation. The LC is the largest noradrenergic center of the brain and signals via both ascending projections from the dorsal part of LC to a wide variety of forebrain targets and descending projections from the ventral LC to the spinal cord (Li et al., 2016; Hirschberg et al., 2017). Interestingly, however, there appears to have been considerable disagreement early in the field regarding the importance of LC in descending modulation and its role in opioid antinociception. First, confusion about how LC may modulate sensory signals, which are processed largely in the spinal dorsal horn, arose as it was determined that different commonly used laboratory rat strains exhibited

divergent patterns of LC terminals in the spinal cord. Using retrograde tracing strategies, in one strain, it was determined that the LC provides a majority of the NAergic input to the motor-focused ventral spinal horn (Clark et al., 1991; Clark and Proudfit, 1991b; Proudfit and Clark, 1991). Additionally, lesion studies aiming to determine the noradrenergic structures that contribute to systemic opioid antinociception produced unconvincing results on whether lesions in the LC or other areas around the LC were more responsible for deficits in the antinociception, with different studies producing opposite results (Sasa et al., 1977; Hammond and Proudfit, 1980).

However, the use of the most up-to-date anatomical and behavioral techniques in more recent papers, including Chapter 2 of this dissertation, have once again established an important role for LC in nociceptive modulation. Exogenous stimulation of ventral LC using electrical, optogenetic, and chemogenetics methods produces antinociception that depends on spinal NA signaling, whereas stimulation of the dorsal, ascending portion of LC has been shown to be pronociceptive or anxiety-producing (West et al., 1993; Hickey et al., 2014; Hirschberg et al., 2017). As a result, more current models of the DPMS now include the LC, among other structures, with the canonical PAG-RVM pathway (Ossipov et al., 2010).

Does LC interface with canonical DPMS nodes?

Although the field now better understands the importance of LC-mediated descending NA in DPMS-driven pain modulation, the circuitry by which the LC may be harnessed in concert with other descending pathways as it is drawn into circuit models of the canonical DPMS requires further study (**Figure 1.1B**). Interestingly, both the vlPAG and the medial portion of the RVM exhibit anatomical projections to all three noradrenergic nuclei (Clark and Proudfit, 1991a;

Bajic and Proudfit, 1999), positioning both PAG and RVM to have influence over spinal NA signaling.

vlPAG projections to LC are better studied, but with sometimes contrasting results. Rabies tracing studies posit a relatively strong projection from vlPAG to LC NAergic neurons, including LC neurons that project to the spinal cord (Schwarz et al., 2015; Kim et al., 2018). Additionally, a recent slice electrophysiology study established an excitatory projection from lateral PAG to LC NAergic neurons (Barcomb et al., 2022). However, *in vivo* electrophysiological studies report relatively weak projections from PAG to LC that serve to inhibit LC output (Ennis et al., 1991). While one study reports that these projections are opioid-sensitive (Kim et al., 2018), this finding appears to be at odds with the notion that opioids cause PAG to drive descending NA release in the spinal cord. For these reasons, the sign, opioid sensitivity, and behavioral relevance in nociception and opioid antinociception of this projection all require further investigation.

To our knowledge, there is only one study that has investigated the anatomical connections between the medial RVM (which receives many of the projections from the vlPAG and is therefore highly implicated in pain) and the pericoerulear region and LC (Clark and Proudfit, 1991a). Interestingly, a large body of literature establishes an excitatory projection from the rostroventro*lateral* medulla (RVLM) to the LC, but these studies noticeably avoid the medial RVM referenced throughout this dissertation (Ennis and Aston-Jones, 1988; Ennis et al., 1992). Similarly, the caudal ventrolateral medulla (cVLM) provides noradrenergic excitatory inputs to LC (Gu et al., 2023). Virtually nothing is known about the projections from the medial aspect of RVM to LC.

Chapters 2 and 3 of this dissertation endeavor to answer many of the questions posed above. First, we establish a significant role for LC activity in opioid-mediated antinociception using two modern viral methods in mice that avoid off target effects that confound the results of lesion studies. Next, using slice physiology and behavior, we not only determine the excitatory or inhibitory nature and opioid sensitivity of the vlPAG and RVM inputs to LC, but also extend our investigation of these circuit elements into their role in complex nociceptive and systemic opioid antinociceptive behavior using pathway specific chemogenetics and activity measurement via fiber photometry.

Chronic Pain in the DPMS

While acute pain assays in rodents like those employed in Chapters 2 and 3 remain important tools for neuroscientists to define new circuitry and uncover roles for endogenous signaling mechanisms in healthy individuals, translational efforts require researchers to go further into these newly defined circuits and mechanisms to determine how they may function in the context of chronic pain. Acute pain is deserving of study as an important survival mechanism and options for treating it are certainly needed for individuals experiencing debilitating short-term pain after injury. However, as noted earlier, the greatest burden on human health arises from the high prevalence of *chronic* pain, which affects patients' ability to function on the timescale of months to years. Chronic pain carries many definitions in different fields, but usually refers to pain that persists after the site of injury has healed (a useful metric in rodent studies) or pain that persists from more than three months in humans (Apkarian et al., 2009; Rikard et al., 2023). An open challenge that exists in the pain field is whether brain circuits shown to hold

antinociceptive promise by testing healthy individuals *remain* antinociceptive in subjects experiencing chronic pain.

The reason to pose this question is that chronic pain causes plasticity at virtually every level of the nervous system that contributes to pain perception and modulation. Studies have found structural and functional alterations from the peripheral nociceptors themselves to spinal circuitry, cortical representations, grey matter volume and even glial activity (Kuner and Flor, 2016). Within the DPMS, imbalances between descending pain facilitation and inhibition from the RVM are often cited as driving forces in establishing chronic hypersensitivity (Porreca et al., 2002; Ren and Dubner, 2002; Heinricher, 2016; Chen and Heinricher, 2019). Additionally, hypofunction in PAG may hamper the pain inhibitory capabilities of the canonical descending pathway (Ho et al., 2013). Existing literature also has investigated the role of noradrenergic signaling in chronic pain states, but with conflicting results. While descending NAergic signaling appears to maintain its pain inhibitory properties and protect against chronic hypersensitivity (Ossipov et al., 2014), some groups have hypothesized that the LC actually generates chronic pain and comorbid anxiodepressive behaviors by shifting signaling away from descending antinociceptive NA release to pain and anxiety-driving ascending signaling (Brightwell and Taylor, 2009; Taylor and Westlund, 2017; Llorca-Torralba et al., 2019). How LC activity changes in response to chronic pain appears up for debate (Viisanen and Pertovaara, 2007; Kimura et al., 2015; Hayashida and Obata, 2019; Alba-Delgado et al., 2021).

Chapter 4 of this dissertation aims to study changes in LC activity and inputs to LC that may occur in the context of persistent inflammatory pain on a relatively short timescale. We establish that although LC intrinsic properties are unchanged in a slice preparation from injured vs. uninjured animals, glutamatergic inputs to LC are upregulated by persistent pain, especially

in ventral LC neurons that are putatively involved in descending NA release. The implications of these results in light of the circuit elements uncovered in Chapters 2 and 3, as well as important future directions for similar studies in a chronic neuropathic (referring to pain caused by damage to the nervous system itself) pain context are discussed.

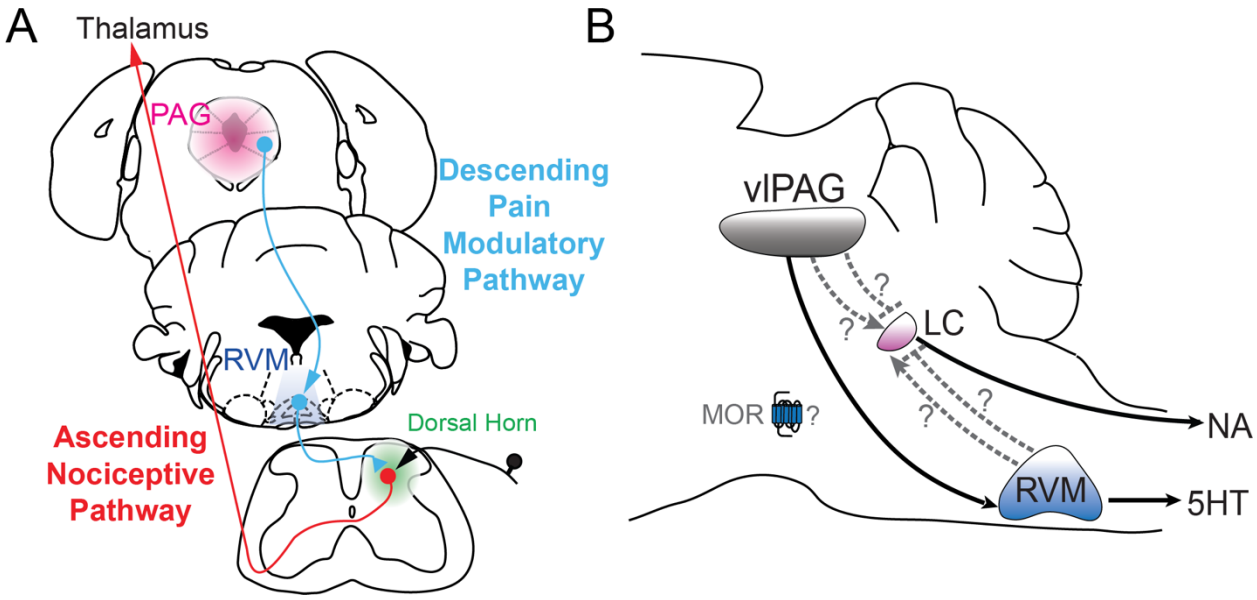

Figure 1.1. Schematics and outstanding questions of the ascending and descending pain pathways.

A. Coronal slice schematic of the ascending nociceptive pathway (red arrow) that is triggered by input from nociceptors to the dorsal horn (black arrow) and the descending pain modulatory pathway (blue arrows) that contacts nociceptor terminals in the dorsal horn. **B.** Sagittal diagram delineating the known descending pathways from vlPAG, RVM and LC (black, solid) and the outstanding questions of circuit connectivity between vlPAG and RVM to the LC (grey, dashed). Open questions include the neurotransmitters (excitatory vs. inhibitory) released at these synapses, as well as the presence of the MOR within these circuit elements.

References

Alba-Delgado, C., Mico, J. A., and Berrocoso, E. (2021). Neuropathic pain increases spontaneous and noxious-evoked activity of locus coeruleus neurons. *Prog Neuropsychopharmacol Biol Psychiatry* 105. doi: 10.1016/j.pnpbp.2020.110121.

Apkarian, A. V., Baliki, M. N., and Geha, P. Y. (2009). Towards a theory of chronic pain. *Prog Neurobiol* 87, 81–97. doi: 10.1016/j.pneurobio.2008.09.018.

Bajic, D., and Proudfit, H. K. (1999). Projections of neurons in the periaqueductal gray to pontine and medullary catecholamine cell groups involved in the modulation of nociception. *Journal of Comparative Neurology* 405, 359–379. doi: 10.1002/(SICI)1096-9861(19990315)405:3<359::AID-CNE6>3.0.CO;2-W.

Barcomb, K., Olah, S. S., Kennedy, M. J., and Ford, C. P. (2022). The Journal of Physiology Properties and modulation of excitatory inputs to the locus coeruleus. *J Physiol* 0, 1–20. doi: 10.1113/JP283605#support-information-section.

Basbaum, A., and Fields, H. L. (1984). Endogenous Pain Control Systems: Brainstem Spinal Pathways and Endorphin Circuitry. *Annu Rev Neurosci* 7, 309–338. doi: 10.1146/annurev.neuro.7.1.309.

Brightwell, J. J., and Taylor, B. K. (2009). Noradrenergic neurons in the locus coeruleus contribute to neuropathic pain. *Neuroscience* 160, 174–185. doi: 10.1016/j.neuroscience.2009.02.023.

Bruinstroop, E., Cano, G., Vanderhorst, V. G. J. M., Cavalcante, J. C., Wirth, J., Sena-Esteves, M., et al. (2012). Spinal projections of the A5, A6 (locus coeruleus), and A7 noradrenergic cell groups in rats. *Journal of Comparative Neurology* 520, 1985–2001. doi: 10.1002/cne.23024.

Chen, Q., and Heinricher, M. M. (2019). Descending Control Mechanisms and Chronic Pain. *Curr Rheumatol Rep* 21, 13. doi: 10.1007/s11926-019-0813-1.

Clark, F. M., and Proudfit, H. K. (1991a). Projections of neurons in the ventromedial medulla to pontine catecholamine cell groups involved in the modulation of nociception. *Brain Res* 540, 105–115. doi: 10.1016/0006-8993(91)90496-I.

Clark, F. M., and Proudfit, H. K. (1991b). The projection of locus coeruleus neurons to the spinal cord in the rat determined by anterograde tracing combined with immunocytochemistry. *Brain Res* 538, 231–245. doi: 10.1016/0006-8993(91)90435-X.

Clark, F. M., and Proudfit, H. K. (1991c). The projection of noradrenergic neurons in the A7 catecholamine cell group to the spinal cord in the rat demonstrated by anterograde tracing combined with immunocytochemistry. *Brain Res* 547, 279–288. doi: 10.1016/0006-8993(91)90972-X.

Clark, F. M., and Proudfit, H. K. (1993). The projections of noradrenergic neurons in the A5 catecholamine cell group to the spinal cord in the rat: anatomical evidence that A5 neurons modulate nociception. *Brain Res* 616, 200–210. doi: 10.1016/0006-8993(93)90210-E.

Clark, F. M., Yeomans, D. C., and Proudfit, H. K. (1991). The noradrenergic innervation of the spinal cord: differences between two substrains of Sprague-Dawley rats determined using retrograde tracers combined with immunocytochemistry. *Neurosci Lett* 125, 155–158. doi: 10.1016/0304-3940(91)90015-L.

Dubin, A. E., and Patapoutian, A. (2010). Nociceptors: The sensors of the pain pathway. *Journal of Clinical Investigation* 120, 3760–3772. doi: 10.1172/JCI42843.

Ennis, M., and Aston-Jones, G. (1988). Activation of locus coeruleus from nucleus paragigantocellularis: a new excitatory amino acid pathway in brain. *The Journal of Neuroscience* 8, 3644–3657. doi: 10.1523/JNEUROSCI.08-10-03644.1988.

Ennis, M., Aston-Jones, G., and Shiekhattar, R. (1992). Activation of locus coeruleus neurons by nucleus paragigantocellularis or noxious sensory stimulation is mediated by intracoerulear excitatory amino acid neurotransmission. *Brain Res* 598, 185–195. doi: 10.1016/0006-8993(92)90182-9.

Ennis, M., Behbehani, M., Shipley, M. T., van Bockstaele, E. J., and Aston-Jones, G. (1991). Projections from the periaqueductal gray to the rostromedial pericoerulear region and nucleus locus coeruleus: Anatomic and physiologic studies. *Journal of Comparative Neurology* 306, 480–494. doi: 10.1002/cne.903060311.

François, A., Low, S. A., Sypek, E. I., Christensen, A. J., Sotoudeh, C., Beier, K. T., et al. (2017). A Brainstem-Spinal Cord Inhibitory Circuit for Mechanical Pain Modulation by GABA and Enkephalins. *Neuron* 93, 822–839. doi: 10.1016/j.neuron.2017.01.008.

Gu, X., Zhang, Y. Z., O'Malley, J. J., De Preter, C. C., Penzo, M., and Hoon, M. A. (2023). Neurons in the caudal ventrolateral medulla mediate descending pain control. *Nat Neurosci*. doi: 10.1038/s41593-023-01268-w.

Hammond, D. L., and Proudfit, H. K. (1980). Effects of locus coeruleus lesions on morphine-induced antinociception. *Brain Res* 188, 79–91. doi: 10.1016/0006-8993(80)90558-2.

Hammond, D. L., and Yaksh, T. L. (1984). Antagonism of stimulation-produced antinociception by intrathecal administration of methysergide or phentolamine. *Brain Res* 298, 329–337. doi: 10.1016/0006-8993(84)91432-X.

Hayashida, K., and Obata, H. (2019). Strategies to treat chronic pain and strengthen impaired descending noradrenergic inhibitory system. *Int J Mol Sci* 20, 822.

Heinricher, M. M. (2016). “Pain Modulation and the Transition from Acute to Chronic Pain,” in *Translational Research in Pain and Itch*, eds. C. Ma and Y. Huang (Dordrecht: Springer), 105–115.

Heinricher, M. M., Morgan, M. M., Tortorici, V., and Fields, H. L. (1994). Disinhibition of off-cells and antinociception produced by an opioid action within the rostral ventromedial medulla. *Neuroscience* 63, 279–288. doi: 10.1016/0306-4522(94)90022-1.

Heinricher, M. M., Tavares, I., Leith, J. L., and Lumb, B. M. (2009). Descending control of nociception: Specificity, recruitment and plasticity. *Brain Res Rev* 60, 214–225. doi: 10.1016/j.brainresrev.2008.12.009.

Hickey, L., Li, Y., Fyson, S. J., Watson, T. C., Perrins, R., Hewinson, J., et al. (2014). Optoactivation of locus ceruleus neurons evokes bidirectional changes in thermal nociception in rats. *Journal of Neuroscience* 34, 4148–4160. doi: 10.1523/JNEUROSCI.4835-13.2014.

Hirschberg, S., Li, Y., Randall, A., Kremer, E. J., and Pickering, A. E. (2017). Functional dichotomy in spinal- vs prefrontal-projecting locus coeruleus modules splits descending noradrenergic analgesia from ascending aversion and anxiety in rats. *Elife* 6, 1–26. doi: 10.7554/elife.29808.

Holden, J. E., Schwartz, E. J., and Proudfit, H. K. (1999). Microinjection of morphine in the A7 catecholamine cell group produces opposing effects on nociception that are mediated by α1- and α2- adrenoceptors. *Neuroscience* 91, 979–990. doi: 10.1016/S0306-4522(98)00673-3.

Ho, Y. C., Cheng, J. K., and Chiou, L. C. (2013). Hypofunction of glutamatergic neurotransmission in the periaqueductal gray contributes to nerve-injury-induced neuropathic pain. *Journal of Neuroscience* 33, 7825–7836. doi: 10.1523/JNEUROSCI.5583-12.2013.

IASP Terminology (n.d.). Available at: https://www.iasp-pain.org/resources/terminology/ [Accessed January 6, 2024].

Kim, J. H., Gangadharan, G., Byun, J., Choi, E. J., Lee, C. J., and Shin, H. S. (2018). Yin-and-yang bifurcation of opioidergic circuits for descending analgesia at the midbrain of the mouse. *Proc Natl Acad Sci U S A* 115, 11078–11083. doi: 10.1073/pnas.1806082115.

Kimmey, B. A., McCall, N. M., Wooldridge, L. M., Satterthwaite, T. D., and Corder, G. (2022). Engaging endogenous opioid circuits in pain affective processes. *J Neurosci Res* 100, 66–98. doi: 10.1002/jnr.24762.

Kimura, M., Suto, S., Morado-Urbina, C. E., Peters, C. M., Eisenach, J. C., and Hayashida, K. I. (2015). Impaired pain-evoked analgesia after nerve injury in rats reflects altered glutamate regulation in the locus coeruleus. *Anesthesiology* 123, 899–908.

Kucharczyk, M. W., Di Domenico, F., and Bannister, K. (2023). A critical brainstem relay for mediation of diffuse noxious inhibitory controls. *Brain* 146, 2259–2267. doi: 10.1093/brain/awad002.

Kuner, R., and Flor, H. (2016). Structural plasticity and reorganisation in chronic pain. *Nat Rev Neurosci* 18, 20–30. doi: 10.1038/nrn.2016.162.

Li, Y., Hickey, L., Perrins, R., Werlen, E., Patel, A. A., Hirschberg, S., et al. (2016). Retrograde optogenetic characterization of the pontospinal module of the locus coeruleus with a canine adenoviral vector. *Brain Res* 1641, 274–290. doi: 10.1016/j.brainres.2016.02.023.

Llorca-Torralba, M., Pilar-Cuéllar, F., Bravo, L., Bruzos-Cidon, C., Torrecilla, M., Mico, J. A., et al. (2019). Opioid Activity in the Locus Coeruleus Is Modulated by Chronic Neuropathic Pain. *Mol Neurobiol* 56, 4135–4150. doi: 10.1007/s12035-018-1361-9.

Millan, M. J. (2002). Descending control of pain. *Prog Neurobiol* 66, 355–474.

Miller, J. F., and Proudfit, H. K. (1990). Antagonism of stimulation-produced antinociception from ventrolateral pontine sites by intrathecal administration of α-adrenergic antagonists and naloxone. *Brain Res* 530, 20–34. doi: 10.1016/0006-8993(90)90653-S.

Nuseir, K., and Proudfit, H. K. (2000). Bidirectional modulation of nociception by GABA neurons in the dorsolateral pontine tegmentum that tonically inhibit spinally projecting noradrenergic A7 neurons. *Neuroscience* 96, 773–783. doi: 10.1016/S0306-4522(99)00603-X.

Ossipov, M. H., Dussor, G. O., and Porreca, F. (2010). Central modulation of pain. *Journal of Clinical Investigation* 120, 3779–3787. doi: 10.1172/JCI43766.

Ossipov, M. H., Morimura, K., and Porreca, F. (2014). Descending pain modulation and chronification of pain. *Curr Opin Support Palliat Care* 8, 143–151. doi: 10.1097/SPC.0000000000000055.

Porreca, F., Ossipov, M. H., and Gebhart, G. F. (2002). Chronic pain and medullary descending facilitation. *Trends Neurosci* 25, 319–325.

Proudfit, H. K., and Clark, F. M. (1991). *The projections of locus coeruleus neurons to the spinal cord*. Elsevier B.V. doi: 10.1016/S0079-6123(08)63803-0.

Proudfit, H. K., and Hammond, D. L. (1981). Alterations in nociceptive threshold and morphine-induced analgesia produced by intrathecally administered amine antagonists. *Brain Res* 218, 393–399.

Raja, S. N., Carr, D. B., Cohen, M., Finnerup, N. B., Flor, H., Gibson, S., et al. (2020). The revised International Association for the Study of Pain definition of pain: concepts, challenges, and compromises. *Pain* 161, 1976–1982. doi: 10.1097/j.pain.0000000000001939.

Ren, K., and Dubner, R. (2002). Topical review Descending modulation in persistent pain: an update. *Pain* 100, 1–6. Available at: www.elsevier.com/locate/pain.

Rikard, S. M., Strahan, A. E., Schmit, K. M., Gery, ;, and Guy, P. (2023). MMWR, Chronic Pain Among Adults — United States, 2019–2021. Available at: https://www.cdc.gov/.

Sasa, M., Munekiyo, K., Osumi, Y., and Takaori, S. (1977). Attenuation of morphine analgesia in rats with lesions of the locus coeruleus and dorsal raphe nucleus.

Schwarz, L. A., Miyamichi, K., Gao, X. J., Beier, K. T., Weissbourd, B., Deloach, K. E., et al. (2015). Viral-genetic tracing of the input-output organization of a central noradrenaline circuit. *Nature* 524, 88–92. doi: 10.1038/nature14600.

Sengul, G., and Watson, C. (2015). "Ascending and Descending Pathways in the Spinal Cord," in *The Rat Nervous System: Fourth Edition* (Elsevier Inc.), 115–130. doi: 10.1016/B978-0-12-374245-2.00008-5.

Taylor, B. K., and Westlund, K. N. (2017). The Noradrenergic Locus Coeruleus as a Chronic Pain Generator. *J Neurosci Res* 95, 1336–1346.

Viisanen, H., and Pertovaara, A. (2007). Influence of peripheral nerve injury on response properties of locus coeruleus neurons and coeruleospinal antinociception in the rat. *Neuroscience* 146, 1785–1794. doi: 10.1016/j.neuroscience.2007.03.016.

Volkow, N. D., Collins, F. S., and Ph, D. (2017). The Role of Science in Addressing the Opioid Crisis. *N Engl J Med* 377, 391–394.

Wager, T. D., Atlas, L. Y., Lindquist, M. A., Roy, M., Woo, C.-W., and Kross, E. (2013). An fMRI-Based Neurologic Signature of Physical Pain. *New England Journal of Medicine* 368, 1388–1397. doi: 10.1056/nejmoa1204471.

West, W. L., Yeomans, D. C., and Proudfit, H. K. (1993). The function of noradrenergic neurons in mediating antinociception induced by electrical stimulation of the locus coeruleus in two different sources of Sprague-Dawley rats. *Brain Res* 626, 127–135. doi: 10.1016/0006-8993(93)90571-4.

Yaksh, T. L. (1979). Direct evidence that spinal serotonin and noradrenaline terminals mediate the spinal antinociceptive effects of morphine in the periaqueductal gray. *Brain Res* 160, 180–185. doi: 10.1016/0006-8993(79)90616-4.

Yeomans, D. C., and Proudfit, H. K. (1992). Antinociception induced by microinjection of substance p into the A7 catecholamine cell group in the rat. *Neuroscience* 49, 681–691. doi: 10.1016/0306-4522(92)90236-U.

CHAPTER 2: Inputs to the locus coeruleus from the periaqueductal gray and rostroventral medulla shape opioid-mediated descending pain modulation

Abstract

The supraspinal descending pain modulatory system (DPMS) shapes pain perception via monoaminergic modulation of sensory information in the spinal cord. However, the role and synaptic mechanisms of descending noradrenergic signaling remain unclear. Here, we establish that noradrenergic neurons of the locus coeruleus (LC) are essential for supraspinal opioid antinociception. Unexpectedly, given prior emphasis on descending serotonergic pathways, we find that opioid antinociception is primarily driven by excitatory output from the ventrolateral periaqueductal gray (vlPAG) to the LC. Furthermore, we identify a previously unknown opioid-sensitive inhibitory input from the rostroventromedial medulla (RVM), the suppression of which disinhibits LC neurons to drive spinal noradrenergic antinociception. We also report the presence of prominent bifurcating outputs from the vlPAG to the LC and the RVM. Our findings significantly revise current models of the DPMS and establish a novel supraspinal antinociceptive pathway that may contribute to multiple forms of descending pain modulation.

Introduction

The midbrain and brainstem descending pain modulatory system (DPMS) alters spinal outflow of ascending nociceptive signals. Current models of the DPMS emphasize excitatory projections from ventrolateral periaqueductal gray (vlPAG) to the rostroventromedial medulla (RVM), which sends projections to the spinal cord dorsal horn that bidirectionally modulate incoming noxious sensory information through serotonergic and opioidergic mechanisms

(Millan, 2002; François et al., 2017). Endogenous and exogenous opioids are thought to produce analgesia via disinhibition of vlPAG-to-RVM projection neurons (Basbaum and Fields, 1984; Heinricher et al., 2009; Lau and Vaughan, 2014). The RVM and, to some extent, the PAG, are comprised of On-, Off-, and neutral cells, which are defined electrophysiologically by their activity preceding a nocifensive response (Fields et al., 1983; Heinricher et al., 1987, 1994).

In addition to serotonin, rodent intrathecal pharmacological studies implicate spinal noradrenaline (NA) signaling in DPMS-driven and opioid-mediated pain suppression (Yaksh, 1979; Proudfit and Hammond, 1981; Hammond and Yaksh, 1984; Jensen and Yaksh, 1984; Aimone et al., 1987). Spinal serotonin can both suppress and facilitate nociceptive processing and pain behaviors (Suzuki et al., 2004; Svensson et al., 2006; Ganley et al., 2023b), whereas spinal NA is more consistently reported as antinociceptive. Previous work implicates midbrain and brainstem catecholaminergic cells groups as the likely sources of spinal NA, especially the locus coeruleus (LC), also known as the A6 nucleus, which sends both ascending projections from dorsal LC to supraspinal areas, and descending projections from ventral LC to the spinal cord (Westlund et al., 1983; Burnett and Gebhart, 1991; Clark and Proudfit, 1991c, 1991b, 1993; Clark et al., 1991; Li et al., 2016; Hirschberg et al., 2017). Stimulation of ventral LC in rats causes antinociception that depends on spinal NA, while stimulation of dorsal LC is pronociceptive or anxiety-producing (West et al., 1993; Hickey et al., 2014; Hirschberg et al., 2017). Yet the role of LC in systemic opioid antinociception remains an open question, as the literature on this topic is sparse and conflicting (Sasa et al., 1977; Hammond and Proudfit, 1980).

Anatomical studies have identified projections from the PAG to the LC (Bajic and Proudfit, 1999). Surprisingly, the synaptic features of these projections and their relevance to pain modulatory behavior have not been established. Although a rabies tracing study reported

inputs to LC-NA neurons from vlPAG, and a slice electrophysiology study found an excitatory connection from lateral PAG to LC-NA neurons (Schwarz et al., 2015; Kim et al., 2018; Barcomb et al., 2022), *in vivo* electrophysiological recordings reported only weak, sparse input that predominantly *inhibits* LC discharge (Ennis et al., 1991). Furthermore, vlPAG-to-LC neurons were reported to be inhibited by mu opioids (Kim et al., 2018), which conflicts with the notion that vlPAG output can drive descending LC neurons in the context of opioid analgesia. Thus, whether vlPAG contributes to the activation of LC to support opioid antinociception remains entirely unclear.

An additional complexity relates to the potential role of the RVM in influencing pain processing via synaptic communication with the LC. One anatomical study reports projections from both the raphe magnus and paragigantocellular nucleus, both components of the medial RVM, to the LC and pericoerulear region (Clark and Proudfit, 1991a), but the sign and functional significance of this anatomical pathway remains unexplored. There is a strong body of literature demonstrating antinociceptive input to LC from excitatory neurons in the rostral ventro*lateral* medulla (RVLM) (Ennis and Aston-Jones, 1988; Ennis et al., 1992) and more recently, noradrenergic excitatory neurons in the caudal ventrolateral medulla (cVLM) (Gu et al., 2023). Yet, to our knowledge, there is no information regarding the nature and behavioral relevance of medial RVM inputs to the LC.

In this study, we use virally- and genetically-mediated anatomical, electrophysiological, and behavioral methods in mice to establish the circuit elements by which the DPMS recruits the LC to produce opioid antinociception. Our findings reveal the necessity of vlPAG input to the LC for systemic morphine antinociception and uncover an unexpected inhibitory input from the

RVM that impacts nociception. These findings place new emphasis on noradrenergic signaling from the LC in opioid analgesia and reveal a novel antinociceptive pathway within the DPMS.

Results

Spinal NA release from the LC underlies systemic morphine antinociception

Intrathecal pharmacological experiments in rats point to a role for spinal noradrenergic and serotonergic signaling in systemic morphine antinociception (Proudfit and Hammond, 1981). We first set out to confirm that spinal NA contributes to systemic morphine antinociception in mice by administering multiple doses of systemic morphine (5, 12, and 20 mg/kg, *s.c.*) in conjunction with intrathecal injections of the vehicle saline, the alpha-adrenergic antagonist phentolamine (5 μg), or, for comparison, the opioid antagonist naltrexone (5 μg) (**Figure 2.1A**). Systemic morphine with intrathecal saline administration increased hot plate withdrawal latencies in a dose-dependent manner (**Figure 2.1B**). At all morphine doses, intrathecal phentolamine blunted the resulting antinociception, and intrathecal naltrexone reduced it to an even greater degree (**Figure 2.1B-C**). These results indicate that spinal NA plays a critical role in the expression of systemic morphine antinociception, especially at low doses of morphine. In contrast, spinal opioid signaling, whether via direct spinal actions of morphine or DPMS-driven endogenous opioid release, is required for systemic morphine antinociception at all doses.

Direct spinal administration of morphine produces antinociception (Yaksh and Rudy, 1977). It is therefore possible that morphine acts within the spinal cord to stimulate NA release, either from descending noradrenergic terminals or from unidentified local NA neurons. To determine whether morphine-driven spinal NA signaling originates from a spinal or supraspinal source, we intrathecally administered morphine (2.5 μg) along with saline, phentolamine, or

naltrexone, prior to the hot plate assay (**Figure 2.1D**). Consistent with a supraspinal source of spinal NA, we found that the effect of intrathecal morphine was not blocked by intrathecal phentolamine, whereas intrathecal naltrexone blocked the antinociception (**Figure 2.1E**). In the absence of morphine, these antagonists did not significantly change withdrawal latency (**Figure 2.1F**).

Previous studies have identified several supraspinal noradrenergic structures that project to the dorsal horn of the spinal cord (Westlund et al., 1983; Clark and Proudfit, 1991c, 1991b, 1993; Clark et al., 1991; Li et al., 2016). Whereas the A5 and A7 nuclei contain only a small fraction of dorsal horn-projecting NA neurons, the LC is the primary source of spinal NA (Li et al., 2016). Stimulation of the spinally-projecting ventral subdivision of LC produces spinal NA-dependent antinociception in mice and rats (West et al., 1993; Hickey et al., 2014; Hirschberg et al., 2017). To determine whether systemic morphine increases the activity of LC-NA neurons, we measured expression of the immediate early gene c-Fos in response to subcutaneous morphine (10 mg/kg) or saline treatment in *DBH-cre:tdTom* mice that express the fluorescent protein tdTomato in dopamine beta-hydroxylase (DBH)-positive neurons. Consistent with LC activation, systemic morphine caused a significant increase in c-Fos expression in LC neurons (**Figure 2.2A-B**), which was significantly blocked by systemic opioid receptor antagonist naloxone (10 mg/kg, s.c.) pretreatment. This presents a paradox, as LC neurons express the mu opioid receptor (MOR), which typically inhibits neuronal output in receptor-expressing neurons. A possible explanation is that the c-Fos induction actually results from direct engagement of mitogen-activated protein kinase cascades downstream of MOR activation (Shoda et al., 2001). However, morphine-induced c-Fos expression was unchanged in *DBH-cre::Oprm1*$^{fl/fl}$ mice (Weibel et al., 2013), which lack MOR in NA neurons (**Figure 2.3A-B**). Taken together, these data suggest that

while MOR expression in LC neurons themselves is not responsible for morphine-induced c-Fos expression, opioid receptors present in the circuit upstream from these neurons are responsible for LC c-Fos expression, possibly via disinhibition of LC activity.

In rat brain slices, MOR agonists strongly hyperpolarize LC neurons via activation of G protein-coupled inward rectifier K^+ (GIRK) channels (Williams et al., 1982; Banghart and Sabatini, 2012). Because nearly all prior observations of MOR-mediated dampening of LC neuronal excitability were made in rats, we asked if mouse LC-NA neurons are similarly affected. Using fluorescent *in situ* hybridization, we first confirmed that *Oprm1* and *TH* transcripts, which encode the MOR and tyrosine hydroxylase, respectively, colocalize in the LC of C57Bl6/J mice (**Figure 2.3D-E**). We next investigated the effects of the MOR agonist DAMGO on LC neuronal excitability using whole cell electrophysiological recordings in acute mouse brain slices. Bath applied DAMGO requires minutes to equilibrate in slices, which can obscure subtle effects on membrane properties. We therefore used the photocaged DAMGO derivative CNV-Y-DAMGO (1 μM) to produce time-locked DAMGO concentration jumps in response to millisecond flashes of light(He et al., 2021; Ma et al., 2023). In current clamp recordings, despite the use of a strong optical stimulus, CNV-Y-DAMGO photoactivation generated only small hyperpolarizations that were accompanied by brief pauses in spontaneous firing and minor subsequent reductions in firing rate (**Figure 2.2C**). In voltage clamp recordings, DAMGO photorelease evoked small outward currents (**Figure 2.2C)**. Consistent with these modest effects, bath application of DAMGO produced no change in evoked action potential firing (**Figure 2.2D).** These small effects stand in stark contrast to the several-hundred pA currents and deep hyperpolarizations evoked by MOR agonists in rat LC, and are consistent with the smaller GIRK currents previously observed in mice on a different genetic background

(Torrecilla et al., 2002). These results suggest that direct MOR-mediated inhibition of LC firing may be insufficient to counteract synaptic drive of LC neurons by upstream circuits in mice. Consistent with this notion, genetic removal of MORs from LC-NA neurons did not alter systemic morphine antinociception on the hot plate (**Figure 2.3C**).

To determine if the LC contributes to morphine antinociception, we employed two loss-of-function approaches. First, we specifically ablated LC-NA neurons via bilateral injection of cre-dependent Caspase 3 (Casp3) into the LC of either *DBH-cre:tdTom* mice or control *tdTom* littermates. Transduction with Casp3 led to near-complete ablation of LC-NA neurons (**Figure 2.2E**). In addition to assessing thermal nociception, we used a pin prick assay to measure mechanical nociception. Somewhat surprisingly, LC ablation had no effect on baseline nocifensive responses in the absence of morphine. However, in comparison to control mice, the morphine-induced increase in hot plate withdrawal latency was strongly attenuated in *DBH-cre:tdTom* mice at both doses of morphine (5 and 10 mg/kg). In addition, the morphine-induced decrease in pin prick response was significantly attenuated at 5 mg/kg morphine and trended toward significance at 10 mg/kg (**Figure 2.2F**).

Casp3-mediated cell ablation is a severe manipulation that may lead to neuroinflammation and/or a loss of structural integrity. We therefore sought to suppress LC activity by overexpressing Kir2.1, a constitutively active inwardly-rectifying K^+ channel, which hyperpolarizes neurons and decreases their excitability. We first analyzed the effect of Kir2.1 overexpression on LC neuronal excitability using brain slice electrophysiology 3 weeks after unilateral LC injection of AAV-DIO-Kir2.1-zsGreen in *DBH-cre* mice. Kir2.1 overexpression decreased resting membrane potential and abolished tonic action potential firing compared to anatomically-identified LC neurons in the uninjected hemisphere (**Figure 2.2G-H**). We also

observed a decrease in evoked action potential firing in response to injection of 50 and 100 pA current steps (**Figure 2.2I**). Taken together, Kir2.1 overexpression effectively decreases both tonic and evoked action potential firing in LC neurons.

For behavioral testing, we injected *DBH-cre:tdTom* or *tdTom* mice bilaterally in the LC with AAV-DIO-Kir2.1-zsGreen. Histological analysis revealed high transduction of LC neurons in cre-expressing mice and negligible expression in cre-negative littermates (**Figure 2.2J**). Kir2.1 overexpression suppressed morphine antinociception on both the hot plate and pin prick assays at both doses of morphine (**Figure 2.2K**). Notably, neither Casp3 nor Kir2.1 produced a difference in locomotion or basal anxiety in the elevated plus maze (**Figure 2.4A-B**). Overall, these results support a critical role for the LC in systemic morphine antinociception.

vlPAG gates LC-mediated morphine antinociception

While LC is crucial for systemic morphine antinociception, it remains unclear how LC activity is recruited by upstream structures in response to opioid drugs. Classic models of opioid antinociception involve the disinhibition of vlPAG output neurons via activation of MORs expressed on inhibitory terminals and/or local GABA neurons within the vlPAG (Basbaum and Fields, 1984; Lau and Vaughan, 2014). Consistent with this, the antinociception produced by local morphine infusion into rat PAG partially depends on spinal NA (Yaksh, 1979). Furthermore, several PAG subregions, including the vlPAG, send excitatory projections to the LC and pericoerulear region (Bajic and Proudfit, 1999; Schwarz et al., 2015; Kim et al., 2018; Barcomb et al., 2022). Although optogenetic and chemogenetic activation of vlPAG glutamatergic neurons produces antinociception in mice (Tovote et al., 2016; Samineni et al.,

2017), whether this is mediated by the LC, and whether vlPAG glutamatergic neurons support morphine antinociception, is not known.

If vlPAG is an important upstream mediator of morphine antinociception, we reasoned that inhibiting vlPAG output should attenuate the antinociception produced by 5 mg/kg morphine, which we found to rely heavily on the LC. To probe the role of vlPAG in morphine antinociception, we bilaterally expressed the inhibitory DREADD HM4D (Roth, 2016) in vlPAG$^{VGLUT2\text{-}cre}$ neurons and inhibited their output with systemic CNO (3 mg/kg, i.p.) in the absence and presence of morphine (5 mg/kg, *s.c.*) (**Figure 2.5A**). In untransduced control mice, CNO had no effect on morphine antinociception. In contrast, CNO completely prevented morphine antinociception in HM4D-expressing mice (**Figure 2.5B**).

To determine if spinal NA signaling mediates vlPAG-driven antinociception, we bilaterally activated vlPAG$^{VGLUT2\text{-}cre}$ neurons with the excitatory DREADD HM3D in conjunction with intrathecal NA antagonism (**Figure 2.5C**). Consistent with prior work (Samineni et al., 2017), systemic CNO (3 mg/kg, i.p.) increased hot plate withdrawal latencies and von Frey mechanical thresholds. Strikingly, this effect was either completely or partially abolished on the thermal and mechanical assays, respectively, by intrathecal administration of either phentolamine or naltrexone (**Figure 2.5D**). However, we also observed that chemogenetic activation of vlPAG$^{VGLUT2\text{-}cre}$ neurons produced a state of active quiescence, in which mice exhibited a marked reduction in voluntary locomotion, distinct from freezing behavior (**Figure 2.6A**). This raises a concern that the apparent antinociception is simply a consequence of general locomotor suppression. However, the active quiescence persisted after intrathecal phentolamine and naltrexone administration, despite significant attenuation of the antinociception. Therefore, DPMS-driven descending antinociception and locomotor suppression are dissociable. Consistent

with vlPAG driving the LC to produce spinal NA-dependent antinociception, we also found that chemogenetic activation of vlPAG$^{VGLUT2\text{-}cre}$ neurons increased c-Fos expression in TH-positive LC neurons (**Figure 2.5E**), yet CNO had no effect in the LC of untransduced wildtype mice (**Figure 2.6B**). Together, these results demonstrate that, like systemic morphine, vlPAG-driven antinociception requires spinal NA signaling. They also establish a role for spinal endogenous opioid signaling in vlPAG-driven antinociception, a point debated in previous literature (Aimone et al., 1987; Morgan et al., 1991).

Anatomy of DPMS input to the LC

To uncover the circuit elements by which the DPMS may recruit the LC, we first mapped projections from the vlPAG and RVM to the LC by virally expressing tdTomato in neurochemically-defined cell types. To label glutamatergic neurons, we used *VGLUT2-cre* mice, as VGLUT2 is the primary vesicular glutamate transporter isoform in both structures. To label inhibitory axons, we used *VGAT-cre* mice, which express cre in both GABAergic and glycinergic neurons (Chaudhry et al., 1998).

After unilateral injection of AAV-DIO-tdTom into the vlPAG of either *VGLUT2-cre* or *VGAT-cre* mice, we observed sparse fibers in the LC somatic region and strong labeling in the surrounding pericoerulear region, including a medial zone corresponding to Barrington's nucleus(Paxinos and Franklin, 2001; Hou et al., 2016) and a dorsolateral zone near the 4th ventricle (**Figure 2.7A-E**). Quantification of pixel intensity of green TH+ LC neurons and red fibers supports dense vlPAG projections just medial to the LC (**Figure 2.7F-G)**. Consistent with axo-dendritic inputs to LC-NA neurons occurring within the pericoerulear region and evidence of pericoerulear interneurons that modulate LC activity(Aston-Jones et al., 1991, 2004; Kuo et al.,

2020), these results establish anatomical substrates by which vlPAG could bidirectionally control LC activity.

As expected, tdTom expression in vlPAG$^{VGLUT2\text{-}cre}$ neurons also labeled axons in the RVM (**Figure 2.8A**). We also observed prominent fluorescent axons in the RVM upon tdTom expression in vlPAG$^{VGAT\text{-}cre}$ neurons. The existence of inhibitory vlPAG-to-RVM projections has been established in rats but refuted in mice (**Figure 2.8B**) (Reichling and Basbaum, 1990; Morgan et al., 2008; Park et al., 2010; Bagley and Ingram, 2020). We verified this inhibitory projection using a retro-FISH approach involving retrobead injection into RVM prior to retrobead-labeled vlPAG cell type identification using fluorescence *in situ* hybridization (**Figure 2.8C**). This analysis revealed that although the vast majority of vlPAG-to-RVM projection neurons contain transcripts encoding glutamatergic (but not GABAergic) markers, ~15% contain only GABAergic markers (**Figure 2.8D**). These results establish that vlPAG sends inhibitory projections to the RVM in mice.

A previous study in mice suggested the presence of two distinct, non-overlapping populations of vlPAG neurons that project to the LC and RVM (Kim et al., 2018). We wondered if vlPAG-to-LC neurons send branches to other brain areas. To address this question, we fluorescently labeled vlPAG neurons that project to the LC using the retrograde virus AAVretro-cre in wild-type mice (**Figure 2.7H**). Consistent with our previous results, we observed mCherry-positive fibers in the medial pericoerulear region. However, we also observed prominent axon fibers in the RVM, with no other apparent midbrain and brainstem targets. To confirm this result, we labeled vlPAG-to-RVM neurons using the same approach and again observed fluorescent axons in the medial pericoerulear region (**Figure 2.7I**). We verified these findings using a dual-color double-retrograde approach by injecting AAVretro-cre into the RVM,

AAVretro-FlpO into the LC, and a mixture of cre- and flp-dependent mCherry and YFP reporter viruses in vlPAG. Importantly, the reporter virus titers were optimized to eliminate recombinase-independent expression and recombinase cross-talk. We observed mCherry and YFP co-expression in 31% of fluorescently labeled neurons (**Figure 2.7J)**, which is likely an underestimate due to incomplete viral uptake. Taken together, these experiments establish that a large number of vlPAG output neurons send bifurcating axons to both the LC and RVM. Importantly, these results imply that vlPAG recruits the LC and RVM in an inseparable, parallel manner.

We next asked if we could detect projections from the RVM to the LC, which were reported a single prior study (Clark and Proudfit, 1991a). Upon injecting AAV-DIO-TdTom into the RVM of *VGLUT2-cre* or *VGAT-cre* mice, red fluorescent fibers were found in the LC and pericoerulear region in innervation patterns distinct from vlPAG axons (**Figure 2.7K-O**). Notably, pixel intensity analysis revealed that $RVM^{VGLUT2\text{-}cre}$ axons were sparse within the LC somatic region and in the medial pericoerulear region, did not innervate Barrington's nucleus, and innervated a region just lateral to LC. In contrast, $RVM^{VGAT\text{-}cre}$ axons appeared to strongly innervate the LC somatic region and symmetrically spill over only slightly into the medial and lateral pericoerulear regions (**Figure 2.7P-Q**). Additionally, analysis of fibers from all four projection origin- and cell type combinations along the dorsal-ventral axis within the LC somatic region suggested that vlPAG largely targets dorsal LC whereas RVM targets ventral LC (**Figure 2.7R**)**.**

To determine if RVM-to-LC neurons send branching axons to other structures, we injected AAVretro-cre in LC and AAV-DIO-tdTom in RVM (**Figure 2.7S**). We observed fluorescent fibers in several brain regions other than the LC. Most prominent was a dense

projection to the parafascicular nucleus of the thalamus, which also receives input from LC (Vogt et al., 2008) (**Figure 2.7T-V**). Notably, we did not find fluorescent axons in the spinal cord dorsal horn, indicating that RVM-LC projection neurons belong to a population distinct from the spinally-projecting RVM neurons that directly modulate incoming noxious sensory information. Taken together, these results suggest that the LC receives neurochemically-diverse synaptic inputs from multiple hindbrain nodes within the DPMS.

Synaptic properties of vlPAG and RVM input to the LC

To gain insight into the functional significance of these pathways, we optogenetically stimulated vlPAG or RVM axons in LC during acute brain slice electrophysiological recording from LC-NA neurons. To achieve high expression of channelrhodopsin (ChR2) in all projection cell types, we injected wild-type mice in either the vlPAG or RVM with a combination of AAVDJ-Ef1a-mCherry-IRES-cre and AAVDJ-Ef1a-DIO-ChR2-mCherry. After 3-4 weeks of expression, we prepared coronal slices and obtained whole-cell recordings from morphologically-identified LC neurons. We targeted cells that were located in the ventral half of LC in order to bias our recordings towards the spinally-projecting population (Li et al., 2016) and confirmed that each recorded neuron exhibited spontaneous tonic firing at ~1.5 Hz.

We first determined the net effect of optogenetic axon stimulation on LC neuron firing using a 2-second blue light stimulus (25 Hz). Upon activating vlPAG inputs, we observed a firing rate increase in 80% of recorded neurons, whereas 20% showed no significant change. Across the population, this resulted in an overall increase in firing rate during the stimulus (**Figure 2.9A-B**). In contrast, upon activating RVM inputs to LC, we observed a firing rate increase in in

only 10% of the recorded neurons, and a decrease in 60%, whereas 30% were not modulated. Across the population, this resulted in an overall decrease in firing rate (**Figure 2.9C,D**).

To gain insight into the synapses driving these changes in action potential firing, we measured optically-evoked postsynaptic currents in voltage clamp recordings. To electrically isolate excitatory and inhibitory postsynaptic currents (oEPSCs and oIPSCs), we applied light while holding neurons at both -70 mV and 0 mV, respectively. Upon stimulating vlPAG axons (1 x 5 ms pulse), we detected oEPSCs in 30/36 neurons. Seven of these 30 neurons also responded with oIPSCs, but we did not observe any neurons displaying oIPSCs only. The relative oEPSC and oIPSC peak amplitudes are consistent with the overall excitatory drive from vlPAG observed in current clamp (**Figure 2.9E**). On the other hand, upon stimulating RVM axons, we found oEPSCs in 32/72 neurons and oIPSCs in 62/72 neurons, while 30/72 LC neurons exhibited both. The relative oEPSC and oIPSC peak amplitudes are consistent with the overall net inhibition of LC firing by the RVM (**Figure 2.9F**).

We next used pharmacology to dissect the underlying synaptic receptors, assess the presence of mono- and/or poly-synaptic connections, and evaluate the mu opioid-sensitivity of each pathway. Consistent with a glutamatergic, monosynaptic excitatory connection, vlPAG-driven oEPSCs were blocked by the AMPA receptor antagonist NBQX (10 μM) and were completely abolished by the voltage-gated sodium channel blocker TTX (1 μM), but could subsequently be rescued by application of the voltage-gated potassium channel antagonist 4-aminopyridine (4-AP; 100 μM) (**Figure 2.9G-H**). Indicative of a mixed GABAergic and glycinergic projection, RVM-driven oIPSCs were partially blocked by the GABA-A receptor antagonist GABAzine (20 μM), and fully blocked by subsequent addition of the glycine receptor antagonist strychnine (10 μM) (**Figure 2.9I**). Demonstrating the presence of a monosynaptic

inhibitory connection, the oIPSCs were abolished and restored by TTX and 4-AP, respectively (**Figure 2.9J**). However, bath application of NBQX and the NMDA antagonist CPP (10 μM each) significantly decreased the oIPSC amplitude, suggesting an additional feed-forward, polysynaptic inhibitory component (**Figure 2.9K**).

Finally, we assayed the opioid sensitivity of vlPAG-driven oEPSCs and RVM-driven oIPSCs by bath applying DAMGO (1 μM) (**Figure 2.9L**). Whereas vlPAG-driven oEPSCs were only slightly suppressed, RVM-driven oIPSCs were strongly attenuated. This suggests that in the presence of opioids, vlPAG excitatory drive to the LC remains largely intact, whereas suppression of inhibitory synaptic transmission from the RVM is poised to disinhibit LC neurons.

vlPAG and RVM inputs to LC modulate nociception

We next aimed to determine the contributions of these synaptic pathways to nociception and systemic morphine antinociception. Due to the prominence of branching axons, we used a chemogenetic loss-of-function strategy that restricts inhibition to synaptic terminals in target structures via CNO infusion through implanted cannulas (Stachniak et al., 2014). We first investigated the contribution of vlPAG output to the LC. After bilateral injection of AAV-DIO-HM4D-mCherry into the vlPAG of *VGLUT2-cre* mice and 3 weeks of expression, we implanted injected mice and control uninjected wildtype mice with cannulas bilaterally over the LC. Following recovery, mice were tested on the hot plate after bilateral infusion of either saline or CNO (3 μM), both in an opioid-naïve state and after injection of morphine (5 mg/kg, *s.c.*). In wildtype mice, intra-LC infusion of CNO had no effect either in the absence or presence of morphine (**Figure 2.10A**). In vlPAG$^{VGLUT2\text{-}cre}$::HM4D mice, although intra-LC infusion of CNO

did not alter baseline nociception, it produced a large, partial reduction in systemic morphine antinociception (**Figure 2.10B**). These results indicate that vlPAG glutamatergic output to LC is crucial for systemic morphine antinociception but may work in tandem with other descending structures (*e.g.*, the RVM) to achieve the full morphine effect.

We next sought to determine if RVM-to-LC inhibitory projections shape nociception. We first challenged RVM$^{VGAT\text{-}cre}$::HM4D mice with systemic CNO to determine the effect of inhibiting all RVM inhibitory neurons. This global inhibition had no effect on baseline nociception or morphine (5 mg/kg) antinociception on the hot plate (**Figure 2.11**). In contrast, suppression of RVM inhibitory output to the LC via local CNO infusion increased hot plate withdrawal latencies, which is consistent with disinhibition of descending LC-NA neurons (**Figure 2.10C**). Confirming this hypothesis, intrathecal phentolamine completely blocked the resulting antinociception. Chemogenetic suppression of this pathway had no effect on morphine antinociception, which is consistent with occlusion of MOR-mediated synaptic suppression by HM4D activation (and vice-versa). Taken together, these pathway-specific manipulations are consistent with direct excitation of LC by vlPAG glutamatergic neurons and tonic inhibition by RVM inhibitory neurons that leads to opioid-driven disinhibition in the presence of opioids to shape nociceptive behavior (**Figure 2.10D**).

Discussion

In this study, we establish a critical and previously underappreciated role for LC activity in systemic morphine antinociception and delineate the synaptic mechanisms by which vlPAG and RVM activate the LC in response to supraspinal opioid signaling. Although the LC is

frequently included in DPMS circuit models, prior lesion studies aimed at identifying the sources of spinal NA concluded that the LC makes only a minor contribution, which led to a focus on the A7 nucleus (Hammond and Proudfit, 1980; Miller and Proudfit, 1990; Yeomans et al., 1992; Holden et al., 1999; Nuseir and Proudfit, 2000). In contrast, our results establish a central role for the LC in morphine antinociception in mice. We find that systemic morphine induces c-Fos in LC NA neurons, consistent with neuronal activation, although other morphine-responsive receptors, such as Gs-coupled Mas-related G protein-coupled receptors (MRGs) (Hu et al., 2019; Yaksh et al., 2019; Hami et al., 2021) could be involved. However, this effect was also significantly blocked by systemic opioid antagonism, pointing to a role for upstream opioid receptors in vlPAG interneurons and/or the inhibitory RVM inputs described in this study. Importantly, our loss-of-function manipulations indicate a major contribution of the LC to systemic morphine antinociception. The apparent discrepancy between our findings and previous work might be attributed to differences in the anatomy and/or neurochemistry of the DPMS in rats and mice. Indeed, in our hands, mouse LC neurons exhibited a comparatively small opioid response, whereas the rat LC is profoundly inhibited by opioids (Williams et al., 1982; Banghart and Sabatini, 2012). In either case, because transgenic mice are widely used in contemporary pain research, understanding their descending pain modulatory circuitry is of great importance.

The vlPAG has been long appreciated to contribute to morphine antinociception due to the initial finding that local vlPAG opioid administration produces potent antinociception. However, its role has not been unequivocally established, as lesion studies in rats arrive at different conclusions (Yeung et al., 1975; Dostrovsky and Deakin, 1977), perhaps due to differences in lesion protocol and the limited precision of this method. Using cell type-specific chemogenetic loss-of-function, our work demonstrates that glutamatergic output from the vlPAG

is critical for morphine antinociception. This is consistent with classic models of opioid-mediated disinhibition of vlPAG neurons that project to the RVM, which we found to send prominent axon collaterals to the LC. This surprising finding suggests that activation of antinociceptive projections neurons in the vlPAG recruits the LC and RVM in parallel. This model is further bolstered by the relatively low mu opioid-sensitivity of vlPAG excitatory synaptic transmission onto LC neurons, such that disinhibited vlPAG output should faithfully drive LC activity in the presence of systemic MOR agonists.

Our results also reveal several distinctions between the role of NA in spinal and supraspinal opioid antinociception. At low doses of morphine (*e.g.*, 5 mg/kg), the antinociception is mediated primarily by supraspinal opioid receptors, as evidenced by nearly complete loss of systemic morphine antinociception upon chemogenetic vlPAG silencing and loss of descending NA. In contrast, higher morphine doses (>10 mg/kg) may directly engage spinal opioid receptors, as intrathecal phentolamine only partially blocks this antinociception. These results are consistent with a proposed multiplicative effect of supraspinal and spinal opioids at lower morphine doses, whereas the effect of either site can mediate antinociception at higher doses (Yaksh and Rudy, 1977; Yeung and Rudy, 1980b, 1980a). Yet, within the spinal cord, NA-opioid interactions are likely critical. In our data, both vlPAG$^{VGLUT2\text{-}Cre}$::HM3D and low-dose systemic morphine antinociception were completely blocked by phentolamine *or* naltrexone. Since both involve the vlPAG, one possibility is that spinal endogenous opioids are recruited via the RVM. Alternatively, because the antinociception produced by intrathecal NA is blocked by intrathecal opioid antagonists (Yang et al., 1994), NA may drive endogenous opioid release in the spinal cord. However, neither spinal NA nor spinal opioids alone are sufficient to support the vlPAG-driven antinociception. Intrathecal naltrexone blocked systemic morphine antinociception at all

doses tested, consistent with spinal opioid signaling being a critical end-point. Because intrathecal morphine antinociception does not require spinal NA signaling, we posit that spinal opioid receptors gate spinal NA-mediated antinociception.

Our results indicate a major role for the LC, as well as the glutamatergic vlPAG projections to it, in systemic morphine antinociception. However, upon inhibition of either, abrogation of antinociception was incomplete. This suggests that other parallel descending pathways also contribute to systemic morphine effects. A likely possibility is that vlPAG projections to RVM contribute to morphine antinociception in a parallel and additive fashion, taking advantage of vlPAG bifurcations to both structures. Alternatively, A5 and A7 are other sources of descending NA that may be involved in morphine antinociception. A large body of literature supports an antinociceptive function for A7 that depends on spinal NA signaling. More recently, A5 has been proposed to mediate diffuse noxious inhibitory control of pain downstream of the LC (Kucharczyk et al., 2022, 2023). Both of these regions also receive anatomical inputs from both vlPAG and RVM (Clark and Proudfit, 1991a; Bajic and Proudfit, 1999). Future experiments are required to assess the contributions of these pathways to systemic opioid antinociception.

Finally, our discovery of a largely inhibitory drive from RVM to LC was unexpected. While chemogenetic inhibition of these RVM outputs specifically to LC caused spinal NA-dependent antinociception, presumably via disinhibition of LC, inhibiting all RVM inhibitory neurons had no effect on either opioid-naïve nociception or morphine antinociception (**Figure S5**). This may be due to interactions between pro- and antinociceptive RVM projections to the spinal cord (François et al., 2017; Ganley et al., 2023a). Interestingly, LC-projecting RVM neurons do not appear to project to the spinal cord and instead send ascending projections to the

thalamus. It is not currently clear how LC-projecting RVM neurons might fit into the canonical On- and Off-cell framework. Additionally, how these LC-projecting RVM neurons become activated remains to be determined.

Overall, this work establishes the LC as a central source of spinal NA that generates systemic morphine antinociception and identifies excitatory input from vlPAG neurons as the critical synapse that drives LC in this context. In addition, it establishes a new synaptic pathway between the medial RVM and LC that can produce acute antinociception via disinhibition of LC-NA neurons, leading to spinal NA release. Although this study utilized an exogenous opioid drug, the circuit elements uncovered are likely involved in other forms of top-down descending pain modulation that rely on endogenous opioids, such as placebo- and stress-induced analgesia.

Materials and Methods

Animals

All procedures were performed in accordance with protocols approved by the University of California San Diego Institutional Animal Care and Use Committee (UCSD IACUC protocol S16171) and guidelines from the US National Institutes of Health Guide for Care and Use of Laboratory Animals. Mice were group housed, maintained on a 12-hour reversed light/dark cycle, and allowed *ad libitum* access to food and water. Experiments were performed under red lighting during the dark period. Strains used include the following: C57Bl/6J (Jackson Laboratory stock #664), *DBH*-cre (MMRRC/GENSAT #032081-UCD, Tg(DBH-cre)HK212Gsat/Mmucd), *VGLUT2*-IRES-cre (Jackson Laboratory stock #028863, B6J.129S6(FVB)-Slc17a6$^{tm2(cre)Lowl}$/MwarJ), and *VGAT*-IRES-cre (Jackson Laboratory stock #028862, B6J.129S6(FVB)-Slc32a1$^{tm2(cre)Lowl}$/MwarJ). Ai14 tdTomato (Jackson Laboratory stock #7914, B6.Cg-Gt(ROSA)$^{26Sortm14(CAG-tdTomato)Hze}$/J) and Oprm1$^{fl/fl}$ (Jackson Laboratory stock #30074, B6;129-Oprm1$^{tm1.1Cgrf}$/KffJ) mice were also obtained from Jackson Labs, but bred in-house to *DBH*-cre mice. Mice were used for experiments between the ages of 8-20 weeks. Both male and female mice were used for all experiments.

Drugs

The following drugs were purchased from HelloBio: CNO (HB1807), NBQX disodium salt (HB0443), Tetrodotoxin citrate (HB1035), GABAzine (SR 95531 hydrobromide; HB0901), and (R)-CPP (HB0021). Naltrexone hydrochloride (N3136), naloxone hydrochloride (N7758), 4-aminopyridine (A78403) and strychnine hydrochloride (S8753) were purchased from Sigma-Aldrich. Morphine sulfate was purchased from Spectrum Chemicals (M1167). Phentolamine

hydrochloride was purchased from Abcam (ab120791). DAMGO was purchased from R&D Systems, Inc. (1171). CNV-Y-DAMGO was prepared in house, as previously reported (Ma et al., 2023). Drugs to be injected or intracranially infused were dissolved in 0.9% saline and sterile filtered before use.

Viral constructs

The following viruses were purchased from Addgene: AAV8-hsyn-DIO-HM4Di-mCherry, (Addgene 44362, titer $2.3x10^{13}$), AAV8-hsyn-DIO-HM3Dq-mCherry (Addgene 44361, titer $2.1x10^{13}$), AAVretro-hsyn-cre (Addgene 105553, titer $2.1x10^{13}$), AAVretro-Ef1a-FlpO (Addgene 55637, titer $1.3x10^{13}$). The following were made and titered in-house using Addgene plasmids: AAVDJ-hsyn-DIO-mCherry (Addgene 50459, titer $3.5x10^{12}$), AAVDJ-ef1a-fDIO-EYFP (Addgene 55641, titer $2x10^{11}$), AAVDJ-Ef1a-mCherry-IRES-cre (Addgene 55632, titer $4.3x10^{12}$), AAVDJ-ef1a-DIO-ChR2(H134R)-mCherry (Addgene 20297, titer $2.55x10^{13}$). AAV1-FLEX-ef1a-taCasp3-TEVP (titer $2.1x10^{12}$) and AAV1-CAG-FLEX-tdTomato (titer $7.6x10^{12}$) were both purchased from the UNC Vector Core. We received AAVDJ-CAG-DIO-Kir2.1-P2A-zsGreen as a gift from the laboratory of Dr. Byungkook Lim.

Intrathecal injections

Intrathecal injections were performed according to the protocol detailed by Hylden and Wilcox (Hylden and Wilcox, 1980). Acute percutaneous intrathecal injections were executed using a 30G 1-inch needle attached to a 10 ul Hamilton syringe via polyethylene tubing. Mice were lightly anesthetized with 2% isoflurane, the fur over their lumbar spine was removed with electric clippers, and the skin disinfected with alternating povidone-iodine solution and isopropyl

alcohol. While firmly holding the pelvic girdle, the needle was inserted into the skin over the lumbar spine at a 20-degree angle. The needle was guided between the vertebrae until it entered the spinal column, which was signified by a tail flick. Each intrathecal injection was given at a volume of 5 μl. Mice were given at least 10-15 minutes to recover from the intrathecal injection before behavioral testing.

Behavior assays

Thermal nociceptive behavior

Mice were habituated to a hot plate (Thermo Fisher Scientific #SP88857100) at room temperature in a clear plastic cylinder for at least 20 minutes. During testing, mice were placed on the hot plate at 52°C and observed for a nocifensive response (hind paw withdrawal, shaking, licking, or jumping). Mice were immediately removed from the hot plate at the first sign of a nocifensive response, and the time to paw withdrawal was recorded. Each trial was terminated after a maximum of 60 seconds, even if no withdrawal occurred, to avoid tissue damage. Mice were tested twice on the hot plate during each session with a 3-5-minute intertrial interval.

Mechanical nociceptive behavior

Mice were tested for mechanical thresholds using either the von Frey or pin prick assay. In both cases, mice were placed in a clear cylinder on an elevated wire grid and allowed to habituate for 20 minutes. Using the up-down method (Chaplan et al., 1994), von Frey filaments (Ugo Basile) of varying stiffnesses were applied to each hindpaw separately, with a 3-minute break until returning to the first paw, until a withdrawal response could be recorded and a 50% withdrawal threshold could be calculated. The resulting threshold values (in grams) for each paw

were averaged together to calculate the mechanical threshold for each mouse. During the pin prick assay, a fine insect pin (size 000, ThermoFisher Scientific NC9295307) was applied to the plantar surface of each hind paw 5 times at 5-minute intervals for a total of 10 trials. Response to pin was calculated as the number out of 10 trials in which the mouse displayed nocifensive withdrawal behavior.

Elevated plus maze and open field

Mice were placed on an elevated plus maze with two open and two closed arms (52 cm diameter) and video recorded (Logitech) for a 20-minute period. The SMARTv3.0 video tracking software (Panlab) was used to measure the percent of time spent in the open vs. closed arms of the apparatus. Additionally, the distance traveled during the 20-minute testing period was reported. Similarly, locomotion in the open field was tested by placing mice in a square arena (18 cm x 18 cm) for a 20-minute testing period and the SMARTv3.0 software was used to track mouse trajectory and calculate distance traveled.

Surgeries

Before surgery, mice were deeply anesthetized by induction at 5% isoflurane, after which anesthesia was maintained by 2% isoflurane (SomnoSuite, Kent Scientific). After mice were placed in a stereotaxic frame (David Kopf Instruments), a midline incision was made through the scalp following fur removal and site preparation by alternating povidone-iodine and 70% isopropyl alcohol. 100-250 nl of virus was injected at a rate of 100 nl/min at defined stereotaxic coordinates. The stereotaxic coordinates used for viral injections are as follows: vlPAG, angle ±10°, AP -4.60 mm, ML ± 0.32 mm, DV 2.85 mm; RVM, angle 10°, AP -7.00 mm, ML +0.26

mm and -0.67 mm, DV 6.30 mm and 6.26 mm; LC, angle ±10°, AP -5.45, ML ±0.75 mm, DV 4.10 mm. For bilateral LC cannula implants, the following coordinates were used: angle ±15°, AP -5.45 mm, ML ±0.9 mm, DV 3.80 mm. Guide cannulas were 26G, included a 5 mm pedestal, and were cut 5 mm below the pedestal. Internal cannulas were 33G and included 1 mm projection from the end of the guide cannula (Plastics One/Protech International, Inc.). Cannulas were secured to the surface of the skull using light-cured dental epoxy and anchored by one screw. For all surgeries, mice were administered 5 mg/kg ketoprofen (MWI Veterinary Supply) before the end of surgery and 24 hours later and monitored for recovery for 5 days.

Brain slice preparation

Mice were anesthetized with isoflurane before rapid decapitation. Brains were removed, blocked, and mounted in a VT1000s vibratome (Leica Instruments). Coronal midbrain slices (190 μm) containing the LC were prepared in ice-cold choline-based artificial cerebrospinal fluid containing 25 mM $NaHCO_3$, 1.25 mM NaH_2PO_4, 2.5 mM KCl, 7 mM $MgCl_2$, 25 mM glucose, 0.5 mM $CaCl_2$, 110 mM choline chloride, 11.6 mM ascorbic acid, and 3.1 mM pyruvic acid, equilibrated with 95% O_2/5% CO_2. Slice were transferred to 32°C oxygenated artificial cerebrospinal fluid (ACSF) containing 125mM NaCl, 2.5 mM KCl, 25 mM $NaHCO_3$, 1.25 mM NaH_2PO_4, 2 mM $CaCl_2$, 1 mM $MgCl_2$, and 10 mM glucose, osmolarity 290. Slices were incubated for 20 minutes, then brought to room temperature before recording.

Slice Electrophysiology

Slice physiology experiments were performed in a chamber continuously perfused with warmed (32°C) ACSF equilibrated with 95% O_2/5% CO_2. Recording pipettes were pulled from

borosilicate glass on a P-1000 Flaming/Brown micropipette puller (Sutter Instruments) to a resistance of 1-3.5 MΩ. Recordings were made with an Axopatch 700B amplifier (Axon Instruments) and data sampled at 10 kHz, filtered at 3 kHz, and acquired using National Instruments acquisition boards and a custom version of ScanImage written in MATLAB (MathWorks). LC neurons were visually identified and confirmed to exhibit tonic action potential spiking of ~1.5 Hz. Recordings were biased toward the ventral portion of LC on each coronal slice. Recordings of action potential spiking were made in current clamp with patch pipettes filled with an internal solution containing 135 mM $KMeSO_3$, 5 mM KCl, 5 mM HEPES, 4 mM MgATP, 0.3 mM NaGTP, 10 mM phosphocreatine, and 1.1 mM EGTA (pH 7.25, 290 mOsm kg^{-1}). Firing rate vs. current input (f-I) curves were constructed using 1-second steps of direct current input (-100, 50, 100, 150, 200, 250, 300 pA) 10 seconds apart. The effect of CNV-Y-DAMGO circulating in the bath on spiking was determined by presenting a single 50 ms flash of UV light (365 nm LED, 84 mW, pE-300ultra, CoolLED) and recording tonic spiking for 20 seconds before and 100 seconds after the flash. Firing rate in the 10 seconds before and after the flash, latency to spike after the flash as a measure of the pause in action potential firing, and the change in membrane potential after the flash were measured. For the effect of optogenetically-mediated excitation of inputs to LC on tonic spiking, 50x2 ms pulses of blue light (470 nm, 18 mW, pE-300ultra LED) at 25 Hz for a total of 2 seconds were delivered. The firing rate in the 2 seconds before and 2 seconds during blue light stimulation were used to compare light-evoked excitation or inhibition.

Recordings of evoked postsynaptic currents were made in voltage clamp with patch pipettes filled with an internal solution containing 135 mM $CsMeSO_3$, 3.3 mM QX314 Cl^- salt, 10 mM HEPES, 4 mM MgATP, 0.3 mM NaGTP, 8 mM phosphocreatine, and 1 mM EGTA (pH

7.2-7.3, 295 mOsm kg^{-1}). Cells were rejected if holding currents became more negative than -200pA or if series resistance exceeded 25 MΩ. Recordings of opioid-evoked currents were recorded in the presence of NBQX (10 μM), CPP (10 μM), GABAzine (20 μM), and strychnine (10 μM) to eliminate synaptic currents. As in current clamp, CNV-Y-DAMGO was photoactivated by a single 50 ms flash of UV light. While recording optogenetically-evoked EPSCs and IPSCs in LC neurons, ChR2 terminals were stimulated with a single 5 ms flash of blue light. Initial characterization of oEPSCs and oIPSCs was done in the absence of synaptic blockers and each current was isolated by holding the LC neuron at -70 mV or 0 mV, respectively. Further pharmacological verification of evoked currents was performed with AMPA blocker NBQX (10 μM), NMDA blocker CPP (10μM), GABA-A receptor blocker GABAzine (SR 95531, 20μM), glycine receptor blocker strychnine (10 μM), sodium channel blocker TTX (1 μM), and potassium channel blocker 4-aminopyridine (100 μM). Opioid sensitivity of evoked postsynaptic currents was assessed by bath perfusion of mu-opioid receptor agonist DAMGO (1 μM). All electrophysiology data were processed in Igor Pro (Wavemetrics).

Fluorescent *in situ* hybridization (FISH)

FISH was performed either in naïve wild type mice or in mice bilaterally injected in RVM with green retrobeads (Lumafluor, Inc.). Mice were deeply anesthetized and decapitated. Brains were quickly removed and frozen in Tissue-Tek OCT medium (Sakura) on dry ice until completely solid. Brain slices (8 μm) were prepared on a cryostat (Leica CM 1950) and adhered to SuperFrost Plus slides (VWR). Samples were fixed with 4% paraformaldehyde and processed according to instructions in the ACD Bio RNAscope Fluorescent Multiplex Assay (Fluorescent Reagent Kit v2) manual and cover slipped with ProLong antifade media (Molecular Probes).

Images were taken on a Keyence microscope (BZ-X710) using a 60x 1.4 NA oil immersion objective configured for structured illumination microscopy. Puncta counting in FISH images was completed using a custom pipeline designed in CellProfiler.

Histology

For all other mice, brains were fixed using chilled 4% paraformaldehyde in phosphate buffered saline (PBS) by transcardial perfusion and cryoprotected in 30% sucrose in PBS solution. In some cases, spinal cords were also removed and processed in the same fashion. Brain slices (40 μm) were prepared on a freezing microtome (ThermoFisher Scientific Microm HM450). For sections selected for immunohistochemistry, slices were blocked in PBS-Triton (0.3% TritonX-100 in 1x PBS) with 5% donkey or goat serum for 1 hour at room temperature. Incubation in primary antibodies occurred in PBS-Triton plus 1% serum at 4°C for 24-72 hours. Following 3 10-minute wash steps in PBS, the slices were incubated in PBS-Triton plus 1% serum with secondary antibodies for 4 hours at room temperature. After 3 more wash steps, slices were mounted and cover slipped with mounting media containing DAPI (Vector Laboratories, H1200). Primary antibodies (1:500) used include rabbit anti-c-Fos (9F6) (#2250, Cell Signaling Technology), rabbit anti-tyrosine hydroxlase (AB152, EMD Millipore), and mouse anti-tyrosine hydroxylase (T2928, Sigma). Secondary antibodies used include Alexa Fluor 488 Donkey anti-rabbit, Alexa Fluor 555 donkey anti-mouse, Alexa Fluor 488 goat anti-rabbit and Alexa Fluor 555 goat anti-rabbit (1:500, Invitrogen). After mounting, slices were imaged on a Keyence microscope (BZ-X710) at 2x, 10x, or 20x magnification. Cell counts and quantification of fluorescent colocalization were performed using custom pipelines in Cell

Profiler. Pixel intensity analysis was performed in Image J, z-scores calculated in Microsoft Excel, and resulting values graphed in GraphPad Prism.

Statistics

Data in each figure are presented as mean ± SEM and individual data points from experimental replicates are plotted in most cases. Statistical analyses were performed in GraphPad Prism. The test performed, number of experimental replicates, mean ± SEM for each condition, statistics provided by ANOVA and two-way ANOVA tests for each variable, and p-values for the overall test are provided in the figure legend. Individual p-values resulting from post hoc tests to correct for multiple comparisons appear in the figures. Repeated measures within individual replicates were taken into account where applicable based on experimental design. Data were tested for normality using the Shapiro Wilk test, and non-parametric statistics were used when necessary and possible. In certain cases, when multiple conditions included different numbers of experimental replicates, a mixed-effects model was used in place of a two-way ANOVA. Raw data for each graph as well as the results of statistical tests are available in the Source Data spreadsheet.

Acknowledgements

We thank B.K. Lim for providing the Kir2.1 virus, A.E. Layden & J. Chang-Weinberg for genotyping support, and B.K. Lim, S. Han, and W. Campana for helpful discussions.

Funding

This work was supported by the Rita Allen Foundation, the Esther A. & Joseph Klingenstein Fund & Simons Foundation, the Brain & Behavior Research Foundation, and the National Institute on Drug Abuse (R00DA034648 to M.R.B.).

Author Contributions: STL, GL, TLY, and MRB conceived the project and designed the work. STL, JP, and JCY performed experiments and analyzed data. STL, TLY, and MRB wrote and edited the manuscript.

Competing Interests: The authors declare that they have no competing interests.

Data and Materials availability: Correspondence and material requests should be addressed to Dr. Matthew Banghart (mbanghart@ucsd.edu). All data, including complete statistics tables, are available in the supplementary materials Source Data file.

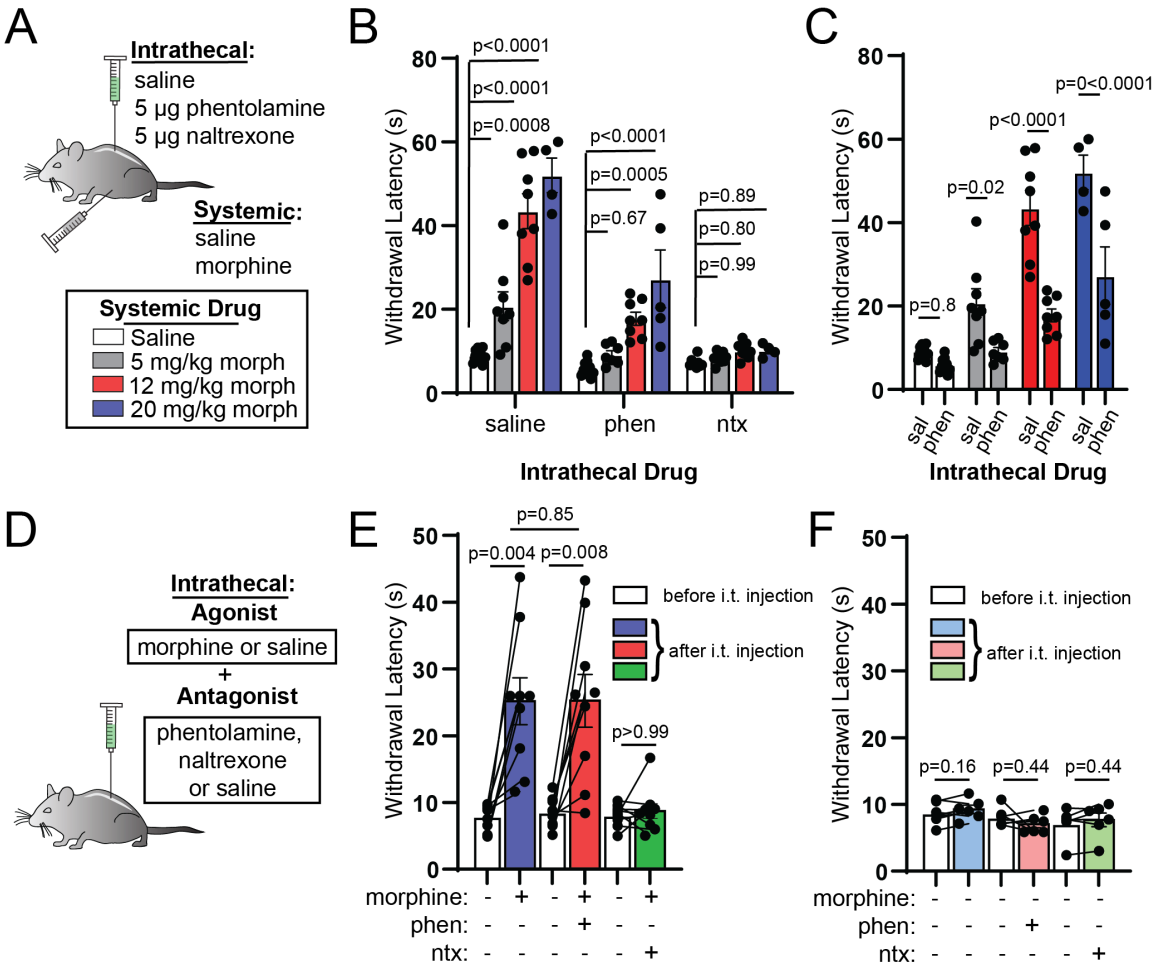

Figure 2.1. Intrathecal noradrenergic and opioidergic antagonists attenuate systemic morphine antinociception.

A. Schematic of intrathecal and systemic injection combinations and morphine doses. **B.** Hot plate (52°C) withdrawal latencies resulting from increasing doses (0, 5, 12, 20 mg/kg) of subcutaneous morphine grouped by intrathecal antagonist administered (saline vs. 5 µg phentolamine vs. 5 µg naltrexone; ordinary two-way ANOVA with post hoc Tukey's multiple comparisons test; intrathecal drug effect, $p<0.0001$, $F(2,81)=95.35$; morphine dose effect, $p<0.0001$, $F(3,81)=56.61$; interaction, $p<0.0001$, $F(6,81)=16.75$). **C.** Same data as in B from intrathecal saline and phentolamine groups organized by systemic morphine dose to facilitate comparisons at each dose (ordinary two-way ANOVA with post hoc Sidak's multiple comparisons test; intrathecal drug effect, $p<0.0001$, $F(1,52)=63.07$; morphine dose effect, $p<0.0001$, $F(3,52)=50.55$; interaction, $p=0.0002$, $F(3,52)=8.037$). **D.** Schematic of intrathecal coadministration of morphine (2.5 µg) or saline with saline, phentolamine (5 µg) or naltrexone (5 µg). **E.** Hot plate withdrawal latencies before (white) and after (blue: saline, red: phentolamine, green: naltrexone) intrathecal injection of morphine and antagonist (pre- vs. post-intrathecal injection, n=9 pairs each, two-sided Wilcoxon matched-pairs signed rank test; post-intrathecal morphine + saline vs. post-intrathecal morphine + phentolamine, n=9 saline, n=9 phentolamine, two-sided Mann-Whitney test). **F.** Hot plate withdrawal latencies before (white) and after (light blue: saline, pink: phentolamine, light green: naltrexone) intrathecal injection of saline and antagonist (pre- vs. post-intrathecal injection, n=6 pairs each, two-sided Wilcoxon matched-pairs signed rank test). All bar graphs depict mean ± SEM and include individual experimental replicate values.

Figure 2.2. LC activity is required for systemic morphine antinociception.

A. Subcutaneous saline, 10 mg/kg morphine, and 10 mg/kg morphine + 10 mg/kg naloxone injections and representative images of resulting c-Fos (green) immunohistochemistry in *DBH-cre::tdTom* mice. Scale bars 150 μm. **B.** Percentage of DBH-positive LC neurons that colocalize with green c-Fos signal (5-8 LC images analyzed per mouse; n=6 saline, n=6 morphine, n=4 morphine + naloxone; saline = 29.9 ± 5.1%, morphine = 71.0 ± 4.5%, morphine + naloxone = 47.9 ± 4.2%; Ordinary One-way ANOVA with post hoc Tukey's multiple comparisons test, $p<0.0001$, $F(2,13) = 20.97$)). **C.** Left: representative traces of CNV-Y-DAMGO light-evoked uncaging (purple arrows: 50 ms, 365 nm LED, 84 mW) during current clamp (top) and voltage clamp (bottom) recordings in whole cell patch clamp from LC neurons in wild type mice. Right: LC neuron opioid response characterized by change in membrane potential after light flash, pause in firing calculated as latency to first spike after light flash, tonic firing rate during the 10 seconds before and 10 seconds after light flash ($p<0.0001$, two-sided Wilcoxon matched-pairs signed rank test), and evoked outward current amplitude (n=16 cells each). **D.** f-I curves recorded from LC neurons in wild type mice before and after bath application of 1 μM DAMGO (n=7 cells; two-sided Wilcoxon matched-pairs signed rank test at 50 pA, 100 pA, 150 pA, and 200 pA). **E.** Injection schematic, representative images and quantification of neuronal ablation of mice after bilateral injection of AAV-DIO-Casp3 in LC (n=11 *DBHcre:TdTom*, n=15 *TdTom* control; *DBH-cre* = 79 ± 15 cells , control = 2376 ± 137 cells; two-sided Mann-Whitney test). **F.** Left, hot plate paw withdrawal latencies of control and *DBH-cre* mice following subcutaneous administration of 0, 5, and 10 mg/kg morphine (Two-way repeated measures ANOVA with post hoc Sidak's multiple comparisons test; n=11 *DBHcre:TdTom* n=15 *TdTom* control; morphine dose effect, $p<0.0001$, $F(1.365,32.75)= 78.80$, genotype effect, $p=0.0006$, $F(1,24)=15.67$, morphine dose x genotype interaction, $p=0.0004$, $F(2,48)=9.328$). Right, Response to 10 hind paw pin pricks following morphine administration (Two-way repeated measures ANOVA with post hoc Sidak's multiple comparisons test; n=11 *DBHcre:TdTom* n=15 *TdTom* control; morphine dose effect, $p<0.0001$, $F(1.690,40.56)=72.20$, genotype effect, $p=0.0006$, $F(1,24)=15.52$, morphine dose x genotype interaction, $p=0.0037$, $F(2,48)=6.294$). **G.** Top, Slice electrophysiology recordings from Kir2.1-positive and -negative LC neurons. Bottom, representative traces of tonic AP firing in control vs. Kir2.1-expressing neurons. **H.** Left, resting membrane potential of control vs. Kir2.1-expressing neurons (n=10 Kir2.1-positive, n=9 control; Kir2.1 RMP = -70.1 ± 3.0 mV, control RMP = -46.9 ± 2.4mV, two-sided Mann-Whitney test). Right, tonic AP firing rate of control vs. Kir2.1-expressing neurons (Kir2.1 tonic firing rate = 0.006 ± 0.006 Hz, control tonic firing rate = 1.61 ± 0.25 Hz, two-sided Mann-Whitney test). **I.** Left, f-I curves of control vs. Kir2.1-expressing neurons for 7 current steps (n=10 Kir2.1-positive, n=9 control; two-sided Mann-Whitney test). Right, representative traces of evoked AP firing from a control (grey) and a Kir2.1-expressing (green) neuron at 50 pA (top) and 200 pA (bottom) current steps. **J.** Injection schematic, representative image of zsGreen expression in the LC of a *DBH-cre::tdTom* mouse (scale bar = 150 μm) and quantification of viral coverage given as % tdTom LC neurons labeled by zsGreen (n=12 *DBHcre:TdTom*, n=13 *TdTom* control; control = 1.2 ± 0.3%, *DBH-cre* = 79.0 ± 2.0%; two-sided Mann-Whitney test). **K.** Left, hot plate paw withdrawal latencies of control and *DBH-cre* mice following 0, 5, and 10 mg/kg morphine, s.c. (Two-way repeated measures ANOVA with post hoc Sidak's multiple comparisons test; n= 12 *DBHcre:TdTom*, n=13 *TdTom* control; hot plate: morphine dose effect, $p<0.0001$, $F(1.092,25.11)=46.27$, genotype effect, $p=0.001$, $F(1,23)=14.30$, morphine dose x genotype interaction, $p=0.013$, $F(2,46)=4.790$). Right, Response to 10 hind paw pin pricks following morphine (Two-way repeated measures ANOVA with post hoc Sidak's multiple comparisons test; n= 12 *DBHcre:TdTom*, n=13 *TdTom* control; morphine dose effect, $p<0.0001$, $F(1.695,38.99)=58.23$, genotype effect, $p=0.0004$, $F(1,23)=17.20$, morphine dose x genotype interaction, $p=0.0044$, $F(2,46)=6.131$). Data in each graph reported as mean ± SEM.

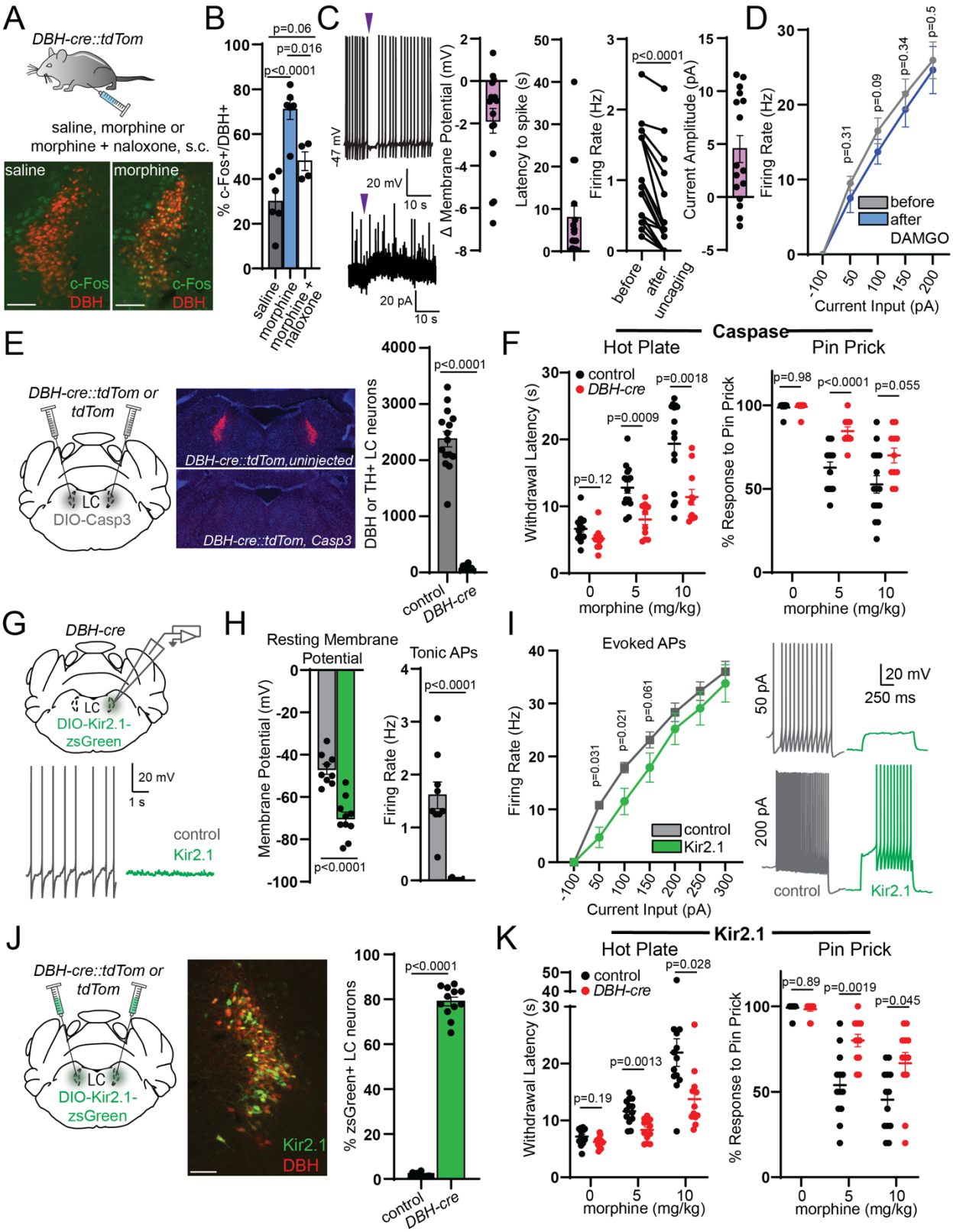
A
DBH-cre::tdTom
saline, morphine or
morphine + naloxone, s.c.
saline
morphine
c-Fos
DBH
B
% c-Fos+/DBH+
p=0.06
p=0.016
p<0.0001
saline
morphine
morphine + naloxone
C
-47 mV
20 mV
10 s
20 pA
10 s
Δ Membrane Potential (mV)
Latency to spike (s)
Firing Rate (Hz)
p<0.0001
Current Amplitude (pA)
before
after uncaging
D
Firing Rate (Hz)
p=0.31
p=0.09
p=0.34
p=0.5
before
after
DAMGO
Current Input (pA)
E
DBH-cre::tdTom or
tdTom
LC
DIO-Casp3
DBH-cre::tdTom,uninjected
DBH-cre::tdTom, Casp3
DBH or TH+ LC neurons
p<0.0001
control
DBH-cre
F
Caspase
Hot Plate
Pin Prick
control
DBH-cre
Withdrawal Latency (s)
p=0.12
p=0.0009
p=0.0018
% Response to Pin Prick
p=0.98
p<0.0001
p=0.055
morphine (mg/kg)
G
DBH-cre
LC
DIO-Kir2.1-
zsGreen
20 mV
1 s
control
Kir2.1
H
Resting Membrane
Potential
Membrane Potential (mV)
p<0.0001
Tonic APs
Firing Rate (Hz)
p<0.0001
I
Evoked APs
Firing Rate (Hz)
p=0.031
p=0.021
p=0.061
control
Kir2.1
Current Input (pA)
50 pA
20 mV
250 ms
200 pA
control
Kir2.1
J
DBH-cre::tdTom or
tdTom
LC
DIO-Kir2.1-
zsGreen
Kir2.1
DBH
% zsGreen+ LC neurons
p<0.0001
control
DBH-cre
K
Kir2.1
Hot Plate
Pin Prick
control
DBH-cre
Withdrawal Latency (s)
p=0.19
p=0.0013
p=0.028
% Response to Pin Prick
p=0.89
p=0.0019
p=0.045
morphine (mg/kg)

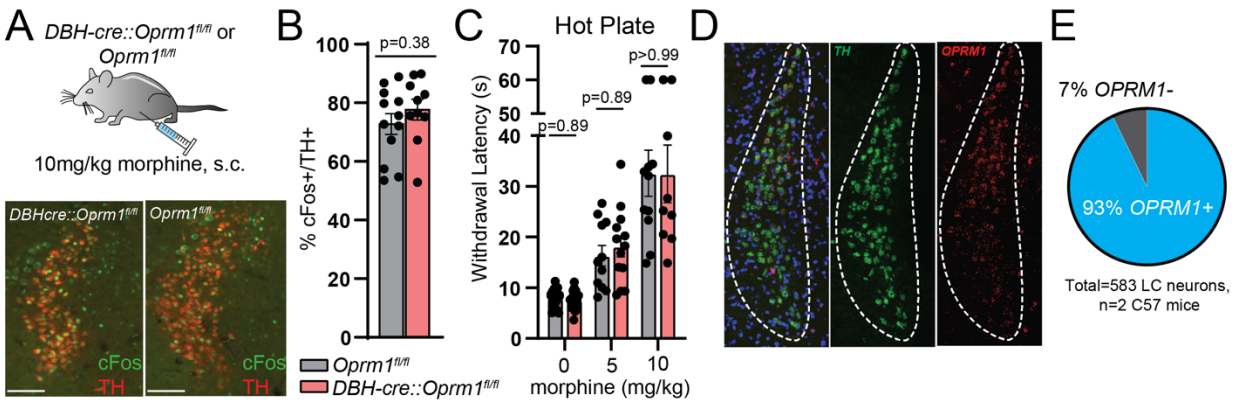

Figure 2.3. MORs in LC are not responsible for morphine induced activity changes or behavior.

A. Top: 10 mg/kg, s.c. morphine injections in *DBH-cre::Oprm1*$^{fl/fl}$ mice and control *Oprm1*$^{fl/fl}$ littermates. Bottom: Representative images of morphine-induced c-Fos expression (green) and immunhistochemical TH LC labeling (red). **B.** Percentage of TH+ LC neurons that colocalize with green c-Fos signal (5-8 images analyzed per mouse; n=10 *DBH-cre::Oprm1*$^{fl/fl}$, n=12 *Oprm1*$^{fl/fl}$; *DBH-cre::Oprm1*$^{fl/fl}$ = 77.6 ± 3.5%, *Oprm1*$^{fl/fl}$ = 72.7 ± 3.5%; p=0.38, two-sided Mann-Whitney test). **C.** Hot plate withdrawal latencies compared between *DBH-cre::Oprm1*$^{fl/fl}$ and *Oprm1*$^{fl/fl}$ littermates at 0, 5, and 10 mg/kg doses of morphine, s.c. (Mixed effects analysis with post hoc Sidak's multiple comparisons test; baseline n=18 *DBH-cre::Oprm1*$^{fl/fl}$, n=18 *Oprm1*$^{fl/fl}$; 5 mg/kg morphine n=13 *DBH-cre::Oprm1*$^{fl/fl}$, n=11 *Oprm1*$^{fl/fl}$; 10 mg/kg morphine n=9 *DBH-cre::Oprm1*$^{fl/fl}$, n=11 *Oprm1*$^{fl/fl}$; morphine dose effect, p<0.0001, F(1.261, 25.22)=50.93; genotype effect, p=0.835, F(1,34)=0.044; morphine dose x genotype interaction, p=0.88, F(2,40)=0.1283). **D.** Representative images of fluorescent *in situ* hybridization of LC with probes against *TH* (green) and *OPRM1* (red). **E.** Quantification of the percentage of *TH*+ LC neurons that express *OPRM1* transcripts.

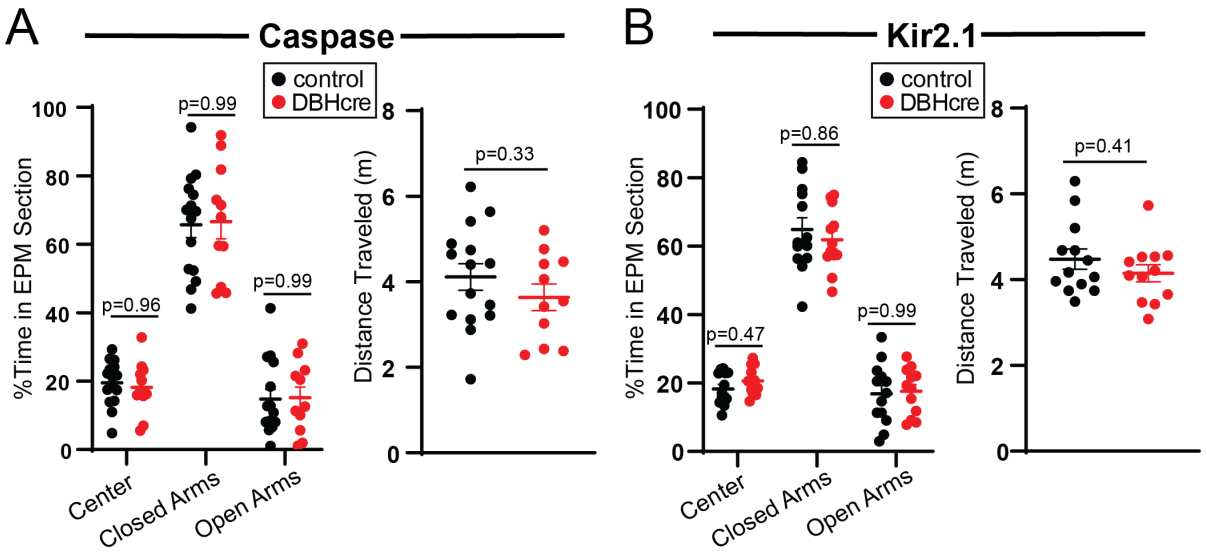

Figure 2.4. LC ablation or silencing does not affect baseline anxiety behavior or locomotion on the elevated plus maze.

A. Left: percentage of time spent in different sections of the elevated plus maze (EPM) during a 20 minute session in *DBH-cre*::tdTom and control *TdTom* mice injected with AAV-DIO-Casp3 (same cohort that underwent hot plate and pin prick behavior in Figure 2.2F; Two-way repeated measures ANOVA with post hoc Sidak's multiple comparisons test; n=11 *DBH-cre* mice, n=15 control; genotype effect, p=0.489, F(1,24)=0.4934). Right: distance traveled during the 20-minute EPM session (two-sided Mann-Whitney test). **B.** Same as in A, but for AAV-DIO-Kir2.1-zsGreen-injected mice from Figure 2.2J-K. Left: Two-way repeated measures ANOVA with post hoc Sidak's multiple comparisons test; n=12 *DBH-cre* mice, n=13 control; genotype effect, p=0.386, F(1,23)=0.7797. Right: two-sided Mann-Whitney test.

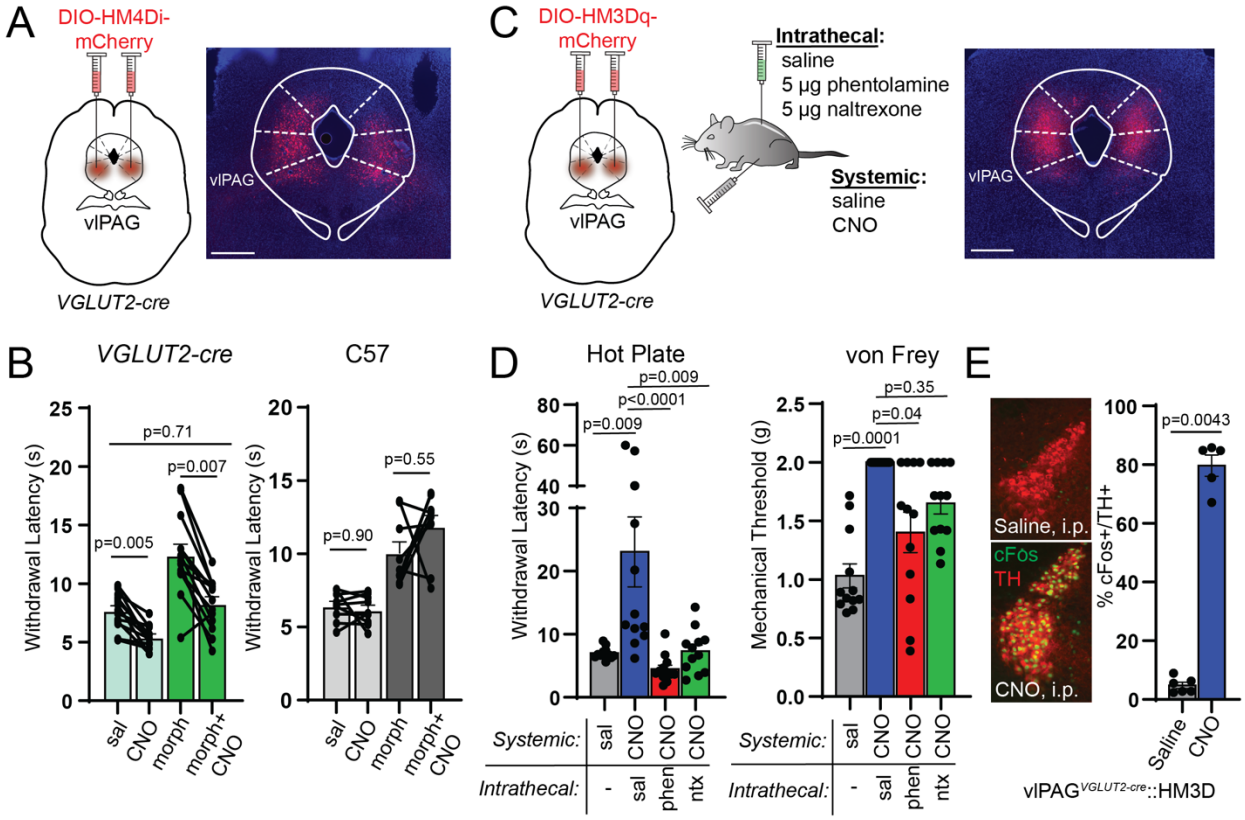

Figure 2.5. vlPAG activity is required for systemic morphine antinociception and drives spinal NA-dependent antinociception.

A. Bilateral AAV-DIO-HM4Di-mCherry injections in vlPAG of *VGLUT2-cre* mice with representative image of viral expression. Scale bar 500 µm. **B.** Left, hot plate withdrawal latencies of vlPAG$^{VGLUT2\text{-}cre}$::HM4D mice administered 3 mg/kg CNO, i.p. vs. saline without (light green bars) and with 5 mg/kg morphine, s.c. (dark green bars) (Two-way repeated measures ANOVA with post hoc Tukey's multiple comparisons test; n=13 mice; sal vs. CNO effect, $p<0.0001$, $F(1,12)=56.93$, morphine effect, $p<0.0001$, $F(1,12)=43.25$, morphine x CNO interaction, $p=0.048$, $F(1,12)=4.837$). Right, hot plate withdrawal latencies of non-virus injected C57 controls (Two-way repeated measures ANOVA with post hoc Tukey's multiple comparisons test; n=9 mice; sal vs. CNO effect, $p=0.32$, $F(1,8)=1.143$, morphine effect, $p<0.0001$, $F(1,8)=75.02$). **C.** Bilateral AAV-DIO-HM3Dq-mCherry injections in vlPAG of *VGLUT2-cre* mice and combinations of systemic CNO (3 mg/kg, i.p.) with intrathecal antagonists and representative image of viral expression. Scale bar 500 µm. **D.** Left, hot plate withdrawal latencies after systemic saline or CNO and intrathecal saline, phentolamine (5 µg), or naltrexone (5 µg) (Friedman test with post hoc Dunn's multiple comparisons test, n=12 subjects, $p<0.0001$, Friedman statistic = 26.40). Right, von Frey mechanical thresholds (Friedman test with post hoc Dunn's multiple comparisons test, n=12 subjects, $p=0.0001$, Friedman statistic = 21.00). **E.** Representative images of c-Fos immunohistochemistry in TH-positive LC neurons of vlPAG$^{VGLUT2\text{-}cre}$::HM3D mice after systemic injection of saline (top) or CNO (bottom). Right, % of TH-positive LC neurons that colocalize with green c-Fos signal (5-8 images analyzed per mouse; n= 6 saline, n=5 CNO; saline = 4.8 ± 1.1%, CNO = 79.6 ± 3.6%, two-sided Mann-Whitney test). Data in each graph reported as mean ± SEM.

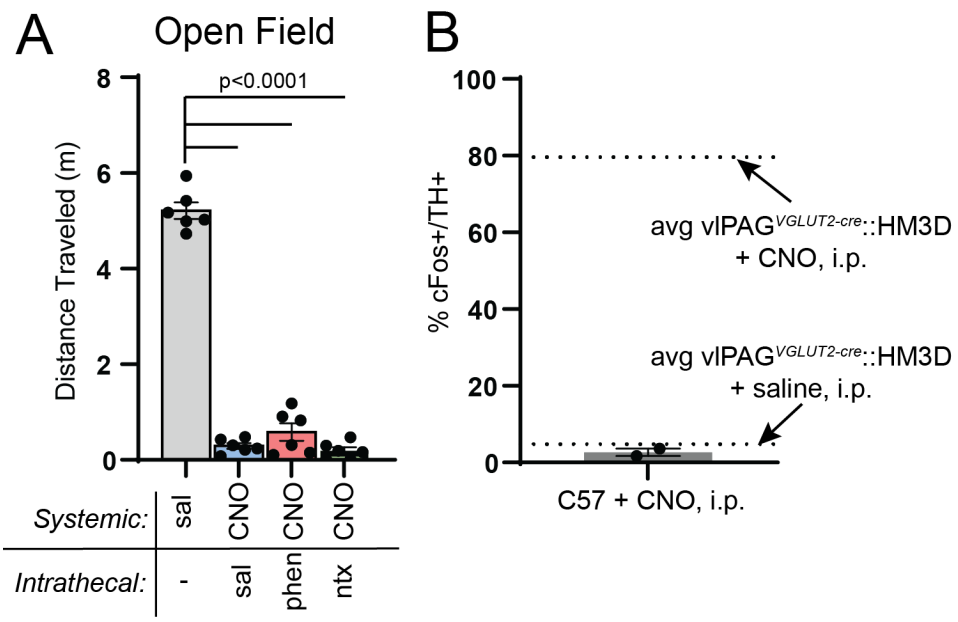

Figure 2.6. Chemogenetic PAG activation leads to decreased locomotion that can be decoupled from antinociception.

A. Distance traveled (m) during a 30-minute open field session after systemic injection of saline or CNO (3 mg/kg, i.p.) with intrathecal saline, phentolamine (5 μg), or naltrexone (5 μg) in vlPAG$^{VGLUT2\text{-}cre}$::HM3D mice (Repeated measures one-way ANOVA with post hoc Tukey's multiple comparisons test, $p<0.0001$, $F(2.467, 12.33)=392.1$). **B.** LC c-Fos expression induced by 3 mg/kg, i.p. CNO injection in uninjected wild type mice expressed as % TH+ LC neurons that colocalize with c-Fos. Dashed lines represent the average c-Fos induction by CNO and saline in the LC of vlPAG$^{VGLUT2\text{-}cre}$::HM3D mice in Figure 2.5E.

Figure 2.7. Anatomical characterization of inputs to LC from vlPAG and RVM.

A. Injection of AAV-DIO-tdTom in vlPAG of *VGLUT2-* or *VGAT-cre* mice. **B.** Injection site in *VGLUT2-cre* mouse. **C.** vlPAG glutamatergic terminals (red) in pericoerulear region defined by TH immunohistochemistry (green). Delineations taken from the Paxinos & Franklin Brain Atlas show that the pericoerulear terminals are largely targeted to the medial Barrington's nucleus. **D.** Injection site in *VGAT-cre* mouse. **E.** vlPAG GABAergic/glycinergic terminals in pericoerulear region. **B-E**. Scale bars 300 μm. **F.** Quantification of red (vlPAG glutamatergic terminals) and green (LC TH immunohistochemistry) pixel intensity in the LC and pericoerulear region normalized by z-score to account for fluorescence differences between animals and during imaging (n=6 LC slices from n=3 mice each). **G.** Same as F for vlPAG GABAergic/glycinergic terminals. **H.** Left: injections of AAVretro-cre in LC and AAV-DIO-mCherry in vlPAG of wild type mice to capture LC-projecting vlPAG neurons. Center: image of mCherry+ vlPAG neurons captured. Right: resulting terminals captured in LC and RVM. Scale bars 500 μm. **I.** Same as H for vlPAG neurons that project to RVM. Scale bars 500 μm. **J.** Left: Orthogonal recombinase strategy to label vlPAG neurons that project to RVM and LC. Center: representative image of mCherry (red) and YFP (green) viral labeling in vlPAG with neurons co-expressing both fluorophores appearing yellow. White arrows indicate examples of double labeled neurons. Scale bar 300 μm. Right: quantification of mCherry and YFP labeling in vlPAG. **K.** Injection of AAV-DIO-tdTom in RVM of *VGLUT2-* or *VGAT-cre* mice. **L.** Injection site in *VGLUT2-cre* mouse. **M.** RVM glutamatergic terminals (red) in LC and pericoerulear region defined by TH immunohistochemistry (green). **N.** Injection site in *VGAT-cre* mouse. **O.** RVM GABAergic/glycinergic terminals in LC and pericoerulear region. **L-O.** Scale bars 300 μm. **P.** Quantification of RVM glutamatergic terminals by pixel intensity z-score similar to F (n=6 LC slices from n=3 mice each). **Q.** Same as P for RVM GABAergic/glycinergic terminals. **R.** Quantification of red pixel intensity normalized by z-score across the dorsal to ventral axis of LC for all four projection origin and cell type combinations (n=6 LC slices from n=3 mice each). **S.** Injections of AAVretro-cre in LC and AAV-DIO-tdTom in RVM of wild type mice to capture LC-projecting RVM neurons. **T.** tdTom+ RVM neurons captured. **U.** Resulting terminals (red) captured in LC (green) and pericoerulear region. Scale bar 300 μm. **V.** tdTom+ fibers located in bilateral parafascicular nucleus of the thalamus. Scale bar 1mm.

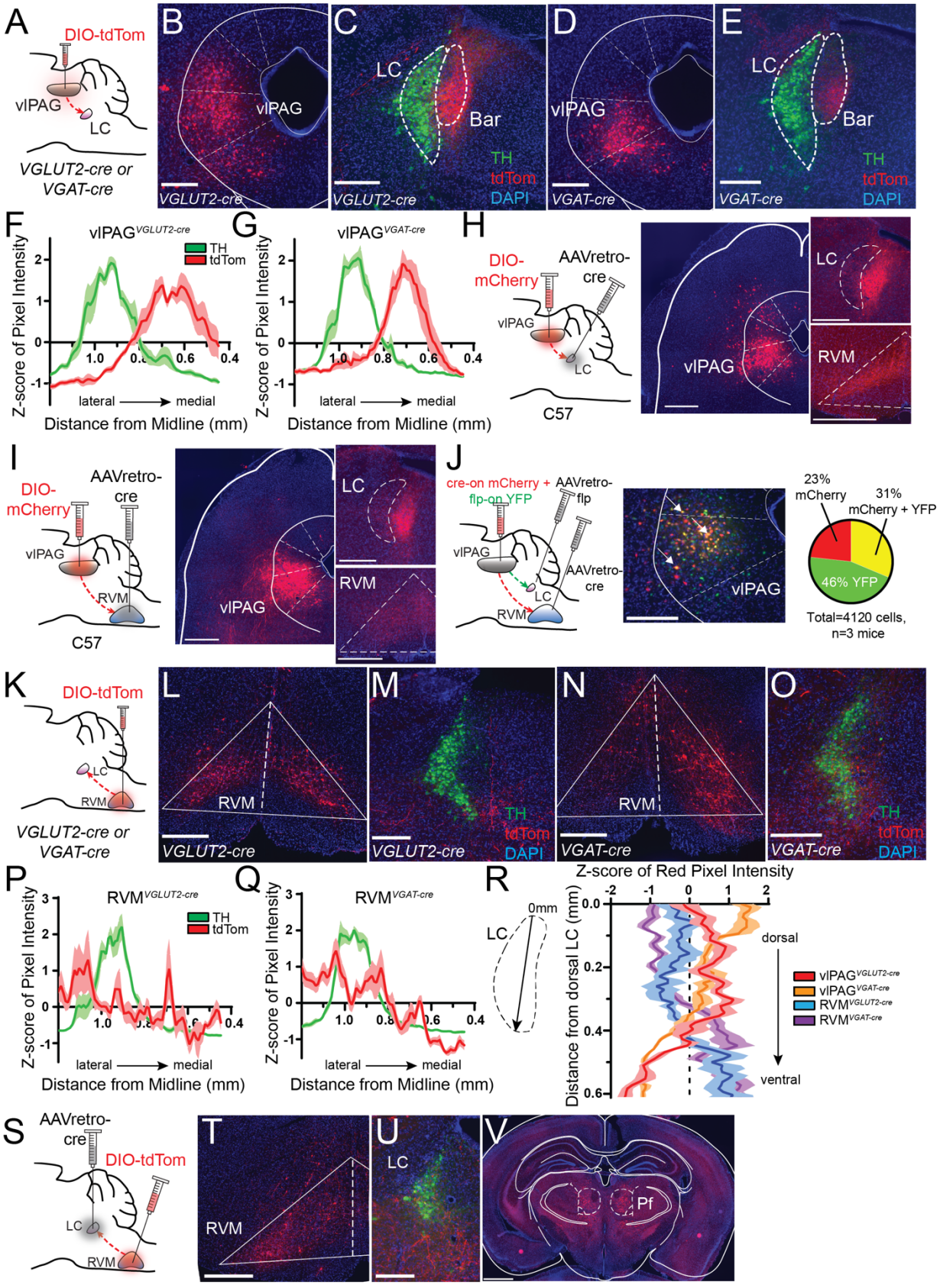
A
DIO-tdTom
vlPAG
LC
VGLUT2-cre or
VGAT-cre
B
vlPAG
VGLUT2-cre
C
LC
Bar
TH
tdTom
DAPI
VGLUT2-cre
D
vlPAG
VGAT-cre
E
LC
Bar
TH
tdTom
DAPI
VGAT-cre
F
vlPAG VGLUT2-cre
TH
tdTom
Z-score of Pixel Intensity
lateral
medial
Distance from Midline (mm)
G
vlPAG VGAT-cre
Z-score of Pixel Intensity
lateral
medial
Distance from Midline (mm)
H
DIO-
mCherry
AAVretro-
cre
vlPAG
LC
C57
vlPAG
LC
RVM
I
DIO-
mCherry
AAVretro-
cre
vlPAG
RVM
C57
vlPAG
LC
RVM
J
cre-on mCherry +
flp-on YFP
AAVretro-
flp
vlPAG
AAVretro-
cre
LC
RVM
vlPAG
23%
mCherry
31%
mCherry + YFP
46% YFP
Total=4120 cells,
n=3 mice
K
DIO-tdTom
LC
RVM
VGLUT2-cre or
VGAT-cre
L
RVM
VGLUT2-cre
M
TH
tdTom
DAPI
VGLUT2-cre
N
RVM
VGAT-cre
O
TH
tdTom
DAPI
VGAT-cre
P
RVM VGLUT2-cre
TH
tdTom
Z-score of Pixel Intensity
lateral
medial
Distance from Midline (mm)
Q
RVM VGAT-cre
Z-score of Pixel Intensity
lateral
medial
Distance from Midline (mm)
R
0mm
LC
Z-score of Red Pixel Intensity
Distance from dorsal LC (mm)
dorsal
ventral
vlPAG VGLUT2-cre
vlPAG VGAT-cre
RVM VGLUT2-cre
RVM VGAT-cre
S
AAVretro-
cre
DIO-tdTom
LC
RVM
T
RVM
U
LC
V
Pf

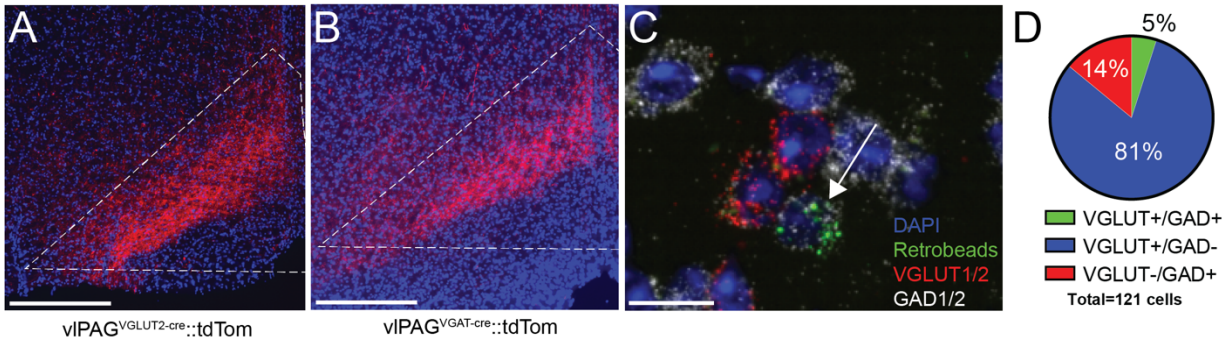

Figure 2.8. vlPAG sends GABAergic projections to RVM.

A. Representative image of glutamatergic terminals in RVM (red) of a *VGLUT2-cre* mouse injected in vlPAG with AAV-DIO-tdTom. Scale bar 300 µm. **B.** Representative image of GABAergic/glycinergic terminals in RVM (red) of a *VGAT-cre* mouse injected in vlPAG with AAV-DIO-tdTom. Scale bar 300 µm. **C.** Representative image of results from the retro-FISH method depicting vlPAG with colocalization of retrobeads from RVM (green) and *GAD1/2* transcripts (white) within a single neuron, as well as nearby neurons expressing *VGLUT1/2* transcripts (red). Scale bar 10 µm. **D.** Quantification of *VGLUT1/2* and *GAD1/2* expression within retrobead-labeled vlPAG neurons.

Figure 2.9. Electrophysiological characterization of inputs from vlPAG and RVM to LC.

A. Top, viral injection of ChR2 into vlPAG for LC slice electrophysiology. Bottom, representative trace of tonic spiking before, during, and after a 2 second blue LED stimulus (470 nm, 50x2 ms pulses at 25 Hz, 18 mW). **B.** Left, firing rate before and during the light stimulus for 20 LC neurons (baseline = 2.4 ± 0.4 Hz, light on = 9.1 ± 1.0 Hz; two-sided Wilcoxon matched-pairs signed rank test). Right, recorded neurons were categorized as "excited" (a z-score of spiking during vs. before light >2), "inhibited" (a z-score of spiking during vs. before light < -2), or "not modulated." **C.** Top, viral injection of ChR2 into RVM for LC slice electrophysiology. Bottom, representative trace of tonic spiking before, during, and after the blue LED stimulus. **D.** Left, firing rate before and during the blue light stimulus for 20 LC neurons (baseline = 2.3 ± 0.2 Hz, light on = 1.3 ± 0.3 Hz; two-sided Wilcoxon matched-pairs signed rank test). Right, categorization of recorded LC neurons as "excited", "inhibited", or "not modulated." **E.** Left, proportions of LC neurons in which optically-evoked EPSCs, EPSCs and IPSCs or no evoked currents were present when stimulating vlPAG terminals (470nm, 1 x 5 ms pulse, 18 mW). Middle, representative example of oEPSC and oIPSC recorded in a single LC neuron via electrical isolation. Right, peak amplitude of oEPSCs and oIPSCs driven by vlPAG terminal stimulation (oEPSCs = -177.8 ± 40.6 pA, oIPSCs = -0.52 ± 12.7 pA, n=12 neurons). **F.** Left, proportions of LC neurons in which optically-evoked EPSCs, IPSCs, both EPSCs and IPSCs or no evoked currents were present when stimulating RVM terminals. Middle, representative example of oEPSC and oIPSC recorded in a single LC neuron via electrical isolation. Right, peak amplitude of oEPSCs and oIPSCs driven by RVM terminal stimulation (oEPSCs = -117.7 ± 39.9 pA, oIPSCs = 466.6 ± 79.5 pA, n=12 neurons). **G-K.** Top, summary bar graphs of oEPSC/IPSC amplitude. Bottom, representative examples. **G.** vlPAG-driven oEPSC amplitude before and after bath application of NBQX (10 μM) (ACSF = -337.1 ± 88.0 pA, +NBQX = -4.9 ± 4.4 pA; two-sided paired t-test: t=3.950, n=4 pairs). **H.** vlPAG-driven oEPSC amplitude before and after bath application of TTX (1 μM) and subsequent application of 4-AP (100 μM) (+TTX = -2.9 ± 1.5 pA, +TTX & 4-AP = -288.5 ± 98.4 pA; two-sided paired t-test: t=2.926, n=5 pairs). **I.** RVM-driven oIPSC amplitude before and after bath application of GABAzine (20 μM) and additional application of strychnine (10 μM) (ACSF = 636.3 ± 154.9 pA, +GABAzine = 286.6 ± 100.8 pA, +GABAzine & strychnine = -2.5 ± 1.7 pA; Repeated Measures One-way ANOVA with Dunnett's multiple comparisons test, p=0.013, F(1.087,4.348)=16.32, n=5 cells). **J.** RVM-driven oIPSC amplitude before and after bath application of TTX (1 μM) and subsequent application of 4-AP (100 μM) (+TTX = 13.1 ± 9.8 pA, +TTX & 4-AP = 443.9 ± 164.6 pA; two-sided Wilcoxon matched-pairs signed rank test, n=6 pairs). **K.** RVM-driven oIPSC amplitude before and after bath application of NBQX (10 μM) + CPP (10 μM) (ACSF = 309.6 ± 36.1 pA, +NBQX/CPP = 207.6 ± 35.8 pA; two-sided paired t-test: t=6.976, n=7 pairs). **L.** Top, example traces of RVM oIPSCs (blue) and vlPAG oEPSCs (red) before and after bath application of DAMGO (1 μM; black). Bottom, opioid sensitivity reported as % suppression of amplitude by DAMGO (RVM oIPSC = 47.6 ± 7.0%, PAG oEPSC = 11.4 ± 4.2%; two-sided unpaired t-test: t=3.785, n=8 RVM IPSC, n=5 PAG EPSC). All summary data reported as mean ± SEM.

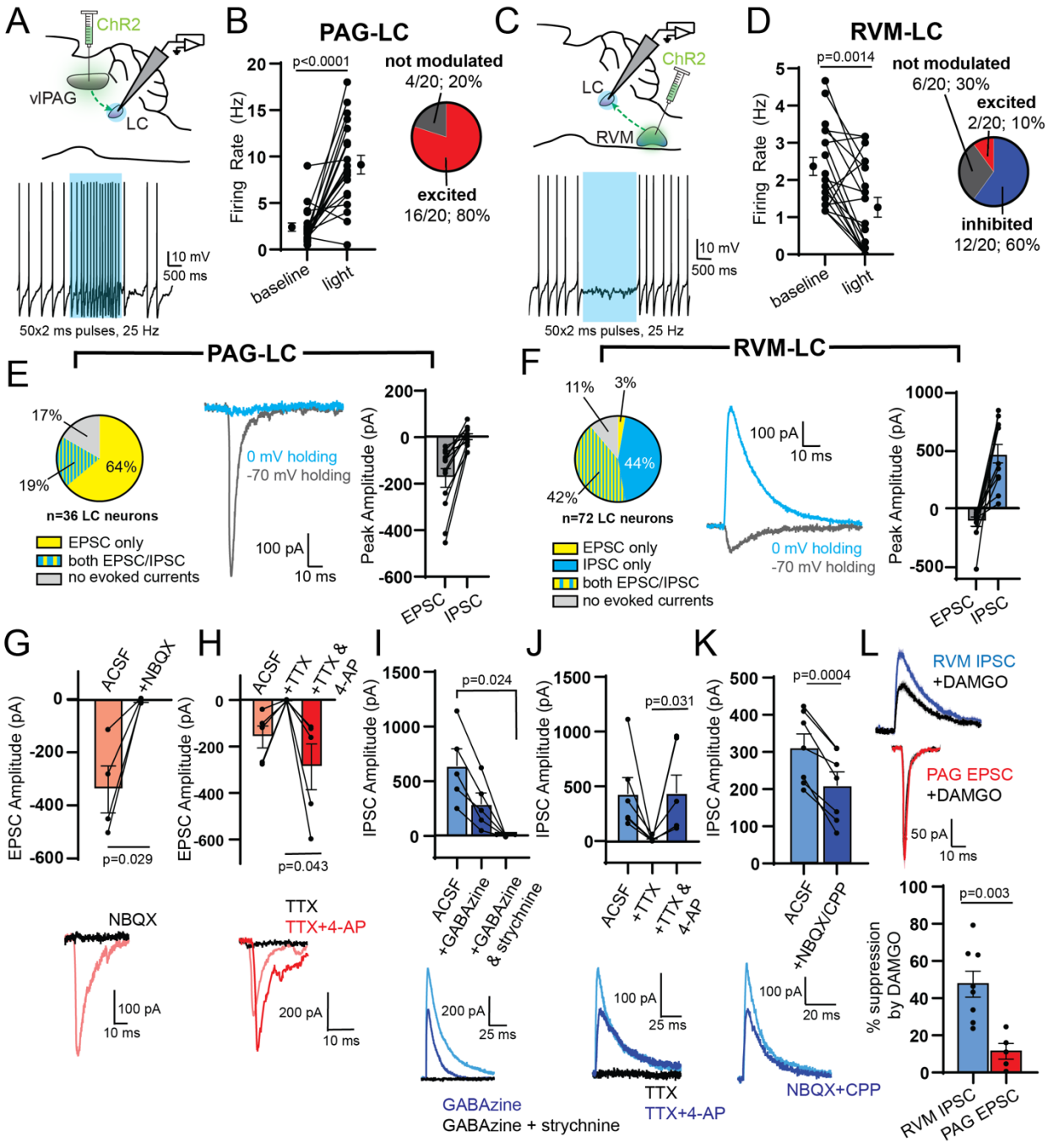
A
ChR2
vlPAG
LC
10 mV
500 ms
50x2 ms pulses, 25 Hz
B
PAG-LC
p<0.0001
Firing Rate (Hz)
baseline
light
not modulated
4/20; 20%
excited
16/20; 80%
C
ChR2
LC
RVM
10 mV
500 ms
50x2 ms pulses, 25 Hz
D
RVM-LC
p=0.0014
Firing Rate (Hz)
baseline
light
not modulated
6/20; 30%
excited
2/20; 10%
inhibited
12/20; 60%
E
PAG-LC
17%
64%
19%
n=36 LC neurons
EPSC only
both EPSC/IPSC
no evoked currents
0 mV holding
-70 mV holding
100 pA
10 ms
Peak Amplitude (pA)
EPSC
IPSC
F
RVM-LC
11%
3%
44%
42%
n=72 LC neurons
EPSC only
IPSC only
both EPSC/IPSC
no evoked currents
100 pA
10 ms
0 mV holding
-70 mV holding
Peak Amplitude (pA)
EPSC
IPSC
G
EPSC Amplitude (pA)
ACSF
+NBQX
p=0.029
NBQX
100 pA
10 ms
H
EPSC Amplitude (pA)
ACSF
+TTX
+TTX & 4-AP
p=0.043
TTX
TTX+4-AP
200 pA
10 ms
I
IPSC Amplitude (pA)
p=0.024
ACSF
+GABAzine
+GABAzine & strychnine
200 pA
25 ms
GABAzine
GABAzine + strychnine
J
IPSC Amplitude (pA)
p=0.031
ACSF
+TTX
+TTX & 4-AP
100 pA
25 ms
TTX
TTX+4-AP
K
IPSC Amplitude (pA)
p=0.0004
ACSF
+NBQX/CPP
100 pA
20 ms
NBQX+CPP
L
RVM IPSC
+DAMGO
PAG EPSC
+DAMGO
50 pA
10 ms
% suppression by DAMGO
p=0.003
RVM IPSC
PAG EPSC

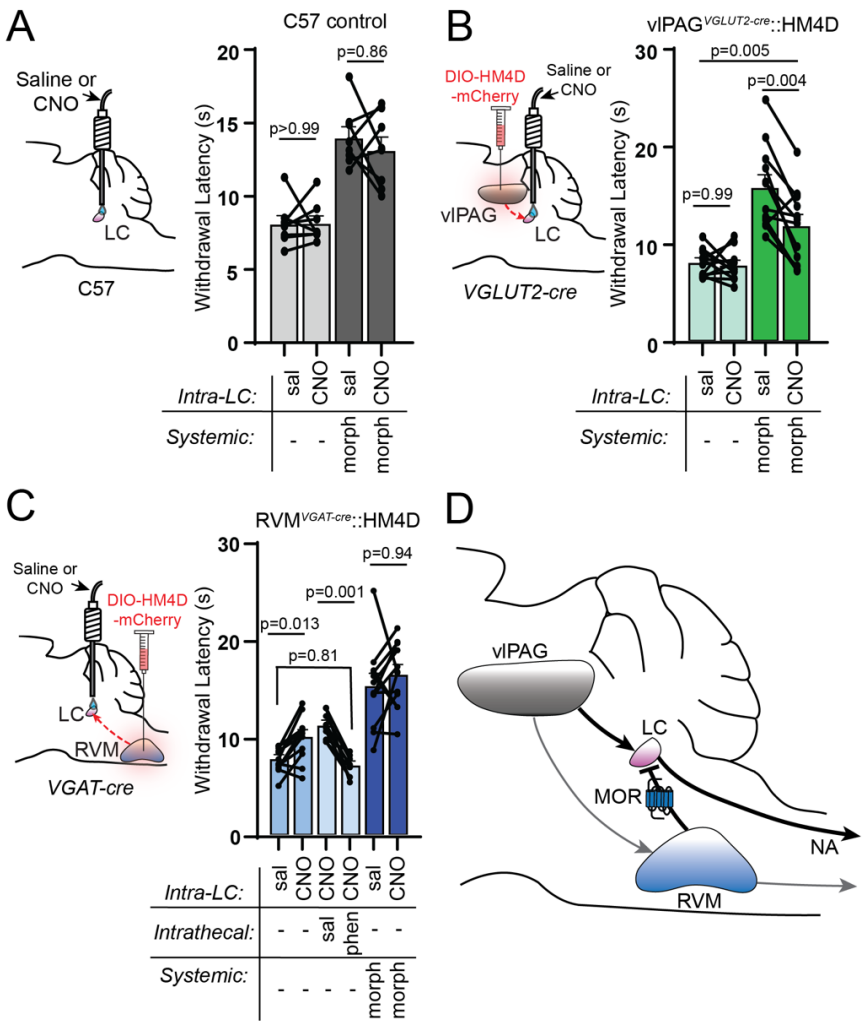

Figure 2.10. Pathway specific modulation of vlPAG and RVM terminals in LC modulates nociceptive behavior.

A. Left: cannula placement over bilateral LC of uninjected C57 control mice. Right: hot plate withdrawal latencies of control mice microinfused in LC with saline (150nl) vs. CNO (3 µM 150nl) without (light grey) and with 5 mg/kg morphine, s.c. (dark grey; Two-way repeated measures ANOVA with post hoc Tukey's multiple comparisons test; n=8 mice; sal vs. CNO effect, p=0.4178, F(1,7)=0.7412, morphine effect, p=0.0001, F(1,7)=57.98; morphine x CNO interaction, p=0.58, F(1,7)=0.3434). **B.** Left: viral injection of AAV-DIO-HM4Di-mCherry in bilateral vlPAG of *VGLUT2-cre* mice with cannula placement over bilateral LC. Right: hot plate withdrawal latencies after microinfusion with saline vs. CNO without (light green) and with 5m/kg morphine, s.c. (dark green; Two-way repeated measures ANOVA with post hoc Sidak's multiple comparisons test; n=12 mice; sal vs. CNO effect, p=0.0022, F(1,11)=15.72, morphine effect, p=0.0003, F(1,11)=27.60; morphine x CNO interaction, p=0.0106, F(1,11)=9.456). **C.** Left: viral injection of AAV-DIO-HM4Di-mCherry in bilateral RVM of *VGAT-cre* mice with cannula placement over bilateral LC. Right: hot plate withdrawal latencies after microinfusion of saline vs. CNO (blue bars n=12 mice), microinfusion of CNO with intrathecal injections of saline vs. phentolamine (5ug, light blue bars, n=9 mice), and microinfusion of saline vs. CNO with 5 mg/kg morphine, s.c. (dark blue, n=12 mice; Mixed effects analysis with matching across row and post hoc Tukey's multiple comparisons test, p<0.0001, F(2.560,25.09)=27.36). **D.** Circuit diagram of DPMS inputs to LC and their opioid sensitivity. Data in each graph reported as mean ± SEM.

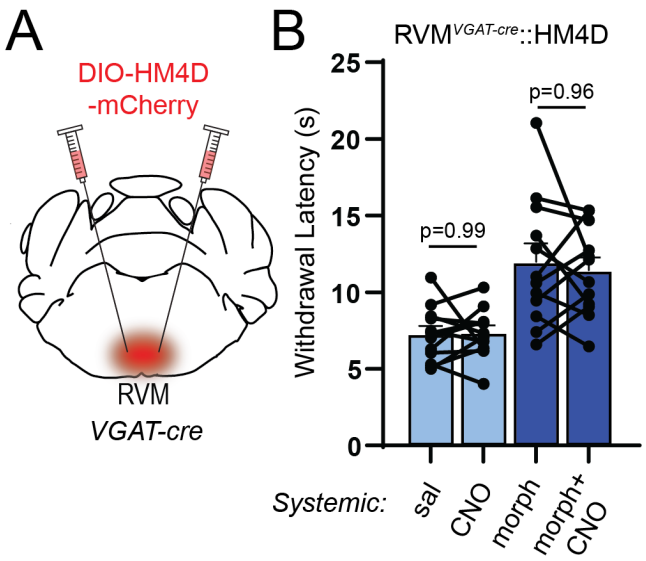

Figure 2.11. Inhibition of RVM GABAergic neurons does not affect baseline pain behavior or morphine antinociception.

A. Viral injections of AAV-DIO-HM4Di-mCherry into bilateral RVM of *VGAT-cre* mice. **B.** Hot plate withdrawal latencies of RVM$^{VGAT\text{-}cre}$::HM4D mice administered 3 mg/kg CNO, i.p. vs. saline without (light blue) and with 5 mg/kg morphine, s.c. (dark blue bars, Two-way repeated measures ANOVA with post hoc Tukey's multiple comparisons test; n=12 mice; saline vs. CNO effect, $p=0.725$, $F(1,11)=0.1307$, morphine effect, $p<0.0001$, $F(1,11)=36.62$, morphine x CNO interaction, $p=0.60$, $F(1,11)=0.2897$).

Chapter 2, in full, has been submitted for publication of the material as it may appear in Science Advances, 2024, Lubejko, Susan T.; Livrizzi, Giulia; Patel, Janki; Yung, Jean C.; Yaksh, Tony L., Banghart, Matthew R. "Inputs to the locus coeruleus from the periaqueductal gray and rostroventral medulla shape opioid-mediated descending pain modulation." The dissertation author was the primary researcher and author of this paper.

References

Aimone, L. D., Jones, S. L., and Gebhart, G. F. (1987). Stimulation-produced descending inhibition from the periaqueductal gray and nucleus raphe magnus in the rat: mediation by spinal monoamines but not opioids. *Pain* 31, 123–136. doi: 10.1016/0304-3959(87)90012-1.

Aston-Jones, G., Shipley, M. T., Chouvet, G., Ennis, M., van Bockstaele, E., Pieribone, V., et al. (1991). "Afferent regulation of locus coeruleus neurons: anatomy, physiology and pharmacology," in *Neurobiolgoy of the Locus Coeruleus*, 47–75. doi: 10.1016/S0079-6123(08)63799-1.

Aston-Jones, G., Zhu, Y., and Card, J. P. (2004). Numerous GABAergic Afferents to Locus Ceruleus in the Pericerulear Dendritic Zone: Possible Interneuronal Pool. *Journal of Neuroscience* 24, 2313–2321. doi: 10.1523/JNEUROSCI.5339-03.2004.

Bagley, E. E., and Ingram, S. L. (2020). Endogenous opioid peptides in the descending pain modulatory circuit. *Neuropharmacology* 173, 108131. doi: 10.1016/j.neuropharm.2020.108131.

Bajic, D., and Proudfit, H. K. (1999). Projections of neurons in the periaqueductal gray to pontine and medullary catecholamine cell groups involved in the modulation of nociception. *Journal of Comparative Neurology* 405, 359–379. doi: 10.1002/(SICI)1096-9861(19990315)405:3<359::AID-CNE6>3.0.CO;2-W.

Banghart, M. R., and Sabatini, B. L. (2012). Photoactivatable Neuropeptides for Spatiotemporally Precise Delivery of Opioids in Neural Tissue. *Neuron* 73, 249–259. doi: 10.1016/j.neuron.2011.11.016.

Barcomb, K., Olah, S. S., Kennedy, M. J., and Ford, C. P. (2022). The Journal of Physiology Properties and modulation of excitatory inputs to the locus coeruleus. *J Physiol* 0, 1–20. doi: 10.1113/JP283605#support-information-section.

Basbaum, A., and Fields, H. L. (1984). Endogenous Pain Control Systems: Brainstem Spinal Pathways and Endorphin Circuitry. *Annu Rev Neurosci* 7, 309–338. doi: 10.1146/annurev.neuro.7.1.309.

Burnett, A., and Gebhart, G. F. (1991). Characterization of descending modulation of nociception from the A5 cell group. *Brain Res* 546, 271–281. doi: 10.1016/0006-8993(91)91491-I.

Chaplan, S. R., Bach, F. W., Pogrel, J. W., Chung, J. M., and Yaksh, T. L. (1994). Quantitative assessment of tactile allodynia in the rat paw. *J Neurosci Methods* 53, 55–63. doi: 10.1016/0165-0270(94)90144-9.

Chaudhry, F. A., Reimer, R. J., Bellocchio, E. E., Danbolt, N. C., Osen, K. K., Edwards, R. H., et al. (1998). The Vesicular GABA Transporter, VGAT, Localizes to Synaptic Vesicles in Sets of Glycinergic as Well as GABAergic Neurons. *Journal of Neuroscience* 18, 9733–9750.

Clark, F. M., and Proudfit, H. K. (1991a). Projections of neurons in the ventromedial medulla to pontine catecholamine cell groups involved in the modulation of nociception. *Brain Res* 540, 105–115. doi: 10.1016/0006-8993(91)90496-I.

Clark, F. M., and Proudfit, H. K. (1991b). The projection of locus coeruleus neurons to the spinal cord in the rat determined by anterograde tracing combined with immunocytochemistry. *Brain Res* 538, 231–245. doi: 10.1016/0006-8993(91)90435-X.

Clark, F. M., and Proudfit, H. K. (1991c). The projection of noradrenergic neurons in the A7 catecholamine cell group to the spinal cord in the rat demonstrated by anterograde tracing combined with immunocytochemistry. *Brain Res* 547, 279–288. doi: 10.1016/0006-8993(91)90972-X.

Clark, F. M., and Proudfit, H. K. (1993). The projections of noradrenergic neurons in the A5 catecholamine cell group to the spinal cord in the rat: anatomical evidence that A5 neurons modulate nociception. *Brain Res* 616, 200–210. doi: 10.1016/0006-8993(93)90210-E.

Clark, F. M., Yeomans, D. C., and Proudfit, H. K. (1991). The noradrenergic innervation of the spinal cord: differences between two substrains of Sprague-Dawley rats determined using retrograde tracers combined with immunocytochemistry. *Neurosci Lett* 125, 155–158. doi: 10.1016/0304-3940(91)90015-L.

Dostrovsky, J. O., and Deakin, J. F. W. (1977). Periaqueductal grey lesions reduce morphine analgesia in the rat. *Neurosci Lett* 4, 99–103.

Ennis, M., and Aston-Jones, G. (1988). Activation of locus coeruleus from nucleus paragigantocellularis: a new excitatory amino acid pathway in brain. *The Journal of Neuroscience* 8, 3644–3657. doi: 10.1523/JNEUROSCI.08-10-03644.1988.

Ennis, M., Aston-Jones, G., and Shiekhattar, R. (1992). Activation of locus coeruleus neurons by nucleus paragigantocellularis or noxious sensory stimulation is mediated by intracoerulear excitatory amino acid neurotransmission. *Brain Res* 598, 185–195. doi: 10.1016/0006-8993(92)90182-9.

Ennis, M., Behbehani, M., Shipley, M. T., van Bockstaele, E. J., and Aston-Jones, G. (1991). Projections from the periaqueductal gray to the rostromedial pericoerulear region and nucleus locus coeruleus: Anatomic and physiologic studies. *Journal of Comparative Neurology* 306, 480–494. doi: 10.1002/cne.903060311.

Fields, H. L., Bry, J., Hentall, I., and Zorman, G. (1983). The activity of neurons in the rostral medulla of the rat during withdrawal from noxious heat.

François, A., Low, S. A., Sypek, E. I., Christensen, A. J., Sotoudeh, C., Beier, K. T., et al. (2017). A Brainstem-Spinal Cord Inhibitory Circuit for Mechanical Pain Modulation by GABA and Enkephalins. *Neuron* 93, 822–839. doi: 10.1016/j.neuron.2017.01.008.

Ganley, R. P., de Sousa, M. M., Ranucci, M., Werder, K., Ozturk, T., Wildner, H., et al. (2023a). Descending GABAergic neurons of the RVM that mediate widespread bilateral antinociception. *bioRxiv*. doi: 10.1101/2023.04.29.538824.

Ganley, R. P., de Sousa, M. M., Werder, K., Öztürk, T., Mendes, R., Ranucci, M., et al. (2023b). Targeted anatomical and functional identification of antinociceptive and pronociceptive serotonergic neurons that project to the spinal dorsal horn. *Elife* 12. doi: 10.7554/eLife.78689.

Gu, X., Zhang, Y. Z., O'Malley, J. J., De Preter, C. C., Penzo, M., and Hoon, M. A. (2023). Neurons in the caudal ventrolateral medulla mediate descending pain control. *Nat Neurosci*. doi: 10.1038/s41593-023-01268-w.

Hami, J., von Bohlen und Halbach, V., Tetzner, A., Walther, T., and von Bohlen und Halbach, O. (2021). Localization and expression of the Mas-related G-protein coupled receptor member D (MrgD) in the mouse brain. *Heliyon* 7, e08440. doi: 10.1016/j.heliyon.2021.e08440.

Hammond, D. L., and Proudfit, H. K. (1980). Effects of locus coeruleus lesions on morphine-induced antinociception. *Brain Res* 188, 79–91. doi: 10.1016/0006-8993(80)90558-2.

Hammond, D. L., and Yaksh, T. L. (1984). Antagonism of stimulation-produced antinociception by intrathecal administration of methysergide or phentolamine. *Brain Res* 298, 329–337. doi: 10.1016/0006-8993(84)91432-X.

Heinricher, M. M., Cheng, Z. F., and Fields, H. L. (1987). Evidence for two classes of nociceptive modulating neurons in the periaqueductal gray. *The Journal of neuroscience* 7, 271–278. doi: 10.1523/JNEUROSCI.07-01-00271.1987.

Heinricher, M. M., Morgan, M. M., Tortorici, V., and Fields, H. L. (1994). Disinhibition of off-cells and antinociception produced by an opioid action within the rostral ventromedial medulla. *Neuroscience* 63, 279–288. doi: 10.1016/0306-4522(94)90022-1.

Heinricher, M. M., Tavares, I., Leith, J. L., and Lumb, B. M. (2009). Descending control of nociception: Specificity, recruitment and plasticity. *Brain Res Rev* 60, 214–225. doi: 10.1016/j.brainresrev.2008.12.009.

He, X. J., Patel, J., Weiss, C. E., Ma, X., Bloodgood, B. L., and Banghart, M. R. (2021). Convergent, functionally independent signaling by mu and delta opioid receptors in hippocampal parvalbumin interneurons. *Elife* 10. doi: 10.7554/eLife.69746.

Hickey, L., Li, Y., Fyson, S. J., Watson, T. C., Perrins, R., Hewinson, J., et al. (2014). Optoactivation of locus ceruleus neurons evokes bidirectional changes in thermal nociception in rats. *Journal of Neuroscience* 34, 4148–4160. doi: 10.1523/JNEUROSCI.4835-13.2014.

Hirschberg, S., Li, Y., Randall, A., Kremer, E. J., and Pickering, A. E. (2017). Functional dichotomy in spinal- vs prefrontal-projecting locus coeruleus modules splits descending

noradrenergic analgesia from ascending aversion and anxiety in rats. *Elife* 6, 1–26. doi: 10.7554/elife.29808.

Holden, J. E., Schwartz, E. J., and Proudfit, H. K. (1999). Microinjection of morphine in the A7 catecholamine cell group produces opposing effects on nociception that are mediated by α1- and α2- adrenoceptors. *Neuroscience* 91, 979–990. doi: 10.1016/S0306-4522(98)00673-3.

Hou, X. H., Hyun, M., Taranda, J., Huang, K. W., Todd, E., Feng, D., et al. (2016). Central Control Circuit for Context-Dependent Micturition. *Cell* 167, 73-86.e12. doi: 10.1016/j.cell.2016.08.073.

Hu, Z., zhao, T., Chen, T., and Wang, D. (2019). Chronic activation of Mas-related gene receptors (Mrg) reduces the potency of morphine-induced analgesia via PKC pathway in naive rats. *Brain Res* 1722, 146363. doi: 10.1016/j.brainres.2019.146363.

Hylden, J. L. K., and Wilcox, G. L. (1980). Intrathecal morphine in mice: a new technique. *Eur J Pharmacol* 67, 313–316.

Jensen, T. S., and Yaksh, T. L. (1984). Spinal Monoamine and Opiate Systems Partly Mediate the Antinociceptive Effects Produced by Glutamate at Brainstem Sites. *Brain Res* 321, 287–297.

Kim, J. H., Gangadharan, G., Byun, J., Choi, E. J., Lee, C. J., and Shin, H. S. (2018). Yin-and-yang bifurcation of opioidergic circuits for descending analgesia at the midbrain of the mouse. *Proc Natl Acad Sci U S A* 115, 11078–11083. doi: 10.1073/pnas.1806082115.

Kucharczyk, M. W., Di Domenico, F., and Bannister, K. (2022). Distinct brainstem to spinal cord noradrenergic pathways inversely regulate spinal neuronal activity. *Brain* 145, 2293–2300. doi: 10.1093/brain/awac085.

Kucharczyk, M. W., Di Domenico, F., and Bannister, K. (2023). A critical brainstem relay for mediation of diffuse noxious inhibitory controls. *Brain* 146, 2259–2267. doi: 10.1093/brain/awad002.

Kuo, C., Hsieh, J., Tsai, H., Kuo, Y., Yau, H., Chen, C., et al. (2020). Inhibitory interneurons regulate phasic activity of noradrenergic neurons in the mouse locus coeruleus and functional implications. *J Physiol* Accepted A, JP279557. doi: 10.1113/JP279557.

Lau, B. K., and Vaughan, C. W. (2014). Descending modulation of pain: The GABA disinhibition hypothesis of analgesia. *Curr Opin Neurobiol* 29, 159–164. doi: 10.1016/j.conb.2014.07.010.

Li, Y., Hickey, L., Perrins, R., Werlen, E., Patel, A. A., Hirschberg, S., et al. (2016). Retrograde optogenetic characterization of the pontospinal module of the locus coeruleus with a canine adenoviral vector. *Brain Res* 1641, 274–290. doi: 10.1016/j.brainres.2016.02.023.

Ma, X., Johnson, D. A., He, X. J., Layden, A. E., McClain, S. P., Yung, J. C., et al. (2023). In vivo photopharmacology with a caged mu opioid receptor agonist drives rapid changes in behavior. *Nat Methods* 20, 682–685. doi: 10.1038/s41592-023-01819-w.

Millan, M. J. (2002). Descending control of pain. *Prog Neurobiol* 66, 355–474.

Miller, J. F., and Proudfit, H. K. (1990). Antagonism of stimulation-produced antinociception from ventrolateral pontine sites by intrathecal administration of α-adrenergic antagonists and naloxone. *Brain Res* 530, 20–34. doi: 10.1016/0006-8993(90)90653-S.

Morgan, M. M., Gold, M. S., Liebeskind, J. C., and Stein, C. (1991). Periaqueductal gray stimulation produces a spinally mediated, opioid antinociception for the inflamed hindpaw of the rat. *Brain Res* 545, 17–23. doi: 10.1016/0006-8993(91)91264-2.

Morgan, M. M., Whittier, K. L., Hegarty, D. M., and Aicher, S. A. (2008). Periaqueductal gray neurons project to spinally projecting GABAergic neurons in the rostral ventromedial medulla. *Pain* 140, 376–386. doi: 10.1016/j.pain.2008.09.009.

Nuseir, K., and Proudfit, H. K. (2000). Bidirectional modulation of nociception by GABA neurons in the dorsolateral pontine tegmentum that tonically inhibit spinally projecting noradrenergic A7 neurons. *Neuroscience* 96, 773–783. doi: 10.1016/S0306-4522(99)00603-X.

Park, C., Kim, J.-H., Yoon, B.-E., Choi, E.-J., Lee, C. J., and Shin, H.-S. (2010). T-type channels control the opioidergic descending analgesia at the low threshold-spiking GABAergic neurons in the periaqueductal gray. *Proceedings of the National Academy of Sciences* 107, 14857–14862. doi: 10.1073/pnas.1009532107.

Paxinos, G., and Franklin, K. B. J. (2001). *The Mouse Brain in Stereotaxic Coordinates, 2nd Edition*. Academic Press.

Proudfit, H. K., and Hammond, D. L. (1981). Alterations in nociceptive threshold and morphine-induced analgesia produced by intrathecally administered amine antagonists. *Brain Res* 218, 393–399.

Reichling, D. B., and Basbaum, A. I. (1990). Contribution of brainstem GABAergic circuitry to descending antinociceptive controls: I. GABA-immunoreactive projection neurons in the periaqueductal gray and nucleus raphe magnus. *Journal of Comparative Neurology* 302, 370–377. doi: 10.1002/cne.903020213.

Roth, B. L. (2016). DREADDs for Neuroscientists. *Neuron* 89, 683–694. doi: 10.1016/j.neuron.2016.01.040.

Samineni, V. K., Grajales-Reyes, J. G., Copits, B. A., O'Brien, D. E., Trigg, S. L., Gomez, A. M., et al. (2017). Divergent Modulation of Nociception by Glutamatergic and GABAergic Neuronal Subpopulations in the Periaqueductal Gray. *eNeuro* 4, ENEURO.0129-16.2017. doi: 10.1523/ENEURO.0129-16.2017.

Sasa, M., Munekiyo, K., Osumi, Y., and Takaori, S. (1977). Attenuation of morphine analgesia in rats with lesions of the locus coeruleus and dorsal raphe nucleus.

Schwarz, L. A., Miyamichi, K., Gao, X. J., Beier, K. T., Weissbourd, B., Deloach, K. E., et al. (2015). Viral-genetic tracing of the input-output organization of a central noradrenaline circuit. *Nature* 524, 88–92. doi: 10.1038/nature14600.

Shoda, T., Fukuda, K., Uga, H., Mima, H., and Morikawa, H. (2001). Activation of-Opioid Receptor Induces Expression of c-fos and junB via Mitogen-activated Protein Kinase Cascade. Available at: www.anesthesiology.org.

Stachniak, T. J., Ghosh, A., and Sternson, S. M. (2014). Chemogenetic Synaptic Silencing of Neural Circuits Localizes a Hypothalamus→Midbrain Pathway for Feeding Behavior. *Neuron* 82, 797–808. doi: 10.1016/j.neuron.2014.04.008.

Suzuki, R., Rahman, W., Hunt, S. P., and Dickenson, A. H. (2004). Descending facilitatory control of mechanically evoked responses is enhanced in deep dorsal horn neurones following peripheral nerve injury. *Brain Res* 1019, 68–76. doi: 10.1016/j.brainres.2004.05.108.

Svensson, C. I., Tran, T. K., Fitzsimmons, B., Yaksh, T. L., and Hua, X. Y. (2006). Descending serotonergic facilitation of spinal ERK activation and pain behavior. *FEBS Lett* 580, 6629–6634. doi: 10.1016/j.febslet.2006.11.012.

Torrecilla, M., Marker, C. L., Cintora, S. C., Stoffel, M., Williams, J. T., and Wickman, K. (2002). G-Protein-Gated Potassium Channels Containing Kir3.2 and Kir3.3 Subunits Mediate the Acute Inhibitory Effects of Opioids on Locus Ceruleus Neurons.

Tovote, P., Esposito, M. S., Botta, P., Chaudun, F., Fadok, J. P., Markovic, M., et al. (2016). Midbrain circuits for defensive behaviour. *Nature* 534, 206–212. doi: 10.1038/nature17996.

Vogt, B. A., Hof, P. R., Friedman, D. P., Sikes, R. W., and Vogt, L. J. (2008). Norepinephrinergic afferents and cytology of the macaque monkey midline, mediodorsal, and intralaminar thalamic nuclei. *Brain Struct Funct* 212, 465–479. doi: 10.1007/s00429-008-0178-0.

Weibel, R., Reiss, D., Karchewski, L., Gardon, O., Matifas, A., Filliol, D., et al. (2013). Mu Opioid Receptors on Primary Afferent Nav1.8 Neurons Contribute to Opiate-Induced Analgesia: Insight from Conditional Knockout Mice. *PLoS One* 8, 1–18. doi: 10.1371/journal.pone.0074706.

Westlund, K. N., Bowker, R. M., Ziegler, M. G., and Coulter, J. D. (1983). Noradrenergic projections to the spinal cord of the rat. *Brain Res* 263, 15–31. doi: 10.1016/0006-8993(83)91196-4.

West, W. L., Yeomans, D. C., and Proudfit, H. K. (1993). The function of noradrenergic neurons in mediating antinociception induced by electrical stimulation of the locus coeruleus in two

different sources of Sprague-Dawley rats. *Brain Res* 626, 127–135. doi: 10.1016/0006-8993(93)90571-4.

Williams, J. T., Egan, T. M., and North, R. A. (1982). Enkephalin opens potassium channels on mammalian central neurones. *Nature* 299, 74–77.

Yaksh, T. L. (1979). Direct evidence that spinal serotonin and noradrenaline terminals mediate the spinal antinociceptive effects of morphine in the periaqueductal gray. *Brain Res* 160, 180–185. doi: 10.1016/0006-8993(79)90616-4.

Yaksh, T. L., Eddinger, K. A., Kokubu, S., Wang, Z., DiNardo, A., Ramachandran, R., et al. (2019). Mast Cell Degranulation and Fibroblast Activation in the Morphine-induced Spinal Mass. *Anesthesiology* 131, 132–147. doi: 10.1097/ALN.0000000000002730.

Yaksh, T. L., and Rudy, T. A. (1977). Studies on the direct spinal action of narcotics in the production of analgesia in the rat. *J Pharmacol Exp Ther* 202.

Yang, S.-W., Zhang, Z.-H., Wang, R., Xie, Y.-F., Qiao, J.-T., Dafny'f', N., et al. (1994). Norepinephrine and Serotonin-induced Antinociception Are Blocked by Naloxone With Different Dosages. *Brain Res Bull* 35, 113–117.

Yeomans, D. C., Clark, F. M., Paice, J. A., and Proudfit, H. K. (1992). Antinociception induced by electrical stimulation of spinally projecting noradrenergic neurons in the A7 catecholamine cell group of the rat. *Pain* 48, 449–461. doi: 10.1016/0304-3959(92)90098-V.

Yeung, J. C., and Rudy, T. A. (1980a). Multiplicative Interaction between Narcotic Agonisms Expressed at Spinal and Supraspinal Sites of Antinociceptive Action as Revealed by Concurrent Intrathecal and Intracerebroventricular Injections of Morphine. *Journal of Pharmacology and Experimental Therapeutics* 215, 633–642.

Yeung, J. C., and Rudy, T. A. (1980b). Sites of Antinociceptive Action of Systemically Injected Morphine: Involvement of Supraspinal Loci as Revealed by Intracerebroventricular Injection of Naloxone. *Journal of Pharmacology and Experimental Therapeutics* 215, 626–632.

Yeung, J. C., Yaksh, T. L., and Rudy, T. A. (1975). Effects of brain lesions on the antinociceptive properties of morphine in rats. *Clin Exp Pharmacol Physiol* 2, 261–268. doi: 10.1111/j.1440-1681.1975.tb03031.x.

CHAPTER 3: Activity measurements correlate descending pain modulatory structures in noradrenaline-mediated pain modulation

Introduction

Activity measurements via calcium imaging from neurons in awake, behaving animals allow for the identification of brain regions that respond to and coordinate complex behaviors. Chapter 2 of this dissertation demonstrates the importance of LC activity, and resulting spinal noradrenaline release, in the expression of systemic morphine antinociception, as well as the antinociception driven by activation of vlPAG as the driver of downstream DPMS activity. While this study utilized a variety of powerful techniques, such as pharmacology, behavior, anatomy, and electrophysiology, it did not investigate the activity of circuit elements uncovered in awake animals experiencing opioid administration or acute pain. This current study endeavors to further investigate the activity of the LC, as well as excitatory inputs to LC from vlPAG posited to drive a large portion of the descending NA from the LC, under these conditions.

As mentioned in Chapter 2, a significant paradox exists regarding how LC activity might be modulated by opioid administration. Seminal slice electrophysiology work in rats demonstrates that LC is profoundly inhibited by opioids due to high expression of the mu-opioid receptor, which couples to G protein-coupled inwardly rectifying potassium channels (Williams et al., 1982; Banghart and Sabatini, 2012). However, stimulation of the ventral portion of LC produces spinal NA-dependent antinociception (West et al., 1993), and our own work in mice in Chapter 2 of this dissertation implies that LC must be activated by opioids to produce full morphine antinociception as evidenced by increased c-fos expression in LC after systemic morphine, as well as the suppression of morphine antinociception on acute pain assays after LC

silencing or ablation. Calcium imaging studies, however, will provide unequivocal evidence of this activity increase and are therefore endeavored here.

Calcium imaging using the calcium indicator GCaMP and fiber photometry via implanted optical cannulas of the NAergic neurons of the LC has been performed in a number of publications on diverse behaviors such as fear memory formation, maternal behavior, and hedonic responses (Chen et al., 2021; Dvorkin and Shea, 2022; Wilmot et al., 2022). To our current knowledge, however, there is only one study investigating LC NAergic neuron activity in response to acute noxious stimuli (Moriya et al., 2019). In this study, LC activity increased upon stimulus onset and persisted for a few seconds after a pinch or heated probe applied to the tail. In contrast, gentle touch and low heat produced no change in LC activity. Additionally, there are no studies that investigate calcium responses during active behavior in the glutamatergic vlPAG inputs to LC.

In this study, we use fiber photometry to measure calcium dynamics of LC NAergic neurons and glutamatergic vlPAG neurons that project to LC. Our findings confirm increased LC activity in response to opioids, as well as noxious stimulation-produced LC and PAG-to-LC calcium activity that may be responsible for downstream release of NA in the spinal cord to modulate incoming pain signals.

Results

Locus coeruleus noradrenergic neurons are activated by systemic morphine

In Chapter 2 of this dissertation, we report that mouse LC neurons express the mu-opioid receptor, which typically inhibits neuronal activity upon ligand binding. However, LC c-Fos expression increases upon systemic morphine administration, and LC activity is required for the

full expression of systemic opioid antinociception. To unequivocally demonstrate the response of LC NAergic neurons to systemic morphine administration, we performed fiber photometry activity measurements in *DBH*-cre mice transduced with AAV-DIO-GCaMP8s and implanted with an optical cannula in the right LC (**Figure 3.1A**). After subcutaneous injection of 10 mg/kg morphine, LC calcium activity increases from baseline within minutes of injection, whereas this increase was not seen when mice were injected with the vehicle saline (**Figure 3.1B**). This difference was captured as a significantly increased area under the curve in the morphine condition versus saline (**Figure 3.1C**).

Locus coeruleus noradrenergic neurons respond to noxious stimuli

To monitor LC NAergic neuron activity during presentation of a variety of modalities of noxious stimuli, we used fiber photometry calcium imaging through an implanted cannula of *DBH*-cre mice transduced with AAV-DIO-GCaMP8s in LC (**Figure 3.2A**). First, we recorded neural activity from mice on the Hargreaves apparatus to assess LC response to thermal heat. Each mouse was tested at 50% light intensity, which caused a paw withdrawal response at an average of 2.77 seconds, and 10% intensity as a relatively non-noxious control. In both cases, LC neurons exhibited a large ~1.5 second "salience" response to the onset of the visible light produced by the Hargreaves apparatus that was significantly larger in the brighter 50% intensity condition. Subsequently, LC activity increased until the paw withdrawal and then quickly decayed to baseline in response to the noxious heat stimulus. In contrast, after the salience response, LC activity remained at baseline in response to the non-noxious 10% intensity heat stimulus (**Figure 3.2B-C**).

Next, mice were challenged with application of single drops of acetone on each hindpaw (or room temperature water as a control) to assay the LC response to a cold thermal stimulus. LC activity increased to a higher peak and exhibited a longer elevation above baseline when the mouse was presented with acetone than the water control (**Figure 3.2D-E**). Finally, LC calcium activity was recorded in response to pin prick or light touch with a 0.16g von Frey filament applied to the hindpaw. In this case, the fluorescence change was short-lived and was slightly but significantly larger in response to the noxious pin prick stimuli (**Figure 3.2F-G**). In all assays, we did not find a difference in the amplitude or pattern of calcium activity when the stimuli were placed on the ipsilateral or contralateral hindpaw. Therefore, we pooled trials from both hindpaws together. Taken together, these results suggest that LC encodes a salience response and subsequent noxious stimulus information in a time-locked and specific fashion that decays quickly after the offset of the stimulus, especially in thermal assays.

PAG neurons that project to LC respond to noxious stimuli

To understand how the inputs to LC established in Chapter 2 respond to noxious stimuli and may therefore shape the acute pain-induced activity changes in LC, we repeated the same fiber photometry recordings in **Figure 3.2**, this time transducing DPMS neurons that input to LC with GCaMP and implanting a fiber optic cannula in that brain region. To isolate the glutamatergic PAG neurons that project to LC and peri-LC, we injected a retrograde AAV encoding flp recombinase (AAVrg-FlpO) in the LC of *VGLUT2*-cre mice and a cre-ON, flp-ON GCaMP6M virus in vlPAG, followed by a fiber optic cannula in PAG (**Figure 3.3A**).

First, PAG-to-LC neural activity was recorded in response the noxious 50% intensity Hargreaves assay compared to a non-noxious 10% intensity. Similar to LC activity on the

Hargreaves assay, PAG-to-LC neurons display a stark increase in fluorescence upon stimulus onset, even before the stimulus becomes noxious (0 to 1.5 s). Unlike the LC, the calcium activity of PAG-to-LC neurons continues to increase until the paw withdrawal response occurs at an average of 2.6 seconds and remains elevated for tens of seconds after the withdrawal response while the mouse is displaying other nocifensive and escape behaviors. As observed with LC neuronal activity, PAG-to-LC neurons exhibited an increased in calcium activity upon onset of the non-noxious 10% intensity stimulus, but this response decayed back to baseline. Interestingly, PAG-to-LC neuron calcium activity in mice subjected to the non-noxious heat displayed a delayed increase in activity that matched the response to the noxious heat by 5-10 seconds after stimulus onset (**Figure 3.3B-C**), although it is unclear whether this increase is due to eventual noxious characteristics of the low heat stimulus or possibly a defensive response to the ongoing light stimulus (which cuts off at 20 seconds in the absence of a nocifensive withdrawal response).

Next, the calcium response in PAG-to-LC neurons to a drop of acetone or room temperature water placed on the paw was measured. While the calcium activity increased upon stimulus onset, the response was larger and remained above baseline past 15 seconds in response to the acetone drop, whereas the response to the control water drop decayed more quickly, leading to a significantly larger area under the curve in response to the acetone drop (**Figure 3.3D-E**). Finally, PAG-to-LC calcium activity was significantly increased in response to a pin prick as compared to light touch with a 0.16 g von Frey filament (**Figure 3.3F-G**). As with our measurements of LC activity, we did not observe differences in the calcium response of PAG-to-LC neurons depending on whether the contralateral or ipsilateral hindpaw was targeted, so we pooled trials from both paws for analysis. Together, these results demonstrate that PAG-to-LC

neurons encode noxious stimulus information by exhibiting increased calcium activity in response to noxious stimuli as compared to non-noxious counterparts, but may also coordinate aspects of nocifensive responses that cause the calcium activity to remain elevated for some time after the painful stimulus is removed.

Discussion

In this study, we have established the presence of opioid-evoked and noxious stimulation-evoked activity in the LC and noxious-evoked activity in inputs to LC that have been implicated in nociceptive and morphine antinociceptive behavior in Chapter 2. Both the LC noradrenergic neurons and glutamatergic PAG neurons that project to the LC appear to exhibit strong responses to the onset of a noxious stimulus (i.e. the visible light of the Hargreaves assay before the heat becomes noxious), as well as increased activity in response to the noxious aspect of the stimulus (i.e. the ramping of the heat stimulus on the Hargreaves) that is separable from a non-noxious control. It is possible that this increased LC activity leads to antinociceptive downstream release of noradrenaline in the spinal cord to blunt the perception of incoming noxious stimuli, although these recordings were not specifically targeted to the ascending or descending module of the LC. Future experiments using retrograde tracers will be necessary to determine whether this general LC activation is segregated to only one module, and how this might affect noradrenaline release in the forebrain and/or spinal cord.

We found that both cell groups tested here exhibited a "salience" response to the onset of the noxious stimulus. This response has been reported in the literature using *in vivo* electrophysiology recordings of LC NAergic neurons, whose phasic activity has been shown to increase in response to a variety of non-noxious stimuli to encode the salience or significance of

a stimulus via downstream targets (Aston-Jones and Bloom, 1981; Sara and Segal, 1991; Sara, 2009; Vazey et al., 2018). However, especially in the LC neurons whose activity quickly returns to baseline after stimulus offset, this salience response is potentially confounding for our interpretation of noxious stimulus-induced activity. We found that in LC NAergic neurons, there was only a small significant difference in calcium response to light touch vs. pin prick, although the behavioral response to the pin was much more pronounced. This may be because the duration of the stimulus is shorter than the potential calcium salience response.

For this reason, we found that the Hargreaves assay was extremely powerful in these studies as the response to the visible light stimulus onset is temporally separated from the onset of the noxious heat and withdrawal response. In LC NAergic neurons, the salience response was visible in the low 10% and high 50% intensity Hargreaves trials, but there was only a subsequent increase in calcium activity in the high intensity trials. Similarly, PAG-to-LC neurons exhibited an increase in calcium signaling at trial onset in at both intensities, but the signal only continued to increase in high intensity trials, while it relaxed back toward baseline in the low intensity trials. Interestingly, this presence of a salience response even in non-noxious trials was not seen by the researchers in Moriya et al. (2019). It is unclear why this might be the case, although some possible differences in the studies might include fiber implantation position, which was not reported, or the fact that the other study performed the photometry recording hours after implantation surgery instead of allowing for days to weeks of recovery.

In addition to the similarities between the LC and PAG-to-LC calcium signals on the same assays, including the initial salience response to the cues and separable response to the noxious stimulus itself, the calcium activity in the two cell groups also exhibits distinct differences. LC activity is extremely time locked to the noxious stimulus and decays quickly

back to baseline after its removal. In contrast, PAG-to-LC neurons exhibit calcium responses that remain elevated above baseline for tens of seconds after the cessation of the noxious stimulus. It is possible that PAG-to-LC neurons encode not only the noxious information, but also are responsible for coordinating nocifensive responses that occur after the initial withdrawal (i.e. escape, licking, attending, etc.). We established in Chapter 2 that a subset of PAG-to-LC neurons bifurcate and project to the RVM. Previous studies have shown that PAG glutamatergic output to RVM-adjacent areas control aspects of nocifensive behavior, such as freezing (Tovote et al., 2016). It is likely that the PAG-to-LC glutamatergic neurons captured in our viral strategy forward noxious stimulus information to the LC but may also coordinate longer lasting nocifensive behaviors by projections to other medullary regions.

Finally, we assayed the hind paws both ipsilateral and contralateral to the recording site in LC or PAG. Interestingly, we did not find any differences in the calcium activity in response to any of our unilateral manipulations. We hypothesized that we might find a lateralized response to the stimulus based on whether the drive to activate these neurons comes from primarily ascending, nociceptive signals from the spinal cord or from upstream in the descending pain modulatory pathway. Incoming nociceptive signals synapse in the ipsilateral dorsal horn and then decussate at the level of the spinal cord to travel contralaterally to supraspinal areas. These ascending spinal neurons appear to project to the PAG and LC, although the evidence for the ascending projections to the LC appear to be debated in the existing literature (Aston-Jones et al., 1991; Benarroch, 2005). If this ascending noxious information directly drives descending LC activity in a closed loop fashion, it might be expected to observe a larger response in LC and PAG-to-LC activity when the noxious information is delivered contralaterally to the recording site.

On the contrary, in our experience, projections within the DPMS at the supraspinal level (i.e, PAG-to-LC) appear to be largely ipsilateral. Therefore, we expected that if LC and PAG-to-LC activity is driven largely by inputs to the DPMS (in this case, LC activity may be driven by our own recorded PAG-to-LC neurons themselves), our calcium recordings might be strongest when the signals that need to be modulated in the spinal cord are ipsilateral to the recording site. However, LC projections to the spinal cord have been shown to terminate bilaterally with only a small bias toward the ipsilateral side (Bruinstroop et al., 2012), suggesting that the DPMS may act in a diffuse manner without much regard for the lateralization of the incoming stimulus. In our case, the signals did not differ in amplitude or time course whether the stimulus was delivered ipsilaterally or contralaterally, so we were unable to use this metric to determine the contributions of ascending and descending inputs.

Overall, this work demonstrates that LC noradrenergic neurons and glutamatergic inputs to the LC from the vlPAG respond with increased activity in response to salient and noxious stimuli. This activation of LC NAergic neurons may lead to the release of NA in the spinal cord to modulate incoming nociceptive signals, although future experiments will be necessary to confirm that these activity measurements reflect the activity of the more specific descending LC module. These results indeed fit with the circuit model established in Chapter 2 that vlPAG is a primary driver of LC activity that causes antinociceptive downstream release of spinal NA.

Materials and Methods

Animals

All procedures were performed in accordance with protocols approved by the University of California San Diego Institutional Animal Care and Use Committee (UCSD IACUC protocol S16171) and guidelines from the US National Institutes of Health Guide for Care and Use of Laboratory Animals. Mice were group housed, maintained on a 12-hour reversed light/dark cycle, and allowed *ad libitum* access to food and water. Experiments were performed under red lighting during the dark period. Strains used include the following: *DBH*-cre (MMRRC/GENSAT #032081-UCD, Tg(DBH-cre)HK212Gsat/Mmucd) and *VGLUT2*-IRES-cre (Jackson Laboratory stock #028863, B6J.129S6(FVB)-Slc17a6$^{tm2(cre)Lowl}$/MwarJ). Mice were used for experiments between the ages of 8-20 weeks. Both male and female mice were used for all experiments.

Viral constructs

The following viruses were purchased from Addgene: AAVretro-Ef1a-FlpO (Addgene 55637, titer 1.3x10^{13}), AAV8-Ef1a-Con/Fon-GCaMP6M (Addgene 137119, titer 2.4 x10^{13}), AAV1-syn-FLEX-jGCaMP8s (Addgene 162377, titer 2.3 x10^{13}), AAV5-hSyn-mCherry (Addgene 114472, titer 2.3 x10^{13}).

Surgeries

Before surgery, mice were deeply anesthetized by induction at 5% isoflurane, after which anesthesia was maintained by 2% isoflurane (SomnoSuite, Kent Scientific). After mice were placed in a stereotaxic frame (David Kopf Instruments), a midline incision was made through the scalp following fur removal and site preparation by alternating povidone-iodine and 70% isopropyl alcohol. 100-250 nl of virus was injected at a rate of 100 nl/min at defined stereotaxic

coordinates. For fiber photometry recordings in LC, *DBH*-cre mice were injected in LC with DIO-GCaMP8s + mCherry unilaterally in the right LC. For recordings from PAG-to-LC neurons, *VGLUT2*-cre mice were injected in unilateral right LC with AAVretro-FlpO and in unilateral right PAG with Cre-on/Flp-on-GCaMP6M. The stereotaxic coordinates used for viral injections are as follows: vlPAG, angle ±10°, AP -4.60 mm, ML ± 0.32 mm, DV 2.85 mm; LC, angle ±10°, AP -5.45, ML ±0.75 mm, DV 4.10 mm. After 3-5 weeks of viral expression, mice were implanted unilaterally with optical fiber implants in LC or PAG. The following coordinates were used for optical implants: vlPAG, angle -10°, AP -4.60 mm, ML ± 0.35 mm, DV 2.60 mm; LC, angle -15°, AP -5.45, ML ±0.90 mm, DV 3.90 mm. Implants used were 200 μm, 0.37 NA optical fibers (Neurophotometrics) and were secured with light-cured dental epoxy. For all surgeries, mice were administered 5 mg/kg ketoprofen (MWI Veterinary Supply) before the end of surgery and 24 hours later and monitored for recovery for 5 days. All mice were given one week to recover from implant surgeries before fiber photometry recordings.

Fiber Photometry

For fiber photometry recordings in LC, *DBH*-cre mice were injected in LC with DIO-GCaMP8s + mCherry and implanted unilaterally in the right LC. For recordings from PAG-to-LC neurons, *VGLUT2*-cre mice were injected in unilateral right LC with AAVretro-FlpO and in unilateral right PAG with Cre-on/Flp-on-GCaMP6M with implants in unilateral right PAG. For fiber photometry recordings, a commercially available fiber photometry system was used (FP3001, Neurophotometrics). Recordings were made through a single fiber optic cable. For LC recordings, a 470 nm LED was used to record GCaMP activity and 560 nm LED for control wavelength. For PAG-to-LC activity recordings, a 470 nm LED was used to record GCaMP

activity and 415 nm LED isosbestic wavelength was used as control. Data analysis of fluorescence recordings was conducted using the pMAT open source photometry analysis package (Bruno et al., 2021) in MATLAB 2021a (Mathworks), which allows for the scaling of the control channel to correct for movement and bleaching, and subsequently calculates peri-event time histograms of ΔF/F and z-score values. Other calculations, such as baseline correction and area under the curve analysis, were completed using custom scripts in Igor Pro (Wavemetrics). Fluorescence traces are presented in the figures as the mean ± SEM of multiple individual traces from all mice (e.g. for recordings from 10 mice with 4 trials each, the figures reflect the mean ± SEM of 40 trials).

Behavior assays

Thermal Assays

Mice were placed on the heated surface (32°C) of a Hargreaves apparatus (IITC Life Science, Model 400 Heated Base, Series 8 Model 390G light source) in a clear plastic cylinder and habituated for 15 minutes. During testing, the Hargreaves apparatus was set to either 10% or 50% intensity. The light stimulus was targeted to one hindpaw at a time and was manually removed when a withdrawal response was observed. Each trial automatically terminated at 20 seconds if no withdrawal response was observed. Mice were tested three times on each paw with a 3-5 minute intertrial interval. The response to the different intensities was tested on different days.

To test response to a cold thermal stimulus, the acetone drop assay was used. Mice were placed in a clear cylinder on an elevated wire grid and allowed to habituate for 15 minutes. A syringe fitted with polyethylene tubing (Braintree Scientific, Inc.) was used to place a single drop

of acetone or room temperature water on the plantar surface of one hind paw at a time. The mice were tested with each solution on different days. Within a recording day, each hindpaw was tested twice, with a 3-5 minute intertrial interval.

Mechanical Assays

Mice were probed for mechanical responses using either a pin prick or non-noxious von Frey fiber. Mice were placed in a clear cylinder on an elevated wire grid and allowed to habituate for 15 minutes. The plantar surface of each hindpaw was probed with either a 0.16 g von Frey fiber (Ugo Basile) or fine insect pin (size 000, ThermoFisher Scientific NC9295307). Each hindpaw was probed 3 times with each stimulus during a single testing session with a 1-3 minute intertrial interval.

Statistics

Data in each figure are presented as mean ± SEM and individual data points from experimental replicates are plotted in summary figures. Statistical analyses were performed in GraphPad Prism. The test performed, test statistic, number of experimental replicates, and mean ± SEM for each condition are provided in the figure legend. Individual p-values appear in the figures. Repeated measures within individual replicates were taken into account where applicable based on experimental design. Data were tested for normality using the Shapiro Wilk test, and non-parametric statistics were used when necessary.

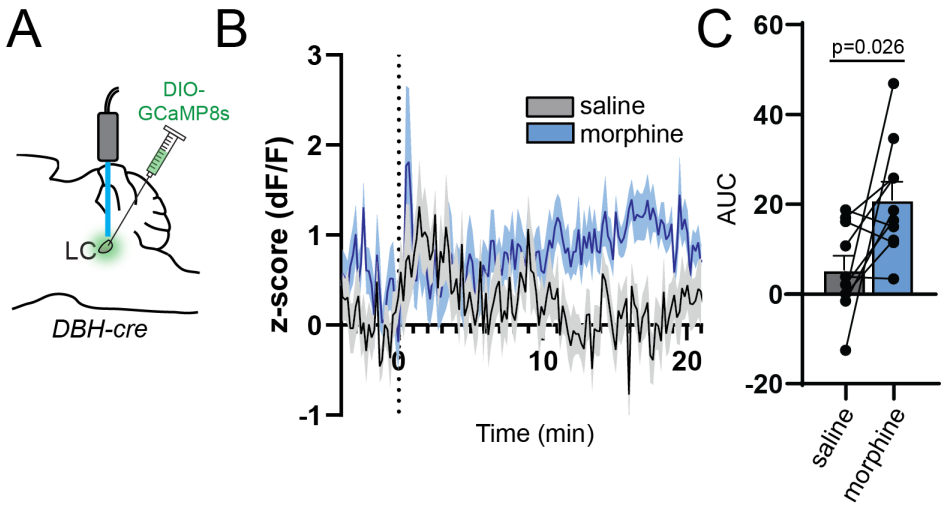

Figure 3.1. LC NAergic neuron calcium activity increases after systemic morphine administration.

A. Viral injection of cre-dependent GCaMP8s and fiber implantation for calcium imaging of LC noradrenergic neurons. **B.** Average GCaMP response to administration of subcutaneous morphine (10 mg/kg) or vehicle saline at time point 0 (n=10 mice, 1 trial each). **C.** Area under the curve analysis from 0 to 20 minutes after injection (saline: 5.44 ± 3.16, morphine: 21.00 ± 4.01; Two-sided paired t-test: t=2.652, n=10 pairs).

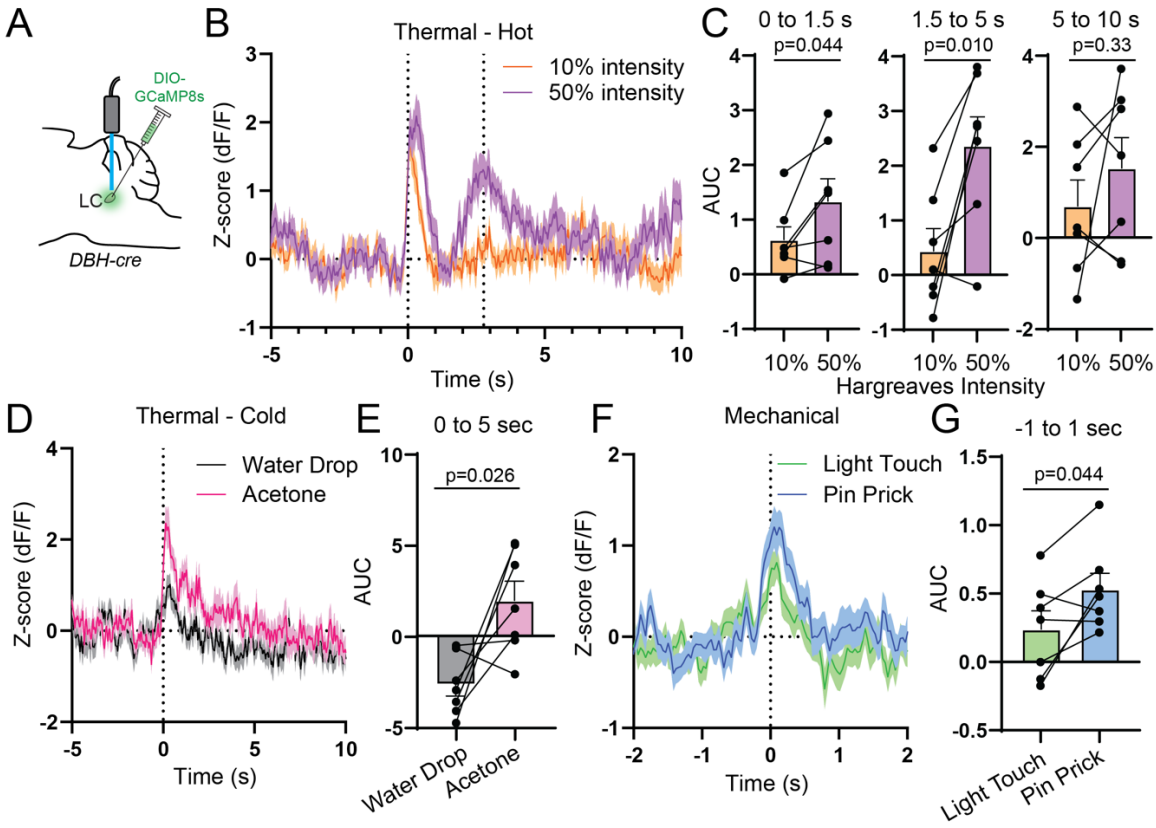

Figure 3.2. LC NAergic neural activity encodes salience and noxious stimulus presentation.

A. Viral injection of cre-dependent GCaMP8s and fiber implantation for calcium imaging of LC noradrenergic neurons. **B.** Average GCaMP response to thermal heat on the Hargreaves apparatus at 10% (orange) and 50% (purple) intensity. The average withdrawal response to the 50% intensity light was 2.77 s (n= 7 mice, 6 trials each). **C.** Area under the curve analysis comparing GCaMP fluorescence at 3 time windows after Hargreaves presentation (10% intensity: 0-1.5 s, 0.63 ± 0.23, 1.5-5 s, 0.43 ± 0.41, 5-10 s, 0.69 ± 0.57; 50% intensity: 0-1.5 s, 1.33 ± 0.41, 1.5-5 s, 2.36 ± 0.53, 5-10 s, 1.52 ± 0.66; Two-sided paired t-tests: 0-1.5 s, t=2.547; 1.5-5 s, t=3.681; 5-10 s, t=1.052; n=7 pairs each). **D.** Average GCaMP response to presentation of acetone (pink) vs. room temperature water drop (black) on the hindpaw (n=7 mice, 4 trials each). **E.** Area under the curve analysis comparing GCaMP fluorescence from 0 to 5 seconds after stimulus presentation (Water drop: -2.67 ± 0.61, Acetone: 1.94 ± 1.07; Two-sided paired t-test: t=2.944, n=7 pairs). **F.** Average GCaMP response to pin prick vs. light touch (0.16g von Frey filament) on the hindpaw (n=7 mice, 6 trials each). **G.** Area under the curve analysis comparing GCaMP fluorescence from -1 to 1 seconds after stimulus presentation (light touch: 0.24 ± 0.13; Pin prick: 0.53 ± 0.12; Two-sided paired t-test: t=2.541, n=7 pairs). Mean ± SEM for all.

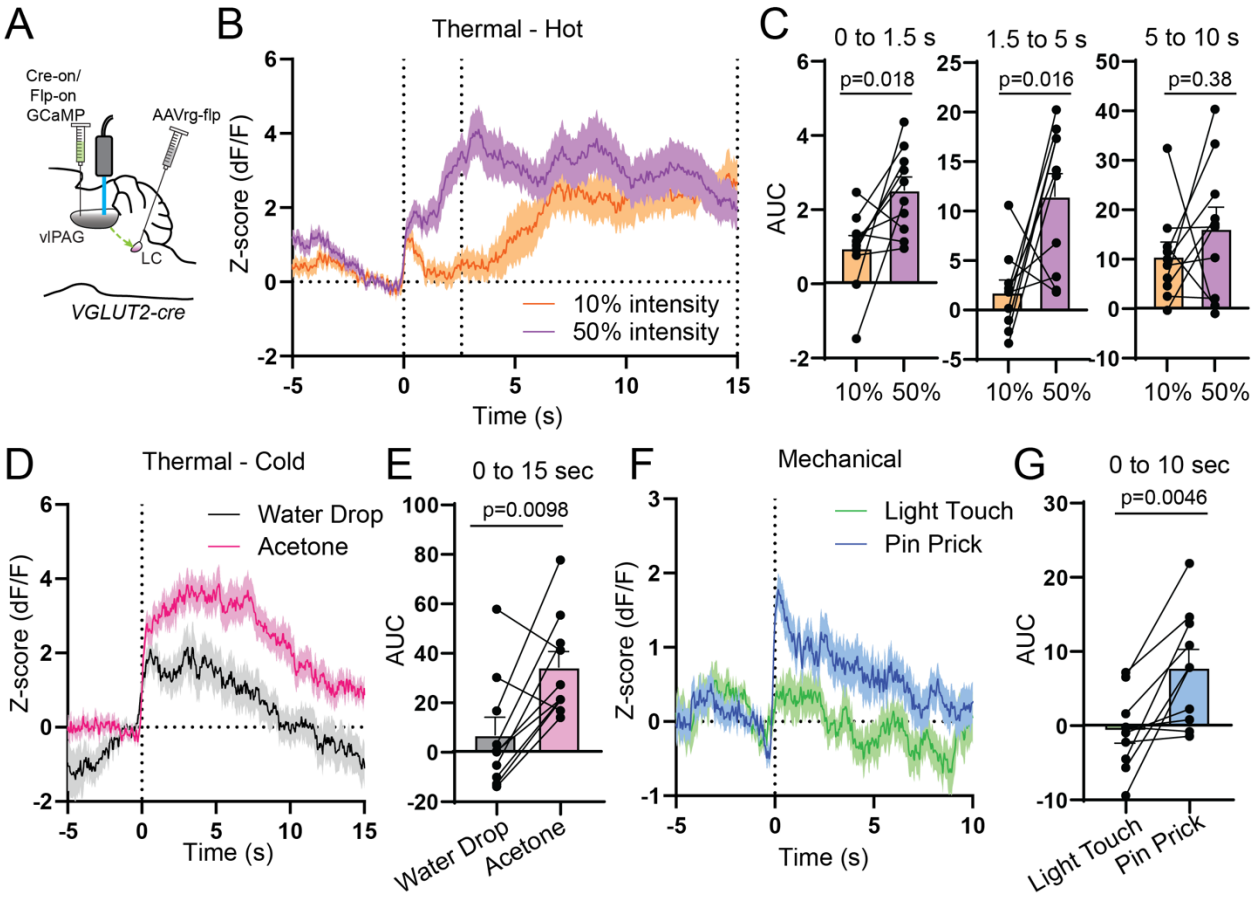

Figure 3.3. PAG neurons that project to LC respond strongly to noxious stimulus presentation.

A. Viral scheme to express GCaMP6M in PAG neurons that project to LC and fiber implantation in PAG for calcium imaging. **B.** Average GCaMP response to thermal heat on the Hargreaves apparatus at 10% (orange) and 50% (purple) intensity. The average withdrawal response to the 50% intensity light was 2.6 s (n=10 mice, 6 trials each). **C.** Area under the curve analysis comparing GCaMP fluorescence at 3 time windows after Hargreaves presentation (10% intensity: 0-1.5 s, 0.93 ± 0.34, 1.5-5 s, 1.78 ± 1.26, 5-10 s, 10.47 ± 2.90; 50% intensity: 0-1.5 s, 2.49 ± 0.36, 1.5-5 s, 11.49 ± 2.30, 5-10 s, 16.06 ± 4.34; Two-sided paired t-tests: 0-1.5 s, t=2.899; 1.5-5 s, t=2.942; 5-10 s, t=0.933, n=10 pairs each). **D.** Average GCaMP response to presentation of acetone (pink) vs. room temperature water drop (black) on the hindpaw (n=10 mice, 4 trials each). **E.** Area under the curve analysis comparing GCaMP fluorescence from 0 to 15 seconds after stimulus presentation (Water drop: 6.66 ± 7.15, Acetone: 34.0 ± 6.47; Wilcoxon matched-pairs signed rank test, n=10 pairs). **F.** Average GCaMP response to pin prick vs. light touch (0.16g von Frey filament) on the hindpaw (n=10 mice, 6 trials each). **G.** Area under the curve analysis comparing GCaMP fluorescence from 0-10 seconds after stimulus presentation (light touch: -0.79 ± 1.62; Pin prick: 7.78 ± 2.42; Two-sided paired t-test: t=3.750, n=10 pairs). Mean ± SEM for all.

Chapter 3, in part, is being prepared for submission for publication of the material. Lubejko, Susan T; Banghart, Matthew R. The dissertation author was the primary investigator and author of this material.

References

Aston-Jones, G., and Bloom, F. E. (1981). Norepinephrine-containing locus coeruleus neurons in behaving rats exhibit pronounced responses to non-noxious environmental stimuli. *The Journal of Neuroscience* 1, 887–900.

Aston-Jones, G., Shipley, M. T., Chouvet, G., Ennis, M., van Bockstaele, E., Pieribone, V., et al. (1991). "Afferent regulation of locus coeruleus neurons: anatomy, physiology and pharmacology," in *Neurobiolgoy of the Locus Coeruleus*, 47–75. doi: 10.1016/S0079-6123(08)63799-1.

Banghart, M. R., and Sabatini, B. L. (2012). Photoactivatable Neuropeptides for Spatiotemporally Precise Delivery of Opioids in Neural Tissue. *Neuron* 73, 249–259. doi: 10.1016/j.neuron.2011.11.016.

Benarroch, E. E. (2005). *Basic Neurosciences with Clinical Applications*. Butterworth-Heinemann.

Bruinstroop, E., Cano, G., Vanderhorst, V. G. J. M., Cavalcante, J. C., Wirth, J., Sena-Esteves, M., et al. (2012). Spinal projections of the A5, A6 (locus coeruleus), and A7 noradrenergic cell groups in rats. *Journal of Comparative Neurology* 520, 1985–2001. doi: 10.1002/cne.23024.

Bruno, C. A., O'Brien, C., Bryant, S., Mejaes, J. I., Estrin, D. J., Pizzano, C., et al. (2021). pMAT: An open-source software suite for the analysis of fiber photometry data. *Pharmacol Biochem Behav* 201, 173093. doi: 10.1016/j.pbb.2020.173093.

Chen, H., Xu, D., Zhang, Y., Yan, Y., Liu, J. X., Liu, C. X., et al. (2021). Neurons in the Locus Coeruleus Modulate the Hedonic Effects of Sub-Anesthetic Dose of Propofol. *Front Neurosci* 15. doi: 10.3389/fnins.2021.636901.

Dvorkin, R., and Shea, S. D. (2022). Precise and Pervasive Phasic Bursting in Locus Coeruleus during Maternal Behavior in Mice. *Journal of Neuroscience* 42, 2986–2999. doi: 10.1523/JNEUROSCI.0938-21.2022.

Moriya, S., Yamashita, A., Nishi, R., Ikoma, Y., Yamanaka, A., and Kuwaki, T. (2019). Acute nociceptive stimuli rapidly induce the activity of serotonin and noradrenalin neurons in the brain stem of awake mice. *IBRO Rep* 7, 1–9. doi: 10.1016/j.ibror.2019.05.005.

Sara, S. J. (2009). The locus coeruleus and noradrenergic modulation of cognition. *Nat Rev Neurosci* 10, 211–223. doi: 10.1038/nrn2573.

Sara, S. J., and Segal, M. (1991). Plasticity of sensory responses of locus coeruleus neurons in the behaving rat: implications for cognition. *Prog Brain Res* 88, 571–585.

Tovote, P., Esposito, M. S., Botta, P., Chaudun, F., Fadok, J. P., Markovic, M., et al. (2016). Midbrain circuits for defensive behaviour. *Nature* 534, 206–212. doi: 10.1038/nature17996.

Vazey, E. M., Moorman, D. E., and Aston-Jones, G. (2018). Phasic locus coeruleus activity regulates cortical encoding of salience information. *Proc Natl Acad Sci U S A* 115, E9439–E9448. doi: 10.1073/pnas.1803716115.

West, W. L., Yeomans, D. C., and Proudfit, H. K. (1993). The function of noradrenergic neurons in mediating antinociception induced by electrical stimulation of the locus coeruleus in two different sources of Sprague-Dawley rats. *Brain Res* 626, 127–135. doi: 10.1016/0006-8993(93)90571-4.

Williams, J. T., Egan, T. M., and North, R. A. (1982). Enkephalin opens potassium channels on mammalian central neurones. *Nature* 299, 74–77.

Wilmot, J. H., Puhger, K., Roshgadol, J., Tian, L., and Wiltgen, B. J. (2022). Phasic locus coeruleus activity facilitates hippocampus-dependent trace fear memory formation. *bioRxiv*. doi: 10.1101/2022.10.17.512590.

CHAPTER 4: Inputs to the locus coeruleus are modulated in response to persistent pain

Introduction

Chronic pain, which has many definitions but often refers to pain that persists after the site of injury has recovered or for longer than three months in humans (Apkarian et al., 2009; Rikard et al., 2023), presents an ongoing health crisis. Chapter 2 of this dissertation outlines noradrenergic pathways that are part of the descending pain modulatory system, revealing the importance of excitatory synapses in the LC from the vlPAG in systemic morphine antinociception and uncovering an inhibitory pathway from RVM to the LC whose inhibition is antinociceptive, likely via disinhibition of descending LC activity. While this study establishes these circuit elements in the context of acute pain, it is important to also study antinociceptive circuits in the context of chronic pain, as the results of these studies may provide the most translational benefit for human health.

The descending pain modulatory system (DPMS) has been studied in the context of chronic pain, but with complex and sometimes divergent results. It is thought that the balance, or perhaps the imbalance, of excitation and inhibition from descending structures contributes to behavioral hypersensitivity in chronic pain states. The rostroventral medulla (RVM) is mostly implicated in this research, as it exhibits distinct pain facilitatory and inhibitory neuronal classes that project to the spinal cord, known as On- and Off- cells, respectively. In early inflammatory pain, the facilitatory mechanisms are active. However, as this pain persists, molecular changes rebalance the facilitatory and inhibitory pathways to limit hypersensitivity (Ren and Dubner, 2002; Heinricher, 2016; Chen and Heinricher, 2019). Some studies indicate that RVM facilitation does persist throughout the persistent and chronic pain states, contributing to

hypersensitivity (Porreca et al., 2002). Given this, improper balancing of the pathways may lead to chronic pain states. The mechanisms of how the DPMS governs modulation of primary afferents entering the spinal cord from and around the site of injury may differ depending on the cause of the pain (i.e. inflammation vs. neuropathy, Vanegas and Schaible, 2004), however, further complicating our understanding of how the DPMS strikes the delicate balance between pain facilitation and inhibition. Within the PAG, there is evidence that neuropathic pain produces glutamatergic hypofunction, which possibly decreases the pain inhibitory output of the DPMS (Ho et al., 2013).

Outside of the canonical PAG and RVM pathways, there is evidence for the role of noradrenergic signaling in chronic pain. In models of nerve injury, noradrenergic signaling in the spinal cord appears protective of the onset of chronic hypersensitivity and the development of abnormal pain (Ossipov et al., 2014). However, other studies conversely posit that LC paradoxically results in pain facilitation longer after neuropathic injury (Brightwell and Taylor, 2009) and contributes to anxiodepressive behaviors that are comorbid in chronic neuropathic pain (Llorca-Torralba et al., 2019). At longer timepoints, it has been demonstrated that chronic pain reduces the noxious stimulation-evoked activity in LC, which would decrease the antinociceptive NA release in the spinal cord (Kimura et al., 2015; Hayashida and Obata, 2019), although other studies at similar or later time points refute this result by demonstrating increased noxious-stimulation evoked LC discharge in nerve-injured animals (Viisanen and Pertovaara, 2007; Alba-Delgado et al., 2021). One group has even labeled the LC as a chronic pain generator, and hypothesizes that within a month of neuropathic injury, LC activity shifts from descending inhibition of pain at the level of the spinal cord, to pain facilitation through ascending projections (Taylor and Westlund, 2017). It is possible that all of these viewpoints are true,

however, given that each study may focus on only specific timepoints throughout the probably dynamic LC response to chronic pain, highlighting the importance of taking a longitudinal view of pain chronification.

In this study, we use slice electrophysiology to measure changes in LC intrinsic activity, as well as excitatory inputs to LC, in response to a relatively short timepoint model of persistent inflammatory pain. While we did not find changes in LC intrinsic properties as a result of this manipulation, we observed excitatory hyperfunction of inputs to LC neurons, especially in the ventral portion of LC.

Results

Complete Freund's adjuvant induces persistent pain in mice

Complete Freund's adjuvant was used to induce persistent and long-lasting pain resulting from chronic immune activation and inflammation in the hindpaws of wildtype male and female mice (Stein et al., 1988). CFA-injected and uninjected control littermates were assessed for mechanical allodynia before and 1, 3, 5, and 7 days after bilateral intraplantar injection of undiluted CFA. Although baseline measurements prior to injection did not differ between the injured and uninjured group, robust mechanical allodynia as measured by a significant decrease in mechanical threshold on the von Frey assay was achieved by post-CFA Day 1. This effect persisted for 7 days post-injection (**Figure 4.1A**).

LC excitability is not modulated by persistent pain

To assess the circuit mechanisms by which the descending noradrenergic pain modulatory system described in Chapter 2 may change in the face of persistent pain, we used

whole cell patch clamp electrophysiology to assess alterations in membrane properties and electrical excitability in the LC dorsal and ventral tiers after induction of CFA-mediated allodynia. Recordings were taken from both dorsal and ventral LC neurons in an attempt to roughly segregate recordings to putative ascending and descending LC tiers (Li et al., 2016; Hirschberg et al., 2017).

First, to assess resting membrane properties, we measured resting membrane potential and tonic action potential firing, but found no difference between neurons recorded from control and CFA-injured mice in either the dorsal or ventral LC tier (**Figure 4.1B-C**). Further, we found no change in input resistance as a metric of voltage response in either cell group (**Figure 4.1D**). Finally, to measure LC neuron excitability in response to direct current injection, we performed firing rate versus current input (f-I) curves in the same dorsal and ventral LC neurons from control and CFA-injured mice. We found no difference in evoked firing between the groups in either the dorsal or ventral tier (**Figure 4.1E-F**). Taken together, these results indicate that this relatively short-term persistent pain state did not induce changes in the electrical properties or physiological response of LC neurons themselves.

Persistent pain enhances excitatory neurotransmission onto LC neurons

To assess persistent pain-related modulation of excitatory inputs onto LC neurons, we recorded miniature excitatory postsynaptic currents (mEPSCs) in dorsal and ventral LC neurons from uninjected and CFA-injected mice. In the dorsal LC, although the interevent interval as a measure of mEPSC frequency did not differ between control and CFA mice, the mEPSC amplitude was significantly increased in CFA-injured LC neurons (**Figure 4.2A-C**). In the ventral, putatively spinally-projecting portion of LC, mEPSC amplitude was significantly

increased and interevent interval was significantly decreased in neurons recorded from CFA-injured mice (**Figure 4.2D-F**). Together, these results suggest that LC neurons in both dorsal and ventral LC experience increased excitatory neurotransmission that may drive their downstream activity after a relatively short-term persistent pain experience.

Discussion

In this study, we investigated changes in the physiological properties of the LC and excitatory inputs to LC in response to a week of persistent inflammatory pain to investigate how LC-driven descending noradrenergic signaling may change in response to, and possibly contribute to, chronic pain states. Interestingly, we did not find changes in the intrinsic properties or evoked action potential firing in LC neurons themselves, regardless of whether the neurons recorded from were located in the dorsal, putative ascending, or ventral, putative descending tiers. This suggests that increased or decreased excitability of LC neurons themselves are not responsible for noradrenergic hyper- or hypofunction found in chronic pain states. Although this is a potentially surprising result, other studies utilizing *in vivo* recordings of LC activity in a model of neuropathic pain similarly did not find modulation of LC firing rates (Alba-Delgado et al., 2012).

We did find significant changes in miniature excitatory postsynaptic currents (mEPSCs), however, suggesting glutamatergic hyperfunction in the face of persistent pain in both the dorsal and ventral LC at this timepoint. To our knowledge, there is only one other study that specifically looked at evoked and spontaneous excitatory inputs to LC in slice during a persistent pain state at a similar time point. This study concluded that there were no differences in the frequency of spontaneous excitatory inputs, but did find an increase in amplitude (Rohampour et al., 2017).

While our experiments were performed all at the seven-day post-injury timepoint, differences between the studies include the injury modality (inflammatory vs. nerve constriction), the species (mouse vs. rat), and age used (adult vs. pup). Additionally, LC recordings in the noted study were not segregated by LC location, which revealed quite significant differences in our study.

Analysis of mEPSC amplitude and frequency can be indicative of which circuit elements are modified in the face of persistent pain. In dorsal LC neurons, the amplitude of the mEPSCs, but not the interevent interval, was increased. In the ventral LC, while the amplitude was increased, we also observed a decrease in the interevent interval, indicative of an increased frequency of mEPSCs. mEPSC amplitude changes can result from either presynaptic or postsynaptic modulation. However, increased mEPSC frequency is most likely caused by a change in the presynaptic properties of input neurons to LC. In Chapter 2, we establish a strong excitatory synaptic connection between vlPAG and ventral LC. It is possible that this synaptic connection is strengthened in the face of week-long persistent inflammatory pain. Alternatively, glutamatergic inputs to LC from other brain areas, such as the prefrontal cortex (PFC), lateral hypothalamus (LH), nucleus paragigantocellularis/rostroventrolateral medulla or any number of other brain areas that input strongly to LC (Ennis et al., 1992; Schwarz et al., 2015; Barcomb et al., 2022), may contribute to this modulation, as mEPSC recording is nonspecific to the input region. Future experiments will be required to investigate the modulation of vlPAG or any other LC input region in a pathway specific manner.

Our study focused on excitatory synaptic inputs to LC neurons. However, future studies should also include recordings of miniature postsynaptic inhibitory currents to create a stronger sense of how ascending and descending LC signals are controlled in the face of persistent pain. Our current understanding of inhibitory inputs to LC appears to lag behind excitatory

counterparts. There is an inhibitory GABAergic input to LC from the nucleus prepositus hypoglossi (PrH) (Aston-Jones et al., 1991), and Chapter 2 of this dissertation establishes a strong inhibitory input to ventral LC from the rostroventromedial medulla whose inactivation leads to LC disinhibition and antinociceptive spinal NA release. Additionally, local pericoerulear GABAergic microcircuits have been shown to gate LC phasic activity and arousal (Jin et al., 2016; Breton-Provencher and Sur, 2019; Kuo et al., 2020). It is unknown how inhibitory inputs from these areas or other potential inhibitory input regions may change in the face of persistent pain.

Finally, this study relied on a model of inflammatory persistent pain and assayed the electrophysiological state of LC neurons and their inputs after 7-10 days. Although this is a suitable model for persistent pain, considerable disagreement in the field exists over whether this model can be considered chronic pain, which typically would exhibit an increased duration. Future studies on LC inputs and chronic pain might benefit from the use of a neuropathic pain model, such as peripheral nerve ligation. First, the use of this model would build upon our findings here by comparing any changes in LC physiology that may differ between inflammatory versus neuropathic pain. Additionally, the neuropathic model would provide a long-lasting pain state that could be used to assay LC physiology at different timepoints, from acute injury within a few days of pain onset, to persistent and chronic pain states on the timescale of weeks to months. Understanding the intrinsic physiological responses of LC neurons and their inputs under these conditions will shed light on how any transitions in activity profile may occur and how downstream NA signaling is affected.

Overall, the results of this study begin to provide important insights on the effects of persistent pain on LC and LC input physiology. Although Chapters 2 and 3 demonstrate

important advances in our knowledge of LC and DPMS circuitry in acute pain and opioid antinociception, as well as reveal new antinociceptive pathways through the LC, it is important to determine if these circuit elements remain effective in the face of chronic pain to reveal their promise as future drug targets for patients experiencing long-lasting pain.

Materials and Methods

Animals

All procedures were performed in accordance with protocols approved by the University of California San Diego Institutional Animal Care and Use Committee (UCSD IACUC protocol S16171) and guidelines from the US National Institutes of Health Guide for Care and Use of Laboratory Animals. Mice were group housed, maintained on a 12-hour reversed light/dark cycle, and allowed *ad libitum* access to food and water. Experiments were performed under red lighting during the dark period. These experiments used C57Bl/6J (Jackson Laboratory stock #664) mice. Mice were used for experiments between the ages of 8-20 weeks. Both male and female mice were used.

Complete Freund's Adjuvant (CFA) injections

Persistent inflammatory pain was induced by bilateral intraplantar injection of CFA (Stein et al., 1988). Mice were lightly anesthetized with 2% isoflurane just before injection to minimize movement. Each hindpaw was injected just under the plantar skin with 10 ul of undiluted CFA (Sigma-Aldrich). After recovery from the isoflurane, mice were placed back in their cage and monitored for any signs of severe distress.

von Frey Assay

Mice were tested for mechanical thresholds using the von Frey assay. Mice were placed in a clear cylinder on an elevated wire grid and allowed to habituate for 20 minutes. Using the up-down method (Chaplan et al., 1994), von Frey filaments (Ugo Basile) of varying stiffnesses were applied to each hindpaw separately, with a 3-minute break until returning to the first paw, until a withdrawal response could be recorded and a 50% withdrawal threshold could be calculated. The resulting threshold values (in grams) for each paw were averaged together to calculate the mechanical threshold for each mouse. Mice were tested just before, and 1, 3, 5, and 7 days after the CFA injection.

Brain slice preparation

Mice were anesthetized with isoflurane before rapid decapitation. Brains were removed, blocked, and mounted in a VT1000s vibratome (Leica Instruments). Coronal midbrain slices (190 μm) containing the LC were prepared in ice-cold choline-based artificial cerebrospinal fluid containing 25 mM $NaHCO_3$, 1.25 mM NaH_2PO_4, 2.5 mM KCl, 7 mM $MgCl_2$, 25 mM glucose, 0.5 mM $CaCl_2$, 110 mM choline chloride, 11.6 mM ascorbic acid, and 3.1 mM pyruvic acid, equilibrated with 95% O_2/5% CO_2. Slice were transferred to 32°C oxygenated artificial cerebrospinal fluid (ACSF) containing 125mM NaCl, 2.5 mM KCl, 25 mM $NaHCO_3$, 1.25 mM NaH_2PO_4, 2 mM $CaCl_2$, 1 mM $MgCl_2$, and 10 mM glucose, osmolarity 290. Slices were incubated for 20 minutes, then brought to room temperature before recording.

Slice Electrophysiology

Slice physiology experiments were performed in a chamber continuously perfused with warmed (32°C) ACSF equilibrated with 95% O_2/5% CO_2. Recording pipettes were pulled from borosilicate glass on a P-1000 Flaming/Brown micropipette puller (Sutter Instruments) to a resistance of 1-3.5 MΩ. Recordings were made with an Axopatch 700B amplifier (Axon Instruments) and data sampled at 10 kHz, filtered at 3 kHz, and acquired using National Instruments acquisition boards and a custom version of ScanImage written in MATLAB (MathWorks). LC neurons were visually identified and confirmed to exhibit tonic action potential spiking of ~1.5 Hz. Recordings were taken from both dorsal and ventral LC neurons. Recordings of action potential spiking and resting membrane properties were made in current clamp with patch pipettes filled with an internal solution containing 135 mM $KMeSO_3$, 5 mM KCl, 5 mM HEPES, 4 mM MgATP, 0.3 mM NaGTP, 10 mM phosphocreatine, and 1.1 mM EGTA (pH 7.25, 290 mOsm kg^{-1}). Firing rate vs. current input (f-I) curves were constructed using 1-second steps of direct current input (-100, 50, 100, 150, 200, 250, 300 pA) 10 seconds apart.

Recordings of miniature excitatory postsynaptic currents (mEPSCs) were made in voltage clamp with patch pipettes filled with an internal solution containing 135 mM $CsMeSO_3$, 3.3 mM QX314 Cl^- salt, 10 mM HEPES, 4 mM MgATP, 0.3 mM NaGTP, 8 mM phosphocreatine, and 1 mM EGTA (pH 7.2-7.3, 295 mOsm kg^{-1}). Cells were held at -70 mV and rejected if holding currents became more negative than -200pA or if series resistance exceeded 25 MΩ. Recordings were made in the presence of tetrodotoxin (TTX; 1 μM), GABAzine (20 μM), and strychnine (10 μM). All electrophysiology data were processed in Igor Pro (Wavemetrics).

Statistics

Data in each figure are presented as mean ± SEM and individual data points from experimental replicates are plotted when possible. Statistical analyses were performed in GraphPad Prism. The test performed, number of experimental replicates, mean ± SEM for each condition, statistics provided by ANOVA and two-way ANOVA tests for each variable, and p-values for the overall test are provided in the figure legend. Individual p-values from statistical tests and those resulting from post hoc tests to correct for multiple comparisons appear in the figures. Repeated measures within individual replicates were taken into account where applicable based on experimental design. Data were tested for normality using the Shapiro Wilk test, and non-parametric statistics were used when necessary and possible.

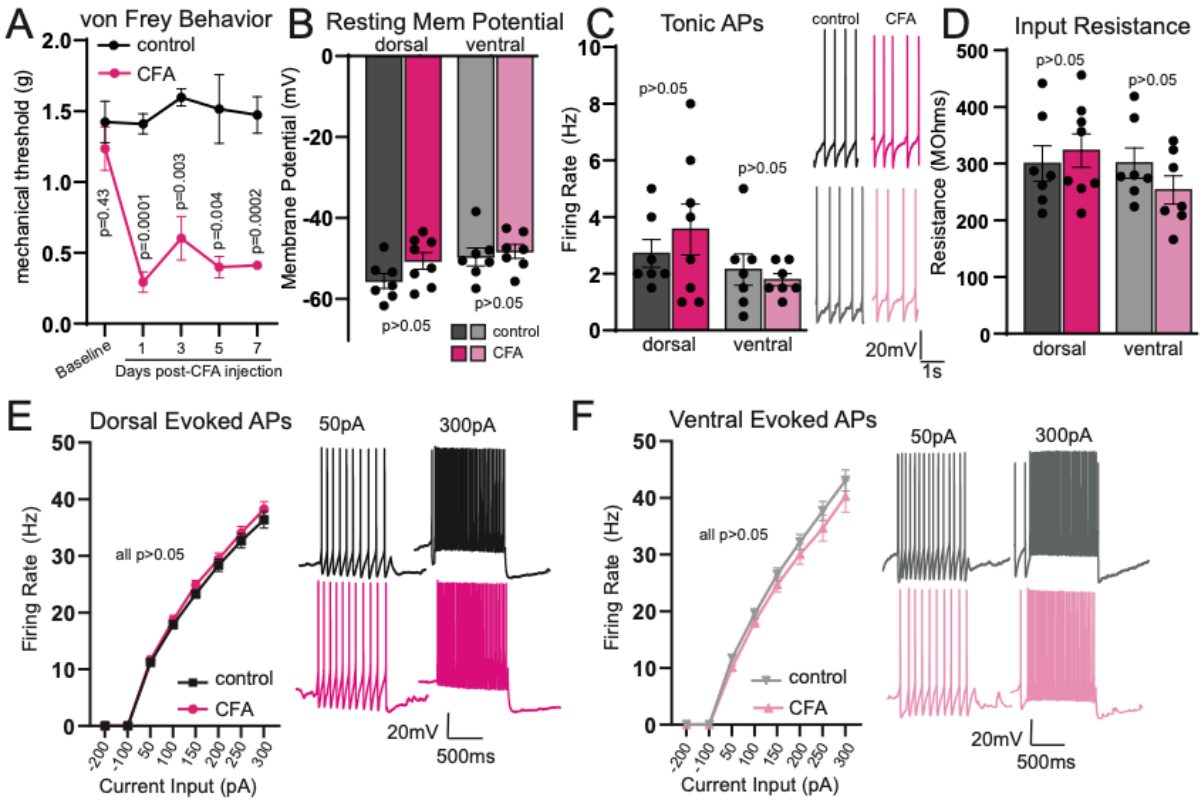

Figure 4.1. Persistent pain does not modulate LC electrical excitability and membrane properties.

A. von Frey mechanical thresholds before and 1, 3, 5, and 7 days after bilateral intraplantar CFA injection presented as the average mechanical threshold of both paws (two-sided unpaired t-test: baseline, t=0.8635, df=5; Day 1, t=10.76; Day 3, t=5.266; Day 5, t=5.036; Day 7, t=9.509; n=3 control, n=4 CFA). **B.** Resting membrane potential of dorsal and ventral LC neurons (two-sided unpaired t-test: dorsal, t=1.792, p=0.0964, n=7 control, n=8 CFA; ventral, t=0.4771, p=0.64, n=7 control, n=7 CFA). **C.** Tonic action potential firing rate of dorsal and ventral LC neurons (two-sided unpaired t-test: dorsal, t=0.7957, p=0.44, n=7 control, n=8 CFA; ventral, t=0.6019, p=0.59, n=7 control, n=7 CFA). **D.** Calculated input resistance of dorsal and ventral LC neurons (two-sided unpaired t-test: dorsal, t=0.5269, p=0.61, n=7 control, n=8 CFA; ventral, t=1.302, p=0.2173, n=7 control, n=7 CFA). **E.** Left, evoked action potential firing rate of dorsal LC neurons as a function of direct current injection (Two-way ANOVA with post hoc Sidak's multiple comparisons test; current input: F(1.484, 19.30)=1156, p<0.0001; CFA treatment: F(1,13)=0.9583, p=0.3455; n=7 control, n=8 CFA). Right, example traces of action potential firing at 50 and 300pA current injection steps for a control (black) vs. CFA (pink) dorsal neuron. **F.** Left, evoked action potential firing rate of ventral LC neurons as a function of direct current injection (Two-way ANOVA with post hoc Sidak's multiple comparisons test; current input: F(1.180, 14.16)=551.6, p<0.0001; CFA treatment: F(1,12)=1.228, p=0.2895; n=7 control, n=7 CFA). Right, example traces of action potential firing at 50 and 300pA current injection steps for a control (grey) vs. CFA (light pink) ventral neuron.

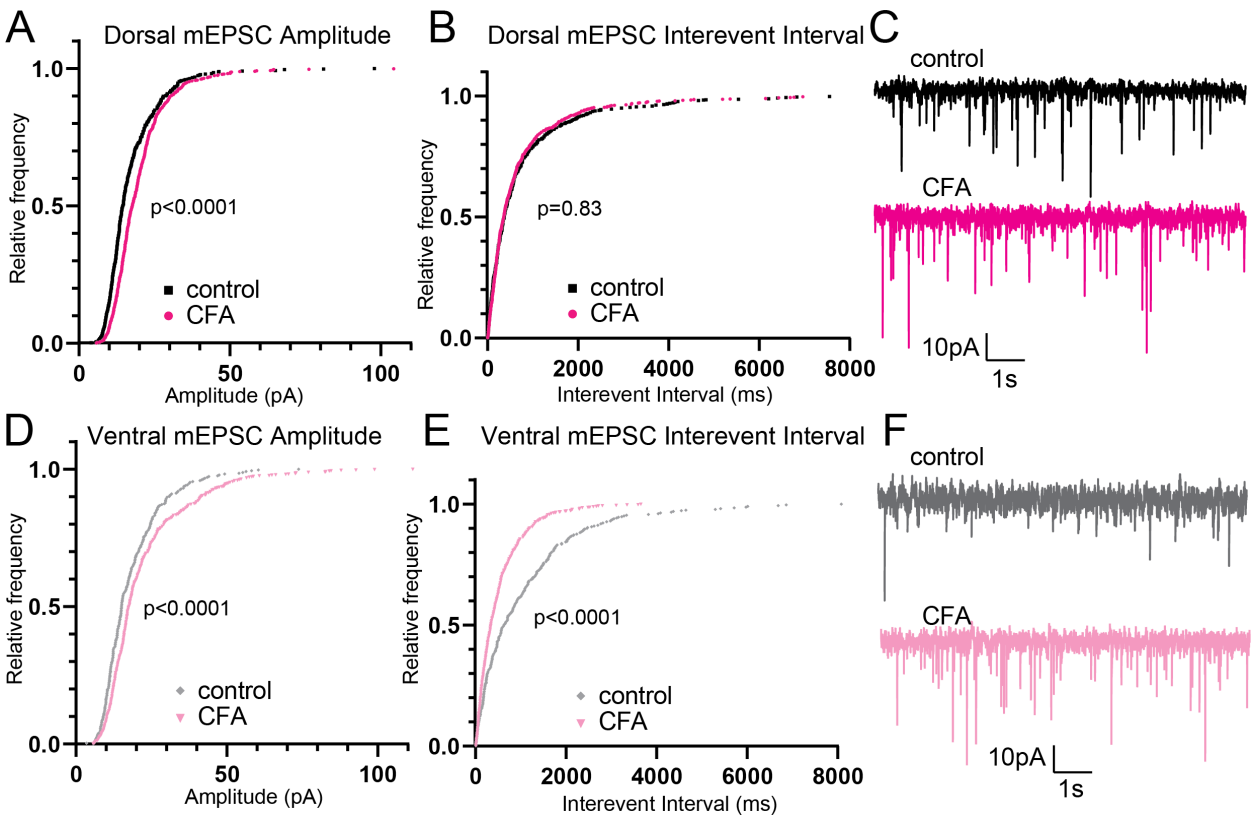

Figure 4.2. Persistent pain increases excitatory input onto LC neurons.

A. Cumulative histogram plot of mEPSC amplitude in dorsal LC (control: n=7 cells, 541 events; CFA: n=8 cells, 689 events; Kolmogorov-Smirnov test: D=0.2143). **B.** Cumulative histogram plot of mEPSC interevent interval in dorsal LC (control: n=7 cells, 541 events; CFA: n=8 cells, 689 events; Kolmogorov-Smirnov test: D=0.0358). **C.** Example traces of mEPSCs from dorsal control (black) and dorsal CFA (pink) LC neurons. **D.** Cumulative histogram plot of mEPSC amplitude in ventral LC (control: n=6 cells, 333 events; CFA: n=6 cells, 690 events; Kolmogorov-Smirnov test: D=0.1740). **E.** Cumulative histogram plot of mEPSC interevent interval in ventral LC (control: n=6 cells, 333 events; CFA: n=6 cells, 690 events; Kolmogorov-Smirnov test: D=0.2467). **C.** Example traces of mEPSCs from ventral control (grey) and ventral CFA (light pink) LC neurons.

Chapter 4 contains unpublished material coauthored with Banghart, Matthew R.

The dissertation author was the primary researcher and author of this chapter.

References

Alba-Delgado, C., Borges, G., Sánchez-Blázquez, P., Ortega, J. E., Horrillo, I., Mico, J. A., et al. (2012). The function of alpha-2-adrenoceptors in the rat locus coeruleus is preserved in the chronic constriction injury model of neuropathic pain. *Psychopharmacology (Berl)* 221, 53–65. doi: 10.1007/s00213-011-2542-7.

Alba-Delgado, C., Mico, J. A., and Berrocoso, E. (2021). Neuropathic pain increases spontaneous and noxious-evoked activity of locus coeruleus neurons. *Prog Neuropsychopharmacol Biol Psychiatry* 105. doi: 10.1016/j.pnpbp.2020.110121.

Apkarian, A. V., Baliki, M. N., and Geha, P. Y. (2009). Towards a theory of chronic pain. *Prog Neurobiol* 87, 81–97. doi: 10.1016/j.pneurobio.2008.09.018.

Aston-Jones, G., Shipley, M. T., Chouvet, G., Ennis, M., van Bockstaele, E., Pieribone, V., et al. (1991). "Afferent regulation of locus coeruleus neurons: anatomy, physiology and pharmacology," in *Neurobiolgoy of the Locus Coeruleus*, 47–75. doi: 10.1016/S0079-6123(08)63799-1.

Barcomb, K., Olah, S. S., Kennedy, M. J., and Ford, C. P. (2022). The Journal of Physiology Properties and modulation of excitatory inputs to the locus coeruleus. *J Physiol* 0, 1–20. doi: 10.1113/JP283605#support-information-section.

Breton-Provencher, V., and Sur, M. (2019). Active control of arousal by a locus coeruleus GABAergic circuit. *Nat Neurosci* 22, 218–228. doi: 10.1038/s41593-018-0305-z.

Brightwell, J. J., and Taylor, B. K. (2009). Noradrenergic neurons in the locus coeruleus contribute to neuropathic pain. *Neuroscience* 160, 174–185. doi: 10.1016/j.neuroscience.2009.02.023.

Chaplan, S. R., Bach, F. W., Pogrel, J. W., Chung, J. M., and Yaksh, T. L. (1994). Quantitative assessment of tactile allodynia in the rat paw. *J Neurosci Methods* 53, 55–63. doi: 10.1016/0165-0270(94)90144-9.

Chen, Q. L., and Heinricher, M. M. (2019). Descending Control Mechanisms and Chronic Pain. *Curr Rheumatol Rep* 21. doi: 10.1007/s11926-019-0813-1.

Ennis, M., Aston-Jones, G., and Shiekhattar, R. (1992). Activation of locus coeruleus neurons by nucleus paragigantocellularis or noxious sensory stimulation is mediated by intracoerulear excitatory amino acid neurotransmission. *Brain Res* 598, 185–195. doi: 10.1016/0006-8993(92)90182-9.

Hayashida, K., and Obata, H. (2019). Strategies to treat chronic pain and strengthen impaired descending noradrenergic inhibitory system. *Int J Mol Sci* 20, 822.

Heinricher, M. M. (2016). “Pain Modulation and the Transition from Acute to Chronic Pain,” in *Translational Research in Pain and Itch*, eds. C. Ma and Y. Huang (Dordrecht: Springer), 105–115.

Hirschberg, S., Li, Y., Randall, A., Kremer, E. J., and Pickering, A. E. (2017). Functional dichotomy in spinal- vs prefrontal-projecting locus coeruleus modules splits descending noradrenergic analgesia from ascending aversion and anxiety in rats. *Elife* 6, 1–26. doi: 10.7554/elife.29808.

Ho, Y. C., Cheng, J. K., and Chiou, L. C. (2013). Hypofunction of glutamatergic neurotransmission in the periaqueductal gray contributes to nerve-injury-induced neuropathic pain. *Journal of Neuroscience* 33, 7825–7836. doi: 10.1523/JNEUROSCI.5583-12.2013.

Jin, X., Li, S., Bondy, B., Zhong, W., Oginsky, M. F., Wu, Y., et al. (2016). Identification of a group of GABAergic neurons in the dorsomedial area of the locus coeruleus. *PLoS One* 11. doi: 10.1371/journal.pone.0146470.

Kimura, M., Suto, S., Morado-Urbina, C. E., Peters, C. M., Eisenach, J. C., and Hayashida, K. I. (2015). Impaired pain-evoked analgesia after nerve injury in rats reflects altered glutamate regulation in the locus coeruleus. *Anesthesiology* 123, 899–908.

Kuo, C., Hsieh, J., Tsai, H., Kuo, Y., Yau, H., Chen, C., et al. (2020). Inhibitory interneurons regulate phasic activity of noradrenergic neurons in the mouse locus coeruleus and functional implications. *J Physiol* Accepted A, JP279557. doi: 10.1113/JP279557.

Li, Y., Hickey, L., Perrins, R., Werlen, E., Patel, A. A., Hirschberg, S., et al. (2016). Retrograde optogenetic characterization of the pontospinal module of the locus coeruleus with a canine adenoviral vector. *Brain Res* 1641, 274–290. doi: 10.1016/j.brainres.2016.02.023.

Llorca-Torralba, M., Pilar-Cuéllar, F., Bravo, L., Bruzos-Cidon, C., Torrecilla, M., Mico, J. A., et al. (2019). Opioid Activity in the Locus Coeruleus Is Modulated by Chronic Neuropathic Pain. *Mol Neurobiol* 56, 4135–4150. doi: 10.1007/s12035-018-1361-9.

Ossipov, M. H., Morimura, K., and Porreca, F. (2014). Descending pain modulation and chronification of pain. *Curr Opin Support Palliat Care* 8, 143–151. doi: 10.1097/SPC.0000000000000055.

Porreca, F., Ossipov, M. H., and Gebhart, G. F. (2002). Chronic pain and medullary descending facilitation. *Trends Neurosci* 25, 319–325.

Ren, K., and Dubner, R. (2002). Topical review Descending modulation in persistent pain: an update. *Pain* 100, 1–6.

Rikard, S. M., Strahan, A. E., Schmit, K. M., Gery, ;, and Guy, P. (2023). MMWR, Chronic Pain Among Adults — United States, 2019–2021. Available at: https://www.cdc.gov/.

Rohampour, K., Azizi, H., Fathollahi, Y., and Semnanian, S. (2017). Peripheral nerve injury potentiates excitatory synaptic transmission in locus coeruleus neurons. *Brain Res Bull* 130, 112–117. doi: 10.1016/j.brainresbull.2017.01.012.

Schwarz, L. A., Miyamichi, K., Gao, X. J., Beier, K. T., Weissbourd, B., Deloach, K. E., et al. (2015). Viral-genetic tracing of the input-output organization of a central noradrenaline circuit. *Nature* 524, 88–92. doi: 10.1038/nature14600.

Stein, C., Millan, M. J., and Herz, A. (1988). Unilateral Inflammation of the Hindpaw in Rats as a Model of Prolonged Noxious Stimulation: Alterations in Behavior and Nociceptive Thresholds. *Pharmacol Biochem Behav* 31, 445–451.

Taylor, B. K., and Westlund, K. N. (2017). The Noradrenergic Locus Coeruleus as a Chronic Pain Generator. *J Neurosci Res* 95, 1336–1346.

Vanegas, H., and Schaible, H. G. (2004). Descending control of persistent pain: Inhibitory or facilitatory? *Brain Res Rev* 46, 295–309. doi: 10.1016/j.brainresrev.2004.07.004.

Viisanen, H., and Pertovaara, A. (2007). Influence of peripheral nerve injury on response properties of locus coeruleus neurons and coeruleospinal antinociception in the rat. *Neuroscience* 146, 1785–1794. doi: 10.1016/j.neuroscience.2007.03.016.

CHAPTER 5: Discussion

The goal of this dissertation is to address long-standing unanswered questions about the role of noradrenergic signaling, specifically from the locus coeruleus, in descending pain modulation and opioid-induced antinociception. In Chapter 2, we establish LC and opioid-insensitive glutamatergic projections from PAG to LC as major contributors to systemic morphine antinociception. Additionally, we reveal a newly described opioid-sensitive inhibitory projection from the medial RVM to LC, inhibition of which can drive antinociception outside of the context of opioid administration, likely through disinhibition of LC activity and subsequent spinal NA release. Next, in Chapter 3, we investigate the activity profile of LC NAergic neurons and PAG-to-LC projection neurons in response to noxious stimuli and determine that both cell groups are responsive to the salience of incoming stimuli, as well as their noxious qualities. Finally, in Chapter 4, we investigate the LC and glutamatergic inputs to LC in the context of persistent pain to begin to translate this newly established circuit model toward understanding its potential role in chronic pain.

How do these results update our understanding of descending NA circuits?

It has been long agreed upon that spinal NA release by DPMS-driven pain modulatory mechanisms is almost purely pain inhibitory and contributes to the antinociceptive effects of systemic opioids. We were surprised to find, then, that the locus coeruleus, which is the largest NAergic center of the brain, was not strongly implicated in systemic morphine analgesia. Existing literature reveals nearly opposite results, with one study using electrolytic lesions of LC reporting abolished morphine analgesia (Sasa et al., 1977) and another utilizing chemical lesions arriving at the conclusion of very little role for LC (Hammond and Proudfit, 1980). To avoid the

conflicting results arising from the lesion methodology, which is not specific for cell type and possibly not spatially restricted enough for the small size of LC, we used two viral methods to ablate or silence LC NAergic neurons specifically. Our results move LC back into position as a major contributor to systemic opioid antinociception, although other circuit elements are almost certainly involved as we did not block the analgesic effects of morphine entirely.

The agreed upon role of spinal NA release in descending pain modulation is recognized such that newer circuit models of the DPMS do often include the LC in addition to the vlPAG and RVM. We believe, however, that some of these models are based on assumptions from anatomical evidence that require much deeper functional understanding. As introduced, vlPAG projections to LC are fairly well established anatomically and physiologically such that these projections largely appear in DPMS circuit diagrams as driving LC activity for downstream NA release. Looking to the literature, however, the functional results of this pathway differ between studying synaptic physiology in slice (Barcomb et al., 2022) and activity patterns *in vivo* (Ennis et al., 1991). Additionally, one study previous study found that vlPAG neurons that project to the pericoerulear area, as labelled by nonspecific retrograde tracers and recorded from vlPAG cell bodies, are inhibited by opioids (Kim et al., 2018), which is at odds with the hypothesis that vlPAG drives LC activity for NA release in the context of opioid antinociception. We believe that our results uphold the assumption that PAG drives LC activity via glutamatergic projections. We report excitatory only drive from PAG that drives action potential spiking and excitatory postsynaptic currents in LC neurons in slice, noxious-evoked calcium activity in both, and a reduction in opioid antinociception when the glutamatergic vlPAG inputs to LC specifically are chemogenetically inhibited. However, our model disagrees with an opioid-sensitive vlPAG input and instead finds that these synapses, using slice electrophysiology, optogenetics, and

pharmacology, are minimally opioid sensitive. It is possible that this difference arises from the use of nonspecific retrograde tracers in Kim et al. (2018) that may capture presynaptic vlPAG cell bodies that do not project directly to LC NAergic neurons whereas our methodology recorded currents in the postsynaptic LC neurons to assay incoming signals.

Our addition to the DPMS circuit model of inhibitory input from RVM to LC is completely novel. Modern DPMS circuit models do occasionally acknowledge communication between the RVM and LC (Ossipov et al., 2010). There is recent evidence that LC projections *to* medial RVM mediate aspects of visceral pain (Kong et al., 2023). However, circuit models that include RVM projections to LC are likely referring to the sizeable body of literature regarding rostroventro*lateral* medullary (RVLM) inputs to LC, which are excitatory and may mediate some sensory inputs to LC (Ennis and Aston-Jones, 1988; Ennis et al., 1992). While this projection is undoubtedly important and well-established, we believe that our viral methods are spatially restricted enough to characterize another RVM input to LC, this time from the rostroventro*medial* medulla. Although we initially hypothesized that this projection would be similarly mediated by excitatory amino acids to drive even further downstream NA release, we were surprised to find a largely inhibitory postsynaptic effect, both on LC spiking as well as evoked postsynaptic currents.

Open questions regarding the RVM-to-LC projection

Our anatomical, electrophysiological, and behavioral results work in concert to establish an inhibitory projection from RVM to LC. However, there are open questions regarding this projection that should be of future study. First, is there a functional role for sparse excitatory synapse from RVM to LC? Although our study focuses on the inhibitory inputs, current clamp

data indicate that a small number of LC neurons recorded were excited by optoactivation of RVM terminals. This result carried into our synaptic physiology data set, which revealed very small excitatory postsynaptic currents in a large proportion of recorded LC neurons. It would be prudent to repeat chemogenetic inhibition of these terminals during systemic morphine to determine whether these projections are required for full expression of antinociception, as was the case with glutamatergic PAG inputs to LC. Alternatively, these inputs could be activated to determine if antinociception that relies on spinal NA signaling results.

Second, what drives activity in RVM-to-LC projections? We report in Chapter 2 that chemogenetic inhibition of RVM GABAergic/glycinergic terminals in LC produces antinociception that can be blocked by intrathecal NA antagonism. These results would suggest that RVM provides tonic inhibition to LC neurons and LC can be disinhibited with release of this inhibition, much like the canonical disinhibitory hypothesis of vlPAG activity in response to opioids. Electrophysiological recordings of tonic activity in these RVM neurons may provide insight. Additionally, RVM-to-LC neurons are likely driven by upstream structures. As of now, we do not know the presynaptic partners of RVM-to-LC neurons. One hypothesis is that vlPAG-to-RVM neurons, possibly even the same ones that project to LC, drive activity in RVM-to-LC neurons, therefore suggesting that PAG excites LC neurons via direct projections and inhibits LC neurons via indirect projections through the RVM. Equally as likely given our current knowledge, the RVM-to-LC neurons may receive input from any number of brain structures that might be involved in the functions of LC, from pain modulation to arousal. In Chapter 2, we reveal that the RVM-to-LC neurons do not bifurcate following the typical DPMS circuit model to the spinal cord and instead send projections to supraspinal areas such as the parafascicular

nucleus of the thalamus, potentially signaling their existence outside of the canonical DPMS framework by input and output.

Finally, what is the purpose of converging excitatory and inhibitory pathways on LC neurons? If indeed the vlPAG and RVM provide excitatory and inhibitory input to LC at the same time, as might be the case during noxious stimulus-evoked activity in the absence of opioids, what is the purpose of this convergent activity? The results of fiber photometry recordings of calcium activity in Chapter 3 provide an interesting starting point for pondering this question. Noxious-evoked responses to LC neurons appear to be much more tightly time locked to the stimulus and decay more quickly toward baseline, whereas glutamatergic PAG-to-LC projection neurons remain in a highly active state for a longer period. It is possible that PAG drives LC activity that is tempered by a concurrent inhibitory input, possibly from the RVM, to temporally restrict LC output. The concept of gain control in the LC to regulate arousal and optimize performance by keeping activity in an intermediate state has been previously proposed (Aston-Jones and Cohen, 2005).

Modulation of newly established circuit elements in chronic pain and tolerance

As mentioned in Chapter 4, how efficacious a circuit is in driving antinociception can change drastically following the plasticity that occurs during the transition from acute to chronic pain. Although our results convincingly exhibit hyperfunction of excitatory inputs onto LC during persistent pain, there is much future work to be done to establish whether the PAG-to-LC pathway contributes to this effect and what might be found in more chronic pain models. Perhaps working against this hypothesis is one study that reports downregulation of glutamatergic function in PAG after neuropathic injury (Ho et al., 2013), which would likely decrease PAG

output and therefore might downregulate PAG-to-LC activity. Additionally, as we have not yet investigated inhibitory inputs onto LC neurons in this context, it is difficult to speculate on a role for RVM-to-LC in modulated inhibitory inputs to LC neurons. Assessing the antinociceptive capabilities of RVM-to-LC inhibition as in Chapter 2 in the context of persistent or chronic pain remains an important first step in evaluating this circuit element's translational potential for treating chronic pain. Changes to the DPMS that are seen during pain chronification are discussed further in Chapter 4.

A parallel concern that arises for chronic pain patients that use opioids to control their pain is opioid tolerance. Although opioids remain the best available treatment for pain, patients become tolerant to the pain-relieving effects, leading to them require higher doses which increase the risk for respiratory depression and overdose. The DPMS contributes to opioid tolerance. Local microinjection of morphine (Yaksh, 1979; Lin et al., 1996; Kim et al., 2018) and electrical stimulation (Mayer et al., 1971) in the ventrolateral periaqueductal gray produces antinociception, but repeated administration of these acutely antinociceptive manipulations leads to strong tolerance (Jacquet and Lajtha, 1976; Morgan and Liebeskind, 1987; Siuciak and Advokat, 1987; Tortorici et al., 2001, 2003; Bagley et al., 2005; Lane et al., 2005; Morgan et al., 2006; Campion et al., 2016). This affect appears limited to the ventral part of the PAG, as electrical stimulation in the dorsal PAG (Morgan and Liebeskind, 1987) and morphine microinjection into the dorsal raphe nucleus (Campion et al., 2016) produce antinociception that is not limited over time by tolerance. PAG-mediated tolerance induced by local microinjection of morphine exhibits two-way cross tolerance with systemic morphine (Jacquet and Lajtha, 1976), but not intrathecal morphine administration (Siuciak and Advokat, 1987).

Mechanistic studies point to decreased effectiveness of opioids in the MOR+ interneurons in PAG after chronic opioid administration (Bagley et al., 2005) as the main driver of these behavioral effects. Muscimol-indued RVM inhibition does not block the development of tolerance (Lane et al., 2005), and PAG microinjection of bicuculline (to produce disinhibition) or kainite (to direct stimulate output) causes antinociception with no development of tolerance (Morgan et al., 2003). While the typical electrophysiological responses of RVM neurons to morphine microinjection in PAG are lost in a tolerant state, the responses are intact after PAG microinjection of kainic acid in morphine-tolerant rats (Tortorici et al., 2001). Together, this body of literature implicates opioid-sensitive PAG neurons, but not PAG projection neurons or other downstream DPMS elements in development of tolerance.

In contrast to this notion, preliminary data from our own lab suggest the possibility of cross tolerance between repeated PAG-to-RVM projection neuron activation and systemic opioids. In these experiments, non-cell type specific PAG-to-RVM projections were captured using a retrograde AAV expressing cre recombinase injected in RVM with a cre-dependent chemogenetic actuator HM3D (or control fluorophore) in PAG (**Figure 5.1A**). Mice were subjected to hot plate nociceptive testing each day at baseline (Day 1 and 2), after systemic CNO injection (Day 3), after repeated twice-daily systemic morphine injection to produce tolerance (Day 4-8), and finally after a second administration of systemic CNO (Day 9) (**Figure 5.1B**). After the induction of morphine tolerance, as evidenced by a decreased hot plate withdrawal latency after repeated morphine administration (**Figure 5.1C**), CNO administration appears less effective at producing antinociception (**Figure 5.1D**), signaling the possibility of cross tolerance between the antinociceptive mechanisms. However, it is important to note that these data are preliminary and further testing is required to make this conclusion.

The effects of long-term opioid administration have been studied in LC on the molecular and cellular level in rats. Acutely, opioids inhibit rat LC neurons through activation of potassium channels and inhibition of downstream intracellular signaling pathways. Chronic opioids appear to upregulate these intracellular pathways and decrease activation of the potassium channels to compensate, resulting in overly excitable LC neurons that contribute to behaviors of dependence and withdrawal and that require more opioids to regulate their activity back down to baseline (Christie, 1991; Nestler, Meenakshi et al., 1994). To determine the effects of tolerance on the circuit elements defined within this dissertation, it will first be prudent to consider any species differences that may make the resulting data hard to interpret. As mentioned in Chapter 2, the opioid effects on LC neurons are much smaller at baseline in mice than in rats. However, there is evidence that assays of LC cellular tolerance in mice follow similar patterns to that found in rats, if qualitatively less effective (Quillinan et al., 2011; Adhikary and Williams, 2022).

Given this, it may be possible to assess changes in PAG-to-LC and RVM-to-LC circuitry in opioid tolerant mice. Following from our results in **Figure 5.1**, if we find that activation of PAG-to-LC projections produces antinociception, we might also find cross tolerance to activation of this circuit element and systemic morphine, as there is significant overlap between PAG neurons that project to RVM and those that project to LC. In line with the presented theory in the literature that tolerance is mainly driven by MOR+ PAG neurons, our PAG-to-LC pathway would be mostly affected if these neurons too are under tonic inhibitory control from local PAG interneurons. This is likely the case given the stated overlap in outputs.

The RVM is less implicated as a driver of tolerance. Enhanced descending facilitation from RVM, however, has been pointed to as a mediator of the paradoxical abnormal pain that can arise from chronic opioid exposure and tolerance (Ossipov et al., 2003). It is unclear how our

RVM-to-LC projection would be affected by chronic opioid exposure. We have established that this projection is largely non-overlapping with the RVM neurons that project to the spinal cord, which would decouple this population from enhanced descending facilitation reported in the literature. Additionally, as discussed, the presynaptic partners of the RVM-to-LC neurons are not known. If PAG-to-RVM neurons directly contact them, our antinociceptive pathway may be subject to tolerance driven by PAG that is already deeply established. Finally, RVM-to-LC neurons are MOR+ themselves, suggesting that intracellular signaling mechanisms might change over time with chronic opioid exposure, as is the case with LC. Experiments regarding the direct effect of repeated opioid exposure on the cells themselves, as well as repeated manipulations that mimic the effect of opioids on this circuit (namely inhibition of the projections) are needed.

Is descending pain modulation a closed loop process?

Our circuit model and methodology established here present an exciting opportunity to investigate *how* the DPMS is triggered to cause descending release of pain modulatory molecules. The ascending and descending pain pathways are largely discussed as two separate entities. While there is evidence that PAG is triggered by and coordinates descending signals from the forebrain, the flow of noxious information through this pathway remains unclear. In addition to a host of forebrain areas, PAG receives afferents directly from the spinal cord and both PAG and RVM receive noxious sensory information from the parabrachial nucleus (Roeder et al., 2016; Chen et al., 2017; Chiang et al., 2020). It is less clear whether the LC receives significant spinal innervation (Aston-Jones et al., 1991; Benarroch, 2005), but our data in Chapter 3 suggest that PAG-to-LC neurons are activated by noxious stimuli and could represent

a pathway by which LC receives sensory information and similar assumptions have been made regarding RVLM excitatory input to LC (Ennis and Aston-Jones, 1988; Ennis et al., 1992).

We hypothesize that the major nodes of the DPMS receive noxious sensory input from the spinal cord or the relays noted above as a closed, negative feedback loop in which noxious, potentially painful stimuli drive activity in the DPMS that inhibits incoming signals back at the level of the spinal dorsal horn. Opioids or inputs to the DPMS from supraspinal regions involved in cognitive modulation likely serve to tune the noxious sensory information within the negative feedback loop in a context-dependent manner. Interesting experiments based on the findings within this dissertation can be used to help clarify how noxious stimulus-evoked activity is represented in this new model of the DPMS. In Chapter 3, we established that LC and PAG-to-LC neurons exhibit noxious stimulus evoked responses. Chemogenetic inhibition of PAG inputs during noxious stimulation and recording of LC responses will help determine if PAG is the brain region that provides crucial noxious information to LC. If LC signaling is not affected by abolishing PAG input, it would indicate that other input regions are responsible for driving noxious stimulus representations in LC. This same line of questioning stands if we find that RVM-to-LC neurons also convey noxious sensory information. Determining how exogenous opioids or persistent/chronic pain modulate the noxious-evoked signals will also be informative.

The updated DPMS in other forms of pain modulation

For many reasons listed throughout this dissertation, we believe that a thorough understanding of how opioids produce antinociception, including which circuit elements are important for downstream NA release, is important for translational potential in human health. By understanding how opioids provide pain relief, we may be able to pinpoint circuits that are

"druggable" to produce analgesia in the absence of negative opioid side effects. Additionally, by studying these same circuits in the context of chronic pain or opioid tolerance, we maximize our chances of producing analgesics that help those burdened most by pain-related negative consequences. However, we also can look at our use of opioids drugs in acute assays as tools in understanding the logic of descending pain modulation in more naturalistic settings. In addition to exogenous opioids like morphine, opioid receptors bind endogenous opioids, such as enkephalins, dynorphin, and endorphins. Endogenous opioids are implicated in a variety of pain modulatory conditions that do not require opioid drugs, such as stress-induced analgesia (Butler and Finn, 2009) and placebo analgesia (Benedetti and Amanzio, 1997). We hypothesize that further study might prove spinal NA signaling to be an important endpoint of these forms of analgesia as well.

Overall, we believe that the work in this dissertation represents an important step forward in understanding the strongly antinociceptive release of NA in the spinal cord. While many portions of the DPMS circuitry, such as canonical projections from PAG to RVM to the dorsal horn and the importance of spinal noradrenergic signaling, have been established in a rich body of literature spanning decades, we believe the efforts herein bring together these important pieces and fill critical gaps in our understanding of how descending NA is triggered to produce antinociception.

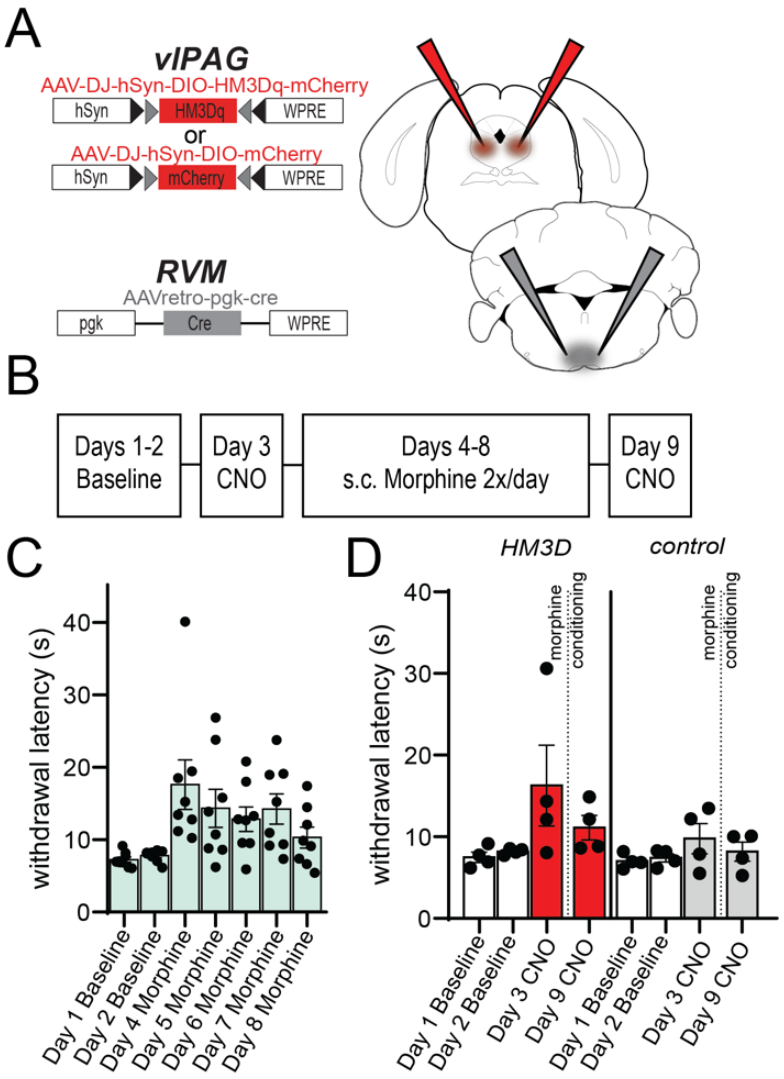

Figure 5.1 Preliminary studies to assess cross tolerance between PAG-to-RVM DPMS activation and systemic morphine.

A. Schematic of viral injections used to chemogenetically activate vlPAG neurons that project to RVM. **B.** Timeline of hot plate testing, including systemic drug used per day. **C.** Hot plate baseline withdrawal latencies and induction of morphine tolerance for both HM3D and control mice. D. Hot plate withdrawal latencies in HM3D (white and red) and control (white and grey) mice at baseline and CNO administration days before (Day 3) and after (Day 9) morphine tolerance induction. All bar graphs represented as mean ± SEM.

Chapter 5 contains unpublished material coauthored with Banghart, Matthew R.

The dissertation author was the primary researcher and author of this chapter.

References

Adhikary, S., and Williams, J. T. (2022). Cellular Tolerance Induced by Chronic Opioids in the Central Nervous System. *Front Syst Neurosci* 16. doi: 10.3389/fnsys.2022.937126.

Aston-Jones, G., and Cohen, J. D. (2005). An integrative theory of locus coeruleus-norepinephrine function: Adaptive gain and optimal performance. *Annu Rev Neurosci* 28, 403–450. doi: 10.1146/annurev.neuro.28.061604.135709.

Aston-Jones, G., Shipley, M. T., Chouvet, G., Ennis, M., van Bockstaele, E., Pieribone, V., et al. (1991). "Afferent regulation of locus coeruleus neurons: anatomy, physiology and pharmacology," in *Neurobiolgoy of the Locus Coeruleus*, 47–75. doi: 10.1016/S0079-6123(08)63799-1.

Bagley, E. E., Chieng, B. C. H., Christie, M. J., and Connor, M. (2005). Opioid tolerance in periaqueductal gray neurons isolated from mice chronically treated with morphine. *Br J Pharmacol* 146, 68–76. doi: 10.1038/sj.bjp.0706315.

Barcomb, K., Olah, S. S., Kennedy, M. J., and Ford, C. P. (2022). The Journal of Physiology Properties and modulation of excitatory inputs to the locus coeruleus. *J Physiol* 0, 1–20. doi: 10.1113/JP283605#support-information-section.

Benarroch, E. E. (2005). *Basic Neurosciences with Clinical Applications*. Butterworth-Heinemann.

Benedetti, F., and Amanzio, M. (1997). The neurobiology of placebo analgesia: from endogenous opioids to cholecystokinin. *Prog Neurobiol* 51, 109–125.

Butler, R. K., and Finn, D. P. (2009). Stress-induced analgesia. *Prog Neurobiol* 88, 184–202. doi: 10.1016/j.pneurobio.2009.04.003.

Campion, K. N., Saville, K. A., and Morgan, M. M. (2016). Relative contribution of the dorsal raphe nucleus and ventrolateral periaqueductal gray to morphine antinociception and tolerance in the rat. *European Journal of Neuroscience* 44, 2667–2672. doi: 10.1111/ejn.13378.

Chen, Q. L., Roeder, Z., Li, M. H., Zhang, Y. M., Ingram, S. L., and Heinricher, M. M. (2017). Optogenetic Evidence for a Direct Circuit Linking Nociceptive Transmission through the Parabrachial Complex with Pain-Modulating Neurons of the Rostral Ventromedial Medulla (RVM). *eNeuro* 4, 202–219. doi: 10.1523/ENEURO.0202-17.2017.

Chiang, M. C., Nguyen, E. K., Canto-Bustos, M., Papale, A. E., Oswald, A. M. M., and Ross, S. E. (2020). Divergent Neural Pathways Emanating from the Lateral Parabrachial Nucleus Mediate Distinct Components of the Pain Response. *Neuron* 106, 927-939.e5. doi: 10.1016/j.neuron.2020.03.014.

Christie, M. J. (1991). Mechanisms of opioid actions on neurons of the locus coeruleus. *Prog Brain Res* 88, 197–205.

Ennis, M., and Aston-Jones, G. (1988). Activation of locus coeruleus from nucleus paragigantocellularis: a new excitatory amino acid pathway in brain. *The Journal of Neuroscience* 8, 3644–3657. doi: 10.1523/JNEUROSCI.08-10-03644.1988.

Ennis, M., Aston-Jones, G., and Shiekhattar, R. (1992). Activation of locus coeruleus neurons by nucleus paragigantocellularis or noxious sensory stimulation is mediated by intracoerulear excitatory amino acid neurotransmission. *Brain Res* 598, 185–195. doi: 10.1016/0006-8993(92)90182-9.

Ennis, M., Behbehani, M., Shipley, M. T., van Bockstaele, E. J., and Aston-Jones, G. (1991). Projections from the periaqueductal gray to the rostromedial pericoerulear region and nucleus locus coeruleus: Anatomic and physiologic studies. *Journal of Comparative Neurology* 306, 480–494. doi: 10.1002/cne.903060311.

Hammond, D. L., and Proudfit, H. K. (1980). Effects of locus coeruleus lesions on morphine-induced antinociception. *Brain Res* 188, 79–91. doi: 10.1016/0006-8993(80)90558-2.

Ho, Y. C., Cheng, J. K., and Chiou, L. C. (2013). Hypofunction of glutamatergic neurotransmission in the periaqueductal gray contributes to nerve-injury-induced neuropathic pain. *Journal of Neuroscience* 33, 7825–7836. doi: 10.1523/JNEUROSCI.5583-12.2013.

Jacquet, Y. F., and Lajtha, A. (1976). THE PERIAQUEDUCTAL GRAY: SITE OF MORPHINE ANALGESIA AND TOLERANCE AS SHOWN BY 2-WAY CROSS TOLERANCE BETWEEN SYS-TEMIC AND INTRACEREBRAL INJECTIONS. *Brain Res* 103, 501–513.

Kim, J. H., Gangadharan, G., Byun, J., Choi, E. J., Lee, C. J., and Shin, H. S. (2018). Yin-and-yang bifurcation of opioidergic circuits for descending analgesia at the midbrain of the mouse. *Proc Natl Acad Sci U S A* 115, 11078–11083. doi: 10.1073/pnas.1806082115.

Kong, D., Zhang, Y., Gao, P., Pan, C., Deng, H., Xu, S., et al. (2023). The locus coeruleus input to the rostral ventromedial medulla mediates stress-induced colorectal visceral pain. *Acta Neuropathol Commun* 11. doi: 10.1186/s40478-023-01537-6.

Lane, D. A., Patel, P. A., and Morgan, M. M. (2005). Evidence for an intrinsic mechanism of antinociceptive tolerance within the ventrolateral periaqueductal gray of rats. *Neuroscience* 135, 227–234. doi: 10.1016/j.neuroscience.2005.06.014.

Lin, Q., Peng, Y. B., and Willis, W. D. (1996). Antinociception and inhibition from the periaqueductal Gray are mediated in part by spinal 5-hydroxytryptamine1A receptors. *Journal of Pharmacology and Experimental Therapeutics* 276, 958–967.

Mayer, D. J., Wolfle, T. L., Akil, H., Carder, B., and Liebeskind, J. C. (1971). Analgesia from electrical stimulation in the brainstem of the rat. *Science (1979)* 174, 1351–1354.

Morgan, M. M., Clayton, C. C., and Lane, D. A. (2003). Behavioral evidence linking opioid-sensitive GABAergic neurons in the ventrolateral periaqueductal gray to morphine tolerance. *Neuroscience* 118, 227–232. doi: 10.1016/S0306-4522(02)00822-9.

Morgan, M. M., Fossum, E. N., Levine, C. S., and Ingram, S. L. (2006). Antinociceptive tolerance revealed by cumulative intracranial microinjections of morphine into the periaqueductal gray in the rat. *Pharmacol Biochem Behav* 85, 214–219. doi: 10.1016/j.pbb.2006.08.003.

Morgan, M. M., and Liebeskind, J. C. (1987). Site specificity in the development of tolerance to stimulation-produced analgesia from the periaqueductal gray matter of the rat. *Brain Res* 425, 356–359.

Nestler,' Meenakshi, E. J., And, A., and Aghajanian, G. K. (1994). Molecular and Cellular Mechanisms of Opiate Action: Studies in the Rat. *Brain Research Builetin* 35, 521–528.

Ossipov, M. H., Dussor, G. O., and Porreca, F. (2010). Central modulation of pain. *Journal of Clinical Investigation* 120, 3779–3787. doi: 10.1172/JCI43766.

Ossipov, M. H., Lai, J., Vanderah, T. W., and Porreca, F. (2003). Induction of pain facilitation by sustained opioid exposure: Relationship to opioid antinociceptive tolerance. *Life Sci* 73, 783–800. doi: 10.1016/S0024-3205(03)00410-7.

Quillinan, N., Lau, E. K., Virk, M., Von Zastrow, M., and Williams, J. T. (2011). Recovery from μ-opioid receptor desensitization after chronic treatment with morphine and methadone. *Journal of Neuroscience* 31, 4434–4443. doi: 10.1523/JNEUROSCI.4874-10.2011.

Roeder, Z., Chen, Q., Davis, S., Carlson, J. D., Tupone, D., and Heinricher, M. M. (2016). Parabrachial complex links pain transmission to descending pain modulation. *Pain* 157, 2697–2708. doi: 10.1097/j.pain.0000000000000688.

Sasa, M., Munekiyo, K., Osumi, Y., and Takaori, S. (1977). Attenuation of morphine analgesia in rats with lesions of the locus coeruleus and dorsal raphe nucleus.

Siuciak, J. A., and Advokat, C. (1987). Tolerance to morphine microinjections in the periaqueductal gray (PAG) induces tolerance to systemic, but not intrathecal morphine.

Tortorici, V. Â., Morgan, M. M., and Vanegas, H. (2001). Tolerance to repeated microinjection of morphine into the periaqueductal gray is associated with changes in the behavior of off-and on-cells in the rostral ventromedial medulla of rats. *Pain* 89, 237–244.

Tortorici, V., Nogueira, L., Salas, R., and Vanegas, H. (2003). Involvement of local cholecystokinin in the tolerance induced by morphine microinjections into the periaqueductal gray of rats. *Pain* 102, 9–16. doi: 10.1016/s0304-3959(02)00153-7.

Yaksh, T. L. (1979). Direct evidence that spinal serotonin and noradrenaline terminals mediate the spinal antinociceptive effects of morphine in the periaqueductal gray. *Brain Res* 160, 180–185. doi: 10.1016/0006-8993(79)90616-4.